

Low Loss Porous Core Photonic Crystal Fiber Design in THz
Regime

by

Md. Sohidul Islam

DOCTOR OF PHILOSOPHY

IN

ELECTRICAL AND ELECTRONIC ENGINEERING



Department of Electrical and Electronic Engineering
Islamic University of Technology (IUT)
Board Bazar, Gazipur-1704, Bangladesh.
September, 2020.

RECOMMENDATION OF THE BOARD OF EXAMINERS

The thesis titled “**Low Loss Porous Core Photonic Crystal Fiber Design in THz Regime**” submitted by **Md. Sohidul Islam**, student number 102703 of Academic Year 2010-2011, has been found as satisfactory and accepted as partial fulfillment of the requirements for the degree of Doctor of Philosophy in Electrical and Electronic Engineering on September 17, 2020.

Board of Examiners:

1.
Dr. Mohammad Rakibul Islam
Professor,
Department of Electrical and Electronic Engineering,
Islamic University of Technology (IUT), Boardbazar, Gazipur-1704. Chairman
(Supervisor)

2.
Dr. Md. Ruhul Amin
Professor and Head,
Department of Electrical and Electronic Engineering,
Islamic University of Technology (IUT), Boardbazar, Gazipur-1704. Member
(Ex-Officio)

3.
Dr. Md. Ashraful Hoque
Professor,
Department of Electrical and Electronic Engineering,
Islamic University of Technology (IUT), Boardbazar, Gazipur-1704. Member

4.
Dr. Rakibul Hasan Sagor
Associate Professor,
Department of Electrical and Electronic Engineering,
Islamic University of Technology (IUT), Boardbazar, Gazipur-1704. Member

5.
Prof. Dr. S. M. Abdur Razzak
Professor,
Department of Electrical and Computer Engineering,
Rajshahi University of Engineering & Technology (RUET) Member
(External)

6.
Prof. Dr. Mohammad Faisal
Professor,
Department of Electrical and Computer Engineering,
Bangladesh University of Engineering & Technology (BUET) Member
(External)

© 2020 Md. Sohidul Islam
All Rights Reserve.

STATEMENT OF CANDIDATE

It is hereby declared that this thesis or any part of it has not been submitted elsewhere for the award of any Degree or Diploma.

I also declare that this thesis is my own work, is not copied from any other person's work, and has not previously submitted for assessment either at this university or elsewhere.

.....

Md. Sohikul Islam

Student No. 102703

Academic Year: 2010-2011

Date: September 17, 2020

Dedicated to Baba, Ma, Sons, and my adorable wife.

TABLE OF CONTENTS

| | |
|---|------|
| RECOMMENDATION OF THE BOARD OF EXAMINERS | II |
| DECLARATION OF CANDIDATE | IV |
| LIST OF FIGURES | VII |
| LIST OF TABLES | X |
| LIST OF ACRONYMS | XI |
| ACKNOWLEDGEMENTS | XII |
| ABSTRACT | XIII |
| CHAPTER 1 | |
| INTRODUCTION | 1 |
| 1.1 Introduction | 1 |
| 1.2 THz Sources and Detectors | 1 |
| 1.2.1 THz Sources | 2 |
| 1.2.2 THz Detectors | 2 |
| 1.3 THz Waveguides | 2 |
| 1.3.1 Solid Core PCF | 4 |
| 1.3.2 Hollow Core PCF | 4 |
| 1.3.3 Kagome PCF | 5 |
| 1.3.4 Porous Core PCF | 5 |
| 1.4 Properties of Porous Core PCF | 7 |
| 1.5 THz Waveguide Characterization | 7 |
| 1.6 THz Applications | 10 |
| 1.7 Performance Parameters for THz Waveguides | 10 |
| 1.8 Fabrication Methods of PC-PCF | 13 |
| 1.9 Background Materials for Fiber Fabrication of PCF | 14 |
| 1.10 Motivation | 16 |
| 1.11 Objectives with Specific Aims | 16 |
| 1.12 Outline of Methodology | 17 |
| 1.13 Thesis Organization | 17 |

CHAPTER 2

| | |
|----------------------------|-----------|
| BACKGROUND STUDIES | 19 |
| 2.1 Background studies | 19 |
| 2.2 Hexagonal Core | 20 |
| 2.3 Hybrid Core | 23 |
| 2.4 Circular Core | 24 |
| 2.5 Other Core | 25 |
| 2.6 Decagonal Cladding | 29 |
| 2.7 Octagonal Cladding | 30 |
| 2.8 Circular Cladding | 32 |
| 2.9 Summary of the Chapter | 32 |

CHAPTER 3

| | |
|--------------------------------------|-----------|
| METHODS OF ANALYSIS | 33 |
| 3.1 Introduction | 33 |
| 3.2 Introduction to Electromagnetism | 33 |
| 3.2.1 Maxwell's Equations | 34 |
| 3.2.2 Boundary Conditions | 35 |
| 3.2.3 Wave Equation Derivation | 36 |
| 3.3 Numerical Techniques | 38 |
| 3.4 Finite Element Method | 38 |
| 3.4.1 Scaler Formulation | 40 |
| 3.4.2 Element Formation in FEM | 42 |
| 3.4.3 Global Matrices Formation | 46 |
| 3.5 Perfectly Match Layer | 49 |
| 3.6 Summary of the Chapter | 49 |

CHAPTER 4

| | |
|---|-----------|
| DECAGONAL CLADDING-HEXAGONAL CORE PC- PCF | 52 |
| 4.1 Introduction | 52 |
| 4.2 Design Methodology of Proposed Decagonal- Hexa Core PC- PCF | 54 |
| 4.3 Results and discussions of the Proposed PC-PCF | 56 |
| 4.4 Concluding Remarks of the Chapter | 60 |

CHAPTER 5

| | |
|--|----|
| OCTAGONAL CLADDING-HEXAGONAL CORE PC- PCF | 61 |
| 5.1 Introduction. | 61 |
| 5.2 Proposed Geometry of Hexagonal PC-PCF | 62 |
| 5.3 Simulation and Results of Proposed Design | 63 |
| 5.4 Comparisons with Octagonal PCFs | 67 |
| 5.5 Fabrication Method of Proposed PC-PCF | 71 |
| 5.6 Summary of the Chapter | 71 |

CHAPTER 6

| | |
|---|----|
| OCTAGONAL CLADDING –HYBRID CORE PC- PCF | 72 |
| 6.1 Introduction | 72 |
| 6.2 Design Methodology of Octa-Hybrid PC-PCF | 72 |
| 6.3 Results and Discussions of the Proposed PC-PCF | 73 |
| 6.4 Octagonal Hybrid PCF Comparisons | 80 |
| 6.5 Summary of the Chapter | 82 |

CHAPTER 7

| | |
|---|----|
| CIRCULAR CORE AND CLADDING PC-PCF | 83 |
| 7.1 Introduction | 83 |
| 7.2 Geometry of the proposed Circular PC-PCF | 83 |
| 7.3 Numerical results and discussions | 85 |
| 7.4 Circular PC-PCF Comparisons | 90 |
| 7.5 Conclusion of the Chapter | 92 |

CHAPTER 8

| | |
|---------------------------------|----|
| CONCLUSION | 93 |
| 8.1 Conclusion of the Thesis | 93 |
| 8.2 Scope for Future Works | 94 |

| | |
|------------|----|
| APPENDICES | 96 |
|------------|----|

| | |
|------------|-----|
| REFERENCES | 101 |
|------------|-----|

| | |
|----------------------|-----|
| LIST OF PUBLICATIONS | 111 |
|----------------------|-----|

LIST OF FIGURES

| | Description | Page |
|-----------|--|-------------|
| Fig. 1.1 | Solid core PCF | 4 |
| Fig. 1.2 | Hollow core PCF | 4 |
| Fig. 1.3 | Cross section of Kagome PCF | 5 |
| Fig. 1.4 | Cross section of porous core fiber | 6 |
| Fig. 1.5 | THz Characterizations | 8 |
| Fig. 1.6 | THz Spectrum | 9 |
| Fig. 2.1 | Cross-sectional view of (a) rotated hexagonal porous core hexagonal PCF, (b) PCF is anti-symmetric inside core and cladding, (c) PCF having hexagonal air holes inside the dense cladding area encircled by circular air holes and a PML in the core, (d) dispersion flattened porous-core honeycomb lattice, (e) dual-core microstructured optical fiber design. | 21 |
| Fig. 2.2 | Cross-sectional diagram of (a) hybrid porous core structure having triangular air hole arrangements, (b) PCF having hybrid air hole configuration inside core accompanied hexagonal cladding. | 23 |
| Fig. 2.3 | Cross-sectional view of (a) porous core PCF, (b) ring-core PCF geometry. | 24 |
| Fig. 2.4 | Cross-sectional view of (a) Topas based PCF having of a conventional hexagonal cladding and a penta-hole elliptical structure in the core, (b) slotted porous core fiber, (c) slotted-core PCF having a hexagonal cladding., (d) diamond-core porous fiber, (e) rhombic-shaped porous-core PCF(f) PC-PCF comprising of a regular octagonal core, (g) COC based diamond-core PCF. | 28 |
| Fig. 2.5 | Cross sectional view of decagonal PCFs | 29 |
| Fig. 2.6 | Cross sectional view of Octagonal PCFs | 30 |
| Fig. 2.7 | Cross sectional view of Circular PCFs | 31 |
| Fig. 3.1 | Mediums with interfaces | 35 |
| Fig. 3.2a | Shape of the elements and mesh size | 41 |
| Fig. 3.2b | Shape of elements for one, two and three dimensions | 41 |

| | | |
|----------|--|----|
| Fig. 3.3 | Meshing at the boundary edge (i) triangular (ii) rectangular elements | 42 |
| Fig. 3.4 | (a) First order, (b) second and (c) third order element | 43 |
| Fig. 3.5 | View of polynomials Pascal triangle | 43 |
| Fig. 3.6 | Perfectly Matched Layer | 49 |
| Fig. 4.1 | Geometry area of the proposed PC-PCF accompanied by zoomed view of porous core | 52 |
| Fig. 4.2 | Modal field of the proposed geometry structure (a) 61.5%porosity (b) 71.5%porosity (c) 81.5%porosity | 53 |
| Fig. 4.3 | V- parameter and D_{core} at $f = 1$ THz | 55 |
| Fig. 4.4 | V-parameter and frequency for $D_{\text{core}} = 280 \mu\text{m}$ | 55 |
| Fig. 4.5 | EML versus core radius at different porosities | 57 |
| Fig. 4.6 | Characteristics of EML, core power fraction and Frequency at $D_{\text{core}} = 280 \mu\text{m}$ | 58 |
| Fig. 4.7 | Calculated confinement versus frequencies at $D_{\text{core}} = 280 \mu\text{m}$ | 58 |
| Fig. 4.8 | Dispersion Characteristics of the proposed PCF versus Frequencies for $D_{\text{core}} = 280 \mu\text{m}$ | 59 |
| Fig. 5.1 | a) Cross section of the proposed structure (b) Zoomed core. | 61 |
| Fig. 5.2 | Modal field at 81% porosity with $324 \mu\text{m}$ at 1 THz | 63 |
| Fig. 5.3 | Normalized frequency as a function of core diameter with $f=1\text{THz}$ and porosity=88% | 63 |
| Fig. 5.4 | V parameter as a function of frequency at $D_{\text{core}}=324\mu\text{m}$ and porosity=88%. | 65 |
| Fig. 5.5 | Effective material loss as a function of core diameter at different porosities with $f=1$ THz. | 65 |
| Fig. 5.6 | Confinement loss versus frequency for $D_{\text{core}}=324\mu\text{m}$, porosity=88%. | 66 |
| Fig. 5.7 | EML versus frequency at $D_{\text{core}}=324 \mu\text{m}$, porosity=88%. | 67 |
| Fig. 5.8 | Power fraction versus frequency at $D_{\text{core}}=324 \mu\text{m}$, porosity=88% | 68 |
| Fig. 5.9 | Dispersion Characteristics at $D_{\text{core}}=324 \mu\text{m}$ and porosity=88% | 69 |
| Fig. 6.1 | (a) Cross section of the proposed Geometry (b) Zoomed core | 73 |
| Fig. 6.2 | Modal field distributions of the PC-PCF geometry at porosity 76%, $D_{\text{core}} = 320\mu\text{m}$, 0.73THz | 74 |

| | | |
|-----------|---|----|
| Fig. 6.3 | Normalized frequency with core diameter where frequency 0.73 THz , porosity of 42% | 75 |
| Fig. 6.4 | Birefringence versus frequency in THz | 76 |
| Fig. 6.5 | Birefringence versus D_{core} | 76 |
| Fig. 6.6 | EML versus core diameters for 63% and 76% at 0.73 THz | 77 |
| Fig. 6.7 | EML versus frequency at core diameter at 320 μ m while porosity 42% | 77 |
| Fig. 6.8 | Core power fraction versus various frequencies while porosity 42% and at core diameter 320 μ m. | 78 |
| Fig. 6.9 | Confinement loss is changing along with frequency at 320 μ m while porosity set to 42% | 79 |
| Fig. 6.10 | Dispersion Characteristics as a function of frequency at 1 THz at core diameter 320 μ m | 80 |
| Fig. 7.1 | Cross-section of the proposed PC-PCF. | 83 |
| Fig. 7.2 | Electric field distributions of the proposed PCF at 84% porosity at core diameter $D_{core} = 350 \mu\text{m}$ for (a) zoomed porous core (b) porous Core fiber | 85 |
| Fig. 7.3 | V parameter versus frequency | 86 |
| Fig. 7.4 | Behaviour of EML with frequency at 350 μ m | 87 |
| Fig. 7.5 | Behaviour of EML with Core diameters at 1.05 THz | 87 |
| Fig. 7.6 | Behaviour of power fraction versus core diameters while frequency 1.05THz. | 88 |
| Fig. 7.7 | Confinement loss vs frequency at 350 μ m using porosity of 84% | 88 |
| Fig. 7.8 | Dispersion as a function of frequency at 350 μ m using porosity 84% | 89 |

LIST OF TABLES

| | Description | Page |
|---------|--|-------------|
| Table 1 | Optimized Parameter for Decagonal PC-PCF at 1 THz | 54 |
| Table 2 | Optimized values for Hexagonal PC-PCF for Simulation | 62 |
| Table 3 | Octagonal PC-PCF Comparisons | 69 |
| Table 4 | Optimize Parameter for the simulation Octa Hybrid at 0.73 THz | 74 |
| Table 5 | Octagonal Hybrid PCF Comparisons | 81 |
| Table 6 | Optimize Parameter for Circular PCF simulations at 1.05 THz | 84 |
| Table 7 | Circular PCF Comparison | 90 |
| Table 8 | Light guiding properties of the proposed PC-PCFs in THz regime | 94 |

LIST OF ACRONYMS

| | |
|---------------|------------------------------------|
| PCF | Photonic Crystal Fiber |
| PC-PCF | Porous Core PCF |
| PGB | Photonic Band Gap |
| THz | Terahertz |
| EML | Effective Material Loss |
| MTIR | Modified Total Internal Reflection |
| PML | Perfectly Matched Layer |
| TIR | Total Internal Reflection |
| LC | Liquid Core |
| FBG | Fiber Bragg Grating |
| SIF | Step Index Fiber |
| GIF | Graded Index Fiber |
| LFM | Localized Function Method |
| FDM | Finite Difference Method |
| FDTD | Finite-Difference Time-Domain |
| FEM | Finite Element Method |
| FFT | Fast Fourier Transform |
| PMC | Perfect Magnetic Conductor |
| PEC | Perfect Electric Conductor |
| PF | Power Fraction |
| CL | Confinement Loss |
| ESMF | Endless Single Mode Fiber |
| BR | Birefringence |
| CPF | Core Power Fraction |

ACKNOWLEDGEMENTS

I would first like to thank my creator who blessed me with the ability to perform this research at Islamic University of Technology. Then I express my gratitude to my supervisor Prof. Dr. Mohammad Rakibul Islam, who played the vital role by providing me with valuable guidelines and all sorts of support. He played the instrumental role behind the research and his motivation in every stage has been the key to the completion of this thesis. I am also very much indebted to Prof. Dr. Md. Ruhul Amin, Head of the Electrical and Electronic Engineering (EEE) Department, for his useful suggestions and encouragement as well as for rendering the administrative support. I would like to gratefully and sincerely thank Prof. Dr. Md. Ashraful Hoque, EEE Department, who has been a constant source of encouragement and enthusiasm. I am also grateful to Prof. Dr. Shaikh Anowarul Fattah for his endless suggestions to my thesis work. I am also grateful to Prof. Dr. Mohammad Faisal as well as Prof. Dr. S. M. Abdur Razzak for their valuable suggestions to this thesis work.

I would like to express my sincere gratitude to all faculty and staff members of EEE Department at IUT for their selfless support, encouragement and love given to me during the course of this thesis. Finally, I take this opportunity to express the profound gratitude to my beloved family members for their patience and moral encouragement to complete my thesis.

Md. Sohidul Islam

September 17, 2020.

ABSTRACT

Photon, the massless particle responsible for electromagnetic radiations travels at the speed of light which is the key element in terahertz (THz) based fiber communications. The efficient transmission of THz wave using waveguides has been a major challenge since early days of this technology. Loss and dispersion play vital part in THz wave guidance. They should be reduced to obtain accurate THz wave propagation. Metallic waveguide tolerates Ohmic losses and dielectric waveguides experience huge material absorption losses. Dry air is the best transparent medium for THz radiations. Considering above losses, the fiber needs to develop. This thesis reports the development of fibers to guide THz radiations. The objective of this research work is to design optical waveguides using more advanced form optical fiber called porous core photonic crystal fiber (PC-PCF) in the terahertz regime. The porous core fiber has an arrangement of sub-wavelength featured air-holes in the cross section. The designed PC-PCF would be a possible candidate for THz wave guidance.

A considerable effort has been put into designing advanced porous core PCF structures with increased flexibility and the ability to minimize losses in terms of geometric structure. In this thesis, different structure is designed to obtain porous core photonic crystal fibers with low effective material loss (EML), low confinement loss (CL), high core power fraction and flatten dispersion for THz wave propagation. The preparation of proposed structure air holes, both in periodic cladding and porous core, made it possible to guide most of the light through low loss air, which is confirmed by numerical analysis of optical properties of the fiber while preserving the single mode condition. Numerical analysis of the proposed geometric structure of the fiber is rigorously performed using finite element method (FEM) with perfectly match layer (PML) boundary conditions to characterize the wave guiding properties. This thesis examines crucial design parameters such as effective material loss, core power fraction, birefringence, dispersion, and confinement loss of the proposed porous core fiber. Topas is used as background material due to its constant refractive index behavior in terahertz regime and its lower bulk absorption loss.

In this thesis work, four PC-PCF structures have been proposed, designed and numerically investigated. The proposed PC-PCF contains different shape and size of air hole dimensions in the cross sections. Among all the proposed PC-PCFs, the circular

cladding and circular core PC-PCF structure exhibits comparatively better results. This circular PC-PCF shows 0.04 cm^{-1} and $1.96 \times 10^{-4} \text{ cm}^{-1}$ of EML and confinement loss respectively. So, the total loss is 0.04 cm^{-1} as the confinement loss is negligible. Also, at 84% porosity the proposed circular PC-PCF exhibits 55.8% of core power fraction which can be considered enough for THz wave propagation. The sol-gel fabrication technique offers more freedom to high porosity geometric structures. Therefore, sol-gel can be considered as the fabrication technique for this proposed circular PC-PCF. Finally, the results of the analysis are further compared with those of previous reported contributions and found comparative. The proposed designs can be taken into consideration for THz communications.

CHAPTER 1

INTRODUCTION

1.1 Introduction

The terahertz (THz) band can be found just after microwave frequency and before optical wavelength windows. Sometimes it refers to millimeter wavelength as it spans from 0.003 mm to 3 mm or 1 THz to 10 THz [1]. Historically, this specific frequency spectrum was used by the physicist in astronomy for different purposes. The investigations of the THz band were evolving in late 1980s in research laboratories for detection and generation but there was toughness in these technologies [1]. With the blessings of more advance microwave and optical waveguide, it poised the THz waveguides with no anomaly. At the present time, the THz frequency band is immensely explored by investigators for designing low loss THz waveguides. The THz waveguides should be less frequency dependent to have better confinement characteristics. There are quite a few profits for designing low-loss and low-dispersion waveguides. The principal responsibility of the waveguides is to carry information from one end to another [2]. Furthermore, the waveguides can be utilized in sensing and imaging applications [3,4]. For the THz regime, the same advantages can be achieved.

Hence, the THz waveguide is promising scientific research areas for researchers. Huge number of research grant and resources have been offered to improve the properties of THz waveguides as well as finding new types of application in various fields such as telecommunication, biosensing, medical use and spectroscopy [5]. In the next section history of THz waveguide will be presented.

1.2 THz Sources and Detectors

Along with designing THz waveguide structure, it is also essential to discuss about THz source and detectors. Recently good numbers of THz source and detectors can be found in the market [6], but the challenging task is developing and THz waveguide. Low loss THz waveguide designing is the focus the research work.

1.2.1 THz Sources

There are good numbers of THz sources in THz spectrum. The carborundum heated rod and mercury lamp [7] sources are generally exploit as THz source in the laboratory. These are from high power laser including klystrons [8], travelling-wave tubes [9], and free-electron lasers [10].

There are other sources for THz is in solid state electronics. They are Gunn diode [11] and high frequency oscillators [12]. Terahertz laser source utilizing Ge-Si can be built efficiently [13]. It has been reported that some gas laser able to generate wave in THz spectrum [14]. The photo conductive dipole antenna exploits optical sampling method to produce THz radiation [15].

1.2.2 THz Detectors

Along with numbers of THz sources, here some of the THz detectors will be presented. They are photoinductive antenna, bolometer and electro-optic sampling techniques. Since first one has been discussed in earlier sub-section, this antenna can detect THz transmission using optical sampling techniques [16]. The bolometer exploits thermal detection techniques to isolate any form of radiation after absorbing it [16]. So, the bolometer has ability to deliver THz wave. In non-linear crystals electron and photon goes through interactions [17]. Hence, this interaction can be exploited to isolate THz transmission.

1.3 THz Waveguides

Traditional silica core structure methodology has enhanced importantly subsequently the first effective silica fiber had introduced in 1957 [18]. Though, the age of optical fiber telecommunications initiated in 1970s, when a fiber with loss around 20 dB/km was hurled [18]. In 1980s, the cost of long-distance communication has been reduced due to the progress of erbium-doped optical amplifier because light signal in the fiber could be amplified without converting it to electrical signal [19]. As a result, the requirement of repeater reduced in long distance communication. Today, conventional optical fibers are one of the best telecommunication media for long-distance telecommunications which is also blessing the THz communication system as well.

There are two major categories of THz waveguides. They are metallic and dielectric waveguides. The metallic waveguide undergoes huge material absorption loss due to the host materials. The dielectric waveguides can be subdivided into three categories and they are solid core, porous core and hollow core.

A photonic crystal is an optical nano structure which affects the motion of photons. Incorporating this specific material, the photonic crystal fiber can be designed. The three types of dielectric THz photonic crystal fiber along with kagome photonic crystal fiber will be presented next.

The periodic refractive index profile of PCF also called microstructured fiber found in transverse detection [20]. The PCF and traditional fiber follow basic wave guidance properties that is TIR. PCF has some geometric properties that is strongly depend on wavelength that is missing in traditional fiber. By tuning these geometric properties losses can be minimized to have application in telecommunication [21]. PCF were first designed in the 1970's but in the 90's they have attracted more attention for fabrication.

Earlier the expansion of current glass optical fiber technology, tubes of the fiber were examined as applicant for optical communications in the sixties [22]. In [22] it was described the first employed instance of a solid core PCF. The wave propagation mechanism of solid core PCF is like traditional optical fiber where light is travelled by modified TIR (mTIR) mechanism. The hollow core PCF was fabricated first time in late nineties [23] follows PGB mechanism to confine optical signal in the core. In hollow core PCF, the refractive index of the core is lower than the cladding as the core is hollow [24]. Due to geometric design flexibility in core of the fiber as well as having wide bandwidth compared to hollow core PCF the porous core PCF introduced in [25] can be apply to design low loss waveguide.

In this kind of fiber optics, the air hole found both in core and cladding regions opens the door of new possibilities in designing. Different types of PCF will be discussed later.

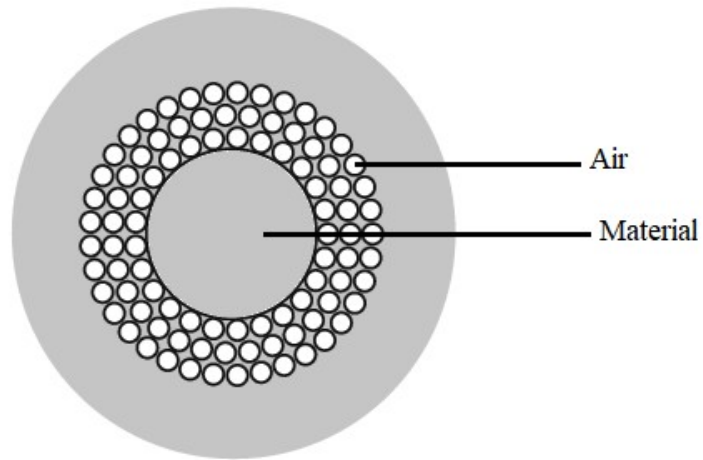


Fig. 1.1 Solid core PCF [26]

1.3.1 Solid Core PCF

This type of PCF is basically index guiding PCFs, with a solid host material in the core region surrounded by air-hole cladding [22]. This solid core fiber opens various novel applications shown in Fig. 1.1. This type of fiber is suitable for small core fiber and for achieving birefringence. Due to extensive material absorption loss in this type of fiber, it is not suitable for long distance communication.

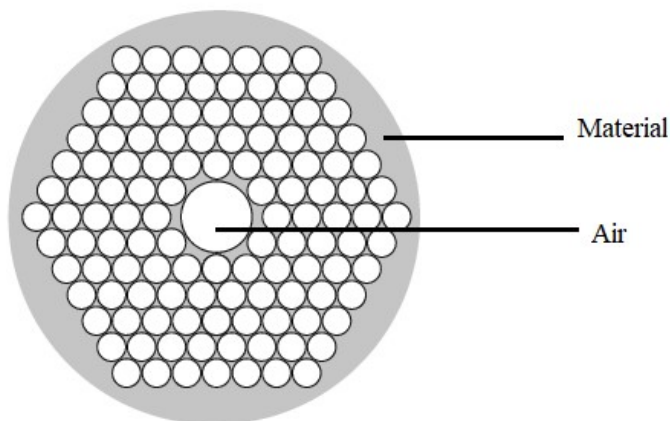


Fig. 1.2 hollow-core PCF [26]

1.3.2 Hollow Core PCF

Hollow core PCF is made of single host material along with a large air hole in the core of the fiber. This air hole is in the direction of the propagation or in the transverse direction.

As it is 2D PBG fiber, its refractive index varies in both direction in the crystal periodically. In the cladding there is air hole to the transverse direction. The fiber core is filled with lossless air opens application sensing, short distance communication, imaging and spectroscopy. It uses PBG effect to guide the light and compared to index guiding fiber loss is higher in this type of fiber [28]. The absence of solid material inside the core makes it damage prone on long distance installation. A diagram of hollow core PCF is shown in Fig. 1.2.

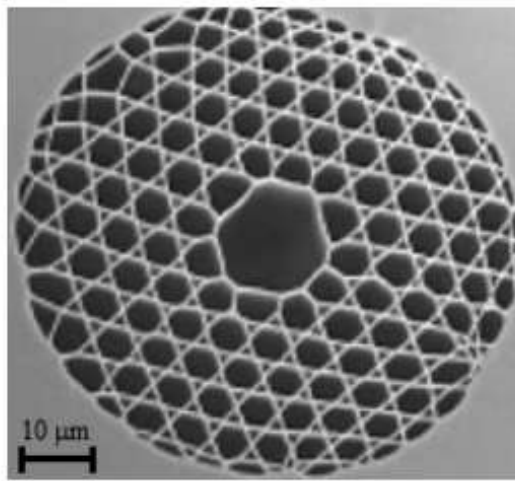


Fig. 1.3 Cross-section of Kagome PCF [28]

1.3.3 Kagome PCF

Another type of fiber known as Kagome fiber was presented in [28] shown in Fig. 1.3. The light guiding mechanism in this fibre is caused by anti-resonant effect. There is no host material in the core of the fiber region and more prone to damage compared to solid and porous core PCFs. The spectrum of this type of fiber is broader than hollow core fiber. In this type of fiber losses can be minimized by increasing core diameter [29]. It has prominent applications in light-matter interaction.

1.3.4 Porous Core Photonic Crystal Fibers

The porous core PCF is new type of PCF proposed for terahertz application in 2008 [25]. A typical porous core PCF has been shown in Fig. 1.4. The THz band ranges from 0.1 to 3 THz in the spectrum. In this fiber, the researchers have introduced sub-wavelength tiny air hole in the fiber core to the transverse direction of the core. Due to the tiny air hole in the solid core, the core of the fiber is become porous. The term porosity

has introduced in the fiber. This is term says about the ratio of total solid area and air hole area of the PCF. If the porosity of the core increased, then the amount of material decreases in the porous core which unique feature of the porous core fiber. If this unique geometric parameter is tuned properly than loss of the fiber due to material absorption can be optimized significantly. The porosity of the fiber can be shown as below.

$$\text{Porosity} = \frac{\text{Area of air holes}}{\text{Total core area}}$$

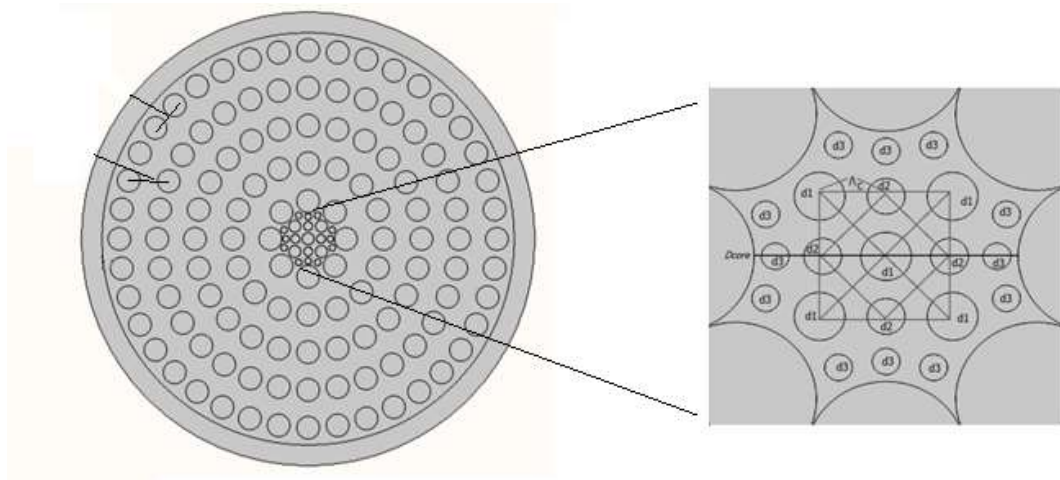


Fig. 1.4 Cross section of porous core fiber

There is significant amount of host material exists in the porous core provides structural strength to the whole fiber during the installation process which a draw back for the hollow and Kagome PCF. There is enormous design scope to optimize geometric parameter of the porous core PCF to achieve better performance. The performance in terms of physical phenomenon are endless single mode condition and minimizing host material loss. This type of fiber also enable large bandwidth along with design flexibly [30] compared to solid and hollow core fibres. As there is refractive index difference between core and cladding it follows index guiding mechanism [25].

Due to the above advantages, scope and applications the author has chosen this porous core PCF for this thesis. More details on porous core PCF will be discussed in chapter 2 in background studies.

1.4 Properties of Porous Core PCF

The behavior of porous core PCF relies on two important properties, one is the intrinsic properties of the host material and the other is geometric structure of the porous core PCF. The first one cannot change for the specific background material. On the other hand, geometric structure can be changed to manage or configure. PCF properties.

The traditional fiber delivers partial improvement to the known features compared with porous fibers. PC-PCF has sole properties that could not be attained by traditional fiber optics. This boundless flexibility in handling light guiding phenomena is because of dispersion characteristics carried by effective refractive index of the cladding structure [31]. The dispersion is altered further efficiently, and several geometric structures have established a better freedom of control. This purpose united with the modal field diameter guides to improvement in long distance THz communication.

Numerous PCFs designs are anticipated and made-up with exceptional optical characteristics for various fields. To mention few of these structures and their implementation: Majority of the structure exhibits endlessly single mode behavior [32] as well as allows lower and flatten dispersion [33]; to introduce asymmetry of the fiber and having high birefringence [34].

In this thesis, novel geometric structures of PC- PCF are proposed. It is based on decagonal, octagonal, hexagonal, and circular PC-PCFs in the cladding region. In this work, above mentioned geometries were enhanced in the simulated structures. The outcomes are presented in next section.

1.5 THz Waveguide Characterization

The analysis of loss and dispersion features belongs to THz characterization [1]. This THz characterization should be function of frequency or wavelength. The alternate orientations of THz source, detectors, lens and other THz components is adopted for the characterization THz system. The THz system is presents in Fig. 1.5. Generally, the PC antennas and nonlinear crystals are used as a source of THz signal. The polymer lenses, parabolic mirrors and THz waveguide together from Fig. 1.5 of option A and B is using to manipulate the generated THz pulse. To acquire smaller spot size at the front part of the waveguide, the polymer lenses are employed at the interface. As a result, there is

higher coupling ratio in the THz waveguide [5]. From the same Fig., option C depicts the alternative way of the placement of the THz source. For example, in [35] the authors have adopted option A. In [36-38], the researchers have taken option B. The option C was adopted to sending signal in the THz waveguide [39-41].

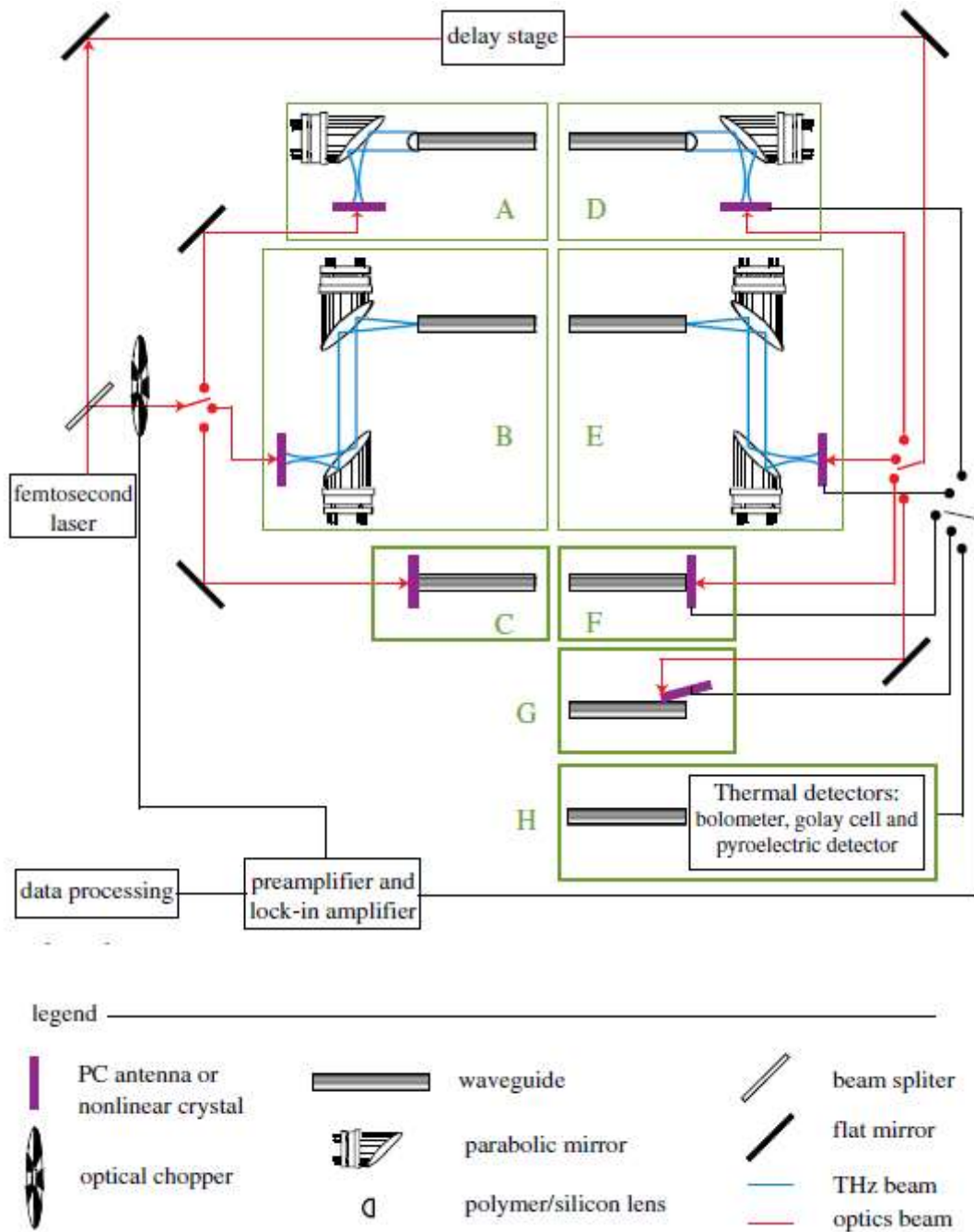


Fig. 1.5: THz Characterization [1]

In the similar way, the orientation used to couple THz signal into the waveguide, coupling out of THz signal from the medium shown (D to F) in the Fig. 1.5. The progress of the photoconductive exploration [42, 43] forwarded the THz imaging. This exploration also helps to examine the THz signal through the corresponding medium [43]. From Fig. 1.5, the path G is best fitted for the THz medium which have additional power at the exterior part where the probe-tips might be placed [44, 45].

The choice D have been adopted in [46, 47] whereas the choice E has been taken into considerations in [39, 48, 40] for sending THz signal into the medium from Fig. 1.5. From the similar Fig., the choice G has been utilized in [40, 41]. The photoconductive detector employs coherent detection techniques used in choice D to G for the measurement of THz signals. Employing this technique, the effective absorption loss and effective refractive index profile can be explored as a function of operating frequency.

As it has been mentioned in section 1.2, the bolometer falls in thermal detector category can be adopted to explore the intensity of the THz wave. Also, from the intensity of THz wave, the absorption loss of the travelling fields can be investigated as a function of wavelength or frequency. For pairing THz signal into the waveguide, the thermal detection techniques (choice H in Fig. 1.5) incorporated in [36,38,49]. Any amalgamation of choices A to C and choices D to H in Fig. 1.13 can be adopted for the characterization of THz waveguides.

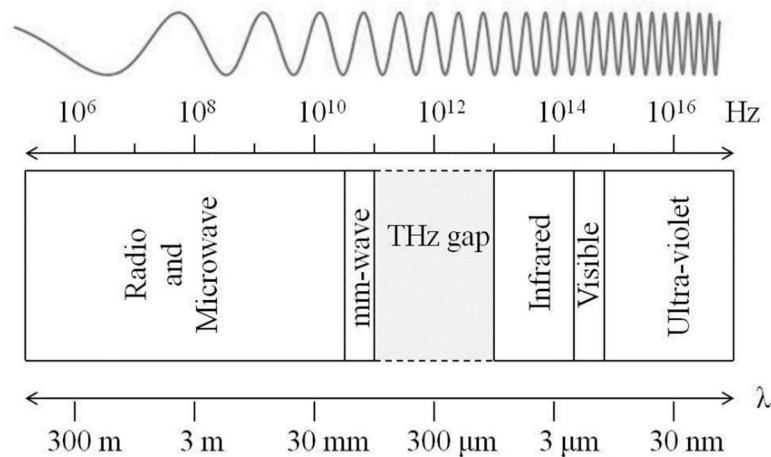


Fig. 1.6 THz Spectrum [50]

1.6 THz Applications

As mentioned earlier, investigators have attentive on a unique sort of frequency spectrum known as terahertz spectrum (0.1-10) THz shown in Fig. 1.6. This unique narrow-band has many prospective usage such as pain-free medical diagnostics, tomography, defence, broadcast/CATV/Cable Television, concealed object recognition, mechanical or industrial, astronomy, and much more [50] In the recent years, considerable advancement has been performed in developing THz waveguides, except majority of current THz structures are uncomfortably bulky along with rely strongly on free space radiation. There are transmission losses in the transmission waveguides due to limitations such as transmitter and receiver misalignment, bulk material absorption loss because of the environmental situation of surrounding area, etc. Therefore, improvement is needed for transmission of long-haul broadband THz waves. Air is used for THz wave transmission at the early stage due to air is clear for THz wave and does not absorb energy. Countless issues arise, like issues linked to transmitter and receiver placement, unexpected loss of absorption affected by the environmental situation of the environment when using unguided medium [50]. To fix these issues different directed media, suppose a metallic waveguide, metal-coated dielectric pipes, Bragg bandgap fibres, polymer photonic band-gap materials are used, but they also show high absorption.

More details of THz waveguides and related literatures have been presented in the chapter 2. In next section, the characteristic parameter of dielectric waveguide will be discussed.

1.7 Performance parameters for THz Waveguide

The dominant waveguide properties which effect the performance of THz waveguides are attenuation, dispersion and non-linearity. The THz signal vanishes as it propagates through the fiber core material [51] causes attenuation. As THz signal travels through the medium the signal spreads this is known as dispersion. For long haul communications, low or zero dispersion is expected [51]. These waveguide loss properties are manageable in porous core PCF than in traditional fiber optics due to the different geometric structure parameter can be optimized to achieve anticipated performance [20]. So, it is essential characteristic to know these characteristics and their

influence, and how they can be managed to have best outcomes. In following subsections, performance parameters will be discussed.

Material Absorption Loss:

Every waveguide material has bulk material loss. Bulk material absorption loss means the loss occurred due to the optical power absorption by the solid material which is quite high in THz range. Material absorption loss is reduced by replacing the solid core with porous core. The effective material loss found in the porous core PCF is define by the below expression [52]

$$\alpha_{\text{eff}} = \sqrt{\frac{\epsilon_0}{\mu_0}} \left(\frac{\int_{\text{mat}} n_{\text{mat}} |E|^2 \alpha_{\text{mat}} dA}{2 \left| \int_{\text{all}} S_z dA \right|} \right) \quad (1.1)$$

Where, ϵ_0 and μ_0 are the relative permittivity and permeability in vacuum respectively, α_{mat} signifies the bulk material absorption loss, n_{mat} denotes the refractive index of material, \mathbf{E} denotes electric field and S_z is the $\hat{\mathbf{z}}$ component of the poynting vector ($S_z = \frac{1}{2}(\mathbf{E} \times \mathbf{H}) \cdot \hat{\mathbf{z}}$), where \mathbf{E} and \mathbf{H} are the electric and magnetic fields respectively. Derivation of above equation has been shown in Appendix B.

Another important term related to material absorption loss is total power propagation inside the core. The amount of power transmits into various areas of fiber is called power fraction of the fibers. Different regions include core air rings, cladding air rings and core background material. The sum of transmitted power through along the length of the fiber above three regions must be equal to the total power. The power flow distribution of different regions can be expressed by the equation [52],

$$\eta' = \frac{\int_X S_z dA}{\int_{\text{all}} S_z dA} \quad (1.2)$$

Where, η' represents mode power fraction (PF) and X represents the area covered by air holes. Derivation of above equation has been shown in Appendix A.

Confinement loss

Finite number of cladding air holes is the only reason of confinement loss (CL). Some of the guided mode breaches through the cladding area due the CL. Index-guiding PCFs follow the same mechanism TIR as the conventional fibers. As in PCFs, the refractive index of the core and the cladding are same except that there are a finite number of air

holes in the cladding. The CL can find from imaginary part of the complex refractive index given by [53],

$$L_C = 8.686 \left(\frac{2\pi f}{c} \right) \text{Im}(n_{eff}) \text{ (dB/cm)} \quad (1.3)$$

Here, f denotes frequency, c light speed through air and $\text{Im}(n_{eff})$ represents the imaginary portion of the complex refractive index.

Dispersion of Single Mode Fiber

The light pulse in the fiber optic is not monochromatic as result pulse broadening occurs as it travels through the material known as dispersion. In other words, this is because of alternation of group velocity for a specific mode as index of refraction of the material has found frequency dependency. The dispersion for single mode fiber can be calculated from effective refractive index (n_{eff}) of the fundamental guided mode of fiber optics. The relation is given by [53].

$$\beta_2 = \frac{2}{c} \frac{dn_{eff}}{d\omega} + \frac{\omega}{c} \frac{d^2 n_{eff}}{d\omega^2} \quad (1.4)$$

Where $\omega = 2\pi f c$ and c is light speed.

V- Parameter

The electric or magnetic field distributed in transverse direction is called mode of the fiber. In different frequencies electromagnetic wave may have identical modes. In a dielectric medium mode states in which manner electromagnetic wave propagates in the waveguide core and it is related to dimension less parameter V in equation 1.5 [54].

$$V = \frac{2\pi a}{\lambda} \sqrt{n_1^2 - n_2^2} \leq 2.405 \quad (1.5)$$

Where a is the radius of the fiber core and λ is the wavelength of the light. To satisfy single mode condition V parameter must be less than equal 2.405. The number of modes propagates through the core can be seen from below Fig. 1.5. Where LP_{01} mode is the fundamental mode.

The above equation is suitable for classical waveguide [54]. For porous core PCF the classical equation of V- parameter can be modified for single mode condition is given below as V_{PCF} [55],

$$V_{PCF} = \frac{2\pi}{\lambda} \Lambda \sqrt{n_1^2 - n_2^2} < \pi \quad (1.6)$$

Where Λ is the air-hole pitch. n_1 and n_2 are core and cladding refractive indices respectively.

Both classical and modified equations of V-parameter have been presented above. For this research work, the classical equation (1.5) has been adopted for numerical investigations [68, 69, 71-74].

Birefringence

In optical waveguide mode propagation, there is two type of guided mode can be seen. One is core guided mode having effective refractive index (n_{eff}) and another is cladding guided mode. If n_1 and n_2 are refractive index of core and cladding respectively then n_{eff} range between $n_2 < n_{eff} < n_1$. The relation among propagation constant, β and k_0 the wave number k_0 and effective refractive index shown in equation 1.7 [56].

$$n_{eff} = \frac{\beta}{k_0} \quad (1.7)$$

When the light propagates through the core of the fiber then degeneracy of fundamental mode may arise due to symmetry of the fiber is altered intentionally, accidentally, or by external stresses. The refractive index differences between two degenerate mode can be expressed as Birefringence (BR) in equation 1.8 [56].

$$BR = \left| n_{eff}^x - n_{eff}^y \right| \quad (1.8)$$

Where n_{eff}^x and n_{eff}^y are the refractive indices of the two degenerated modes. It has application in slotted core, elliptical core and where it is necessary to break symmetry of fiber core.

1.8 Fabrication Methods of PC-PCF

There are several methods for fabrication of PC-PCF which were established to fit the changes in the material characteristics. Hence, proper information of the materials characteristics is essential for selecting the suitable fabrication method. The fabrication

method of PC-PCF includes two phases; preparing a preform that covers the geometric shape on a macroscopic level and drawing the preform to extend to PC-PCF size.

The second phase, sketch of the fiber which does not vary because the identical process, with few variations in parameters that govern the sketch method such that heat temperature, speed and pressure inside PC-PCF air holes to maintain their shape and does not breakdown. Few popular methods of fabrication will be presented next.

The fabrication procedure is vital part in designing and developing novel kind of PC-PCFs. Traditional fibers optics fabricated using silica has been precisely examined, since most traditional fibers optics are created from glued silica [57]. In the fabrication procedure of PC-PCF, a preform requires to be ready primarily. Generally, the greatest exciting phase in the development of fabrication is the preform phase. The Stack and Draw technique were established and presented from the tube stacking method [57]. Because of the increasing investigation in PC-PCF fabrication there are novel designs with complex air-hole arrangement in the porous core which needs different methods of fabrication such extrusion [58], sol-gel method [59] and 3D printing [60] which is a capable technique for complex PC-PCF geometric structures.

In this thesis, there are four proposed PC-PCF design. Along with each proposed design, the author has proposed suitable fabrication method considering the shape of the geometric structure.

1.9 Background Materials for Fabrication of PCF

Polymer materials can yield significant benefit over silica glass. The benefits are lower manufacturing cost, mechanical strength and chemical elasticity [61]. The new polymers offer low loss compared to silica glass and applications can be found in different areas like in THz propagation [62], bio-sensing [63] and optical-imaging. In next, the author will discuss various background material for proposed porous core PCFs.

PMMA

Polymethylmethacrylate (PMMA) is a clear thermoplastic [61] has lightweight, shatter-resistant properties. PMMA has made from synthetic polymer of the organic compound methyl methacrylate (MMA). It is found as an economical substitute to polycarbonate when much more strength is not essentially a rigorous requirement for the

given application. The pure PMMA is brittle, cannot tolerate toughness as well as prone to scratches.

Teflon

Polytetrafluoroethylene (PTFE) it is a synthetic polymer known as teflon. The constituting atoms of Teflon is carbon and fluorine. It has some advantages like higher chemical resistances. The disadvantages are radiation resistance is lower, melting during the fabrication not possible and is costly than other polymers [61].

Topas

Topas is new type of copolymer having lots of advantages over Teflon and PMMA. This generally used in PC-PCFs fiber design [25] in terahertz spectrum. It has constant refractive index profile $n=1.53$ in the THz regime. At 1 terahertz, it has lower bulk material absorption loss 0.2 per centimeter [30]. It also has high chemical and temperature tolerance. It has another property that it does not absorb water vapor. These properties make it suitable for low loss THz long distance communication.

Zeonex

Zeonex [64], a Cyclo Olefin Polymer (COP), is the latest addition in polymer group. Zeonex has several unique qualities including low water absorption, low content of impurities, high heat resistance, low dielectric constant and loss tangent. Moreover, it has low specific gravity, excellent chemical resistance capacity at elevated temperature, high transparency and low absorption loss. Its constant refractive index (1.535) over a wide terahertz frequency band causes negligible material dispersion.

Terahertz PCF has been constructed using various background materials such as PMMA, TOPAS, Teflon, ZEONEX, etc. In most recent designs TOPAS was chosen as the background material over the rest because absorption loss is less than both PMMA and Teflon and a higher glass transition temperature than ZEONEX [64]. Besides there are other advantages of TOPAS [65]: (i) facilitates multi-antibody bio-sensing, (ii) greater refractive index which improves confinement, (iii) comparatively high glass transition temperature, (iv) steady refractive index between 0.1 and 1.5 THz frequency, (v) humidity unaffected and (vi) superb biocompatibility. Furthermore, lots of research

reports has already been reported on topas compare to newer material zeonex. So, topas has been considered as host material for the research work.

1.10 Motivation

Due to the enormous attractiveness, THz wave propagation and detection have been thrived auspiciously in last few years. However, free space propagation is preferred for existing THz systems as all the existing materials for guiding the THz waves are extremely absorbent in this frequency band. Although air in the free space is considered to be non-absorbent, the existing oxygen and water vapor in the air absorb the terahertz signals. Therefore, attention was shifted towards the improvement of various types of terahertz waveguides. A lot of papers on terahertz using several background materials such as Polymethyl Methacrylate (PMMA), High density polyethylene (HDPE), Topas, Teflon, silicon etc. have been proposed so far. However, topas has several favorable characteristics over other dielectric materials such as lower content of impurities, higher heat resistance, lower dielectric constant and loss tangent. Moreover, it has lower specific gravity, higher chemical resistance at elevated temperature, higher transparency etc. Furthermore, lower melt flow index of Topas is very suitable for high quality fiber fabrication compared to other polymer dielectric materials. Also, fluctuations in the fiber diameter are reduced because of the greater stability of fabrication process. This material allows more degrees of freedom in fiber design. In addition, it offers a wide range of drawing stress which makes the fabrication much easier. Hence, there is still a great scope to improve the various modal characteristics of porous core THz fibers using topas as the only host material.

1.11 Objectives with Specific Aims

The objectives of this thesis are:

- i. To design topas based porous core photonic crystal fiber (PC-PCF) with low effective material absorption loss for the better wave guidance in THz regime.
- ii. To design high birefringence PC-PCF to maintain polarization state of the PC-PCF.
- iii. To full fill the objective of the research, the computational simulation will be utilized to obtain various desirable modal characteristics of the proposed fibers.

The possible outcome is a novel topas based waveguide with lower EML and much higher core power fraction and that can be used in THz communications, polarization preserving applications such as sensing and optical coherent communications etc.

1.12 Outline of Methodology

The THz band experiences inevitable loss in metallic wave guide and wireless medium respectively. So, the material can be changed and tailored such way to minimize this inevitable material loss. The author would propose PC-PCFs design that will operate in THz band.

The proposed design will be carried out using COMSOL Multiphysics Software (FEM solver package). The guiding properties and parameters will be evaluated using Finite Element Method in COMSOL Multiphysics for the proposed design. Different steps for this procedure are as follows.

- i. At first, we will design a PC-PCF to meet our objectives.
- ii. Different guiding properties of the PC-PCF will be numerically evaluated by tuning geometrical parameters using Finite Element Method. Perfectly Match Layer (PML) will be applied.
- iii. Simulations will be performed in order to get desired parameters such as effective mode index, confinement loss, effective material loss, dispersion birefringence, and core power fraction.
- iv. The same parameters will be reevaluated for different porosities and core diameters.

Finally, after simulating the complete system, the system performance will be obtained and graphically displayed using MATLAB where necessary and an overall evaluation will be carried out.

1.13 Thesis Organizations

Chapter 1 describes brief introduction of THz spectrum; THz sources and detectors has been described. THz characterization of THz also presented. The key modal features of THz waveguide that effect waveguide structure performance such as attenuation and

dispersion are presented. The various types of host materials also discussed in this chapter along with the fabrication scopes.

In chapter 2, explained the previous works done on the topic. The study and understanding of the fiber optics need physical, mathematical and numerical investigations. The finite element method is used for the numerical investigations described in chapter 3.

The decagonal cladding and hexagonal core structured PCF proposed in this chapter along with design methodology. Also, detailed numerical investigation has been presented in chapter 4. In the same way, octagonal cladding and hexagonal core structure proposed in chapter 5. In chapter 6, Octagonal cladding and hybrid core has been proposed. Circular cladding and circular core have been proposed in chapter 7. Finally, in chapter 8 conclusion and further work scope has been discussed.

CHAPTER 2

BACKGROUND STUDIES

Based on the aim and objective of the research works, the background studies have been done. The author has presented related research paper and their crucial performance parameters in this chapter like effective material losses and core power fractions.

2.1 Background Studies

Optical fiber is a wired transmission medium that is more flexible and authentic than the atmosphere [66]. Optical fibers are till today the transmission medium for long distance communication. Furthermore, low loss optical fibre transmission has trapped to the massive achievement in communication technology. Optical-fiber systems have many advantages [67] such as high bandwidth, immune to electromagnetic interference, signal security, light weight, low transmission loss and many more. To get better guiding properties numerous designs are being made to core-cladding structure regarding shape such as hexagonal, circular, hybrid, octagonal, star, decagonal, diamond porous, Kagome structure, square, rectangular slotted, hexagonal slotted, vertical array, horizontal array, elliptical, spiral and many more. Structural features such as EML, confinement loss, birefringence, dispersion, V-parameter, core power fraction varies for each design and is observed meticulously. Parameters like core diameter, frequency, porosity, pitch value, air hole diameter and PML are varied to observe the overall changes of losses in an optical fiber. In most of the recent researches, the operating frequency is taken 1 THz. So far, there is few numbers of THz theoretical and practical structures have been reported by the investigators for reducing the EML.

In 2013, the authors [68] have suggested a porous-core octagonal photonic crystal fiber [68] where EML was found to be 0.07 cm^{-1} . In 2015, they have also presented a porous core fiber [69] displaying an EML of 0.066 cm^{-1} . In 2016, [70] has presented a porous core structure obtained an EML of 0.028 cm^{-1} . In [71] the authors have introduced a porous-core circular photonic crystal fiber where an EML of 0.043 cm^{-1} was reported in 2016. Later that year, they introduced an optical fiber where inside the core there were rectangular slotted air holes giving an EML of about 0.08 cm^{-1} [72]. In 2017, authors have proposed [73] a slotted cladding with slotted core where a very low EML between

0.0103 cm^{-1} and 0.0145 cm^{-1} were reported. The structure also exhibited dispersion of 0.5 ps/THz/cm. In 2018, the authors have also presented [65] a PCF deploying TOPAS as host material, containing only rectangular slots. The fiber confirmed a minimum EML of 0.009 to 0.01 cm^{-1} within the frequency span of 0.77–1.05 THz. So, it can be said that there is still scoped to minimize the EML and flatten the dispersion characteristics in the communication technology of terahertz with the advancement of time.

In this section, it has been discussed about different core-cladding designs from 2013 to 2018 as well as different structural properties that are related to optical fiber transmission like EML, confinement loss, birefringence, V-parameter and dispersion. Also, it has been shown and compared among different designs according to their respective core-cladding structures and delineated each of the design.

All the optical fiber designs listed in this section are considered in terms of the structural design parameters and properties. The parameters are varied to get the best possible transmission features of a fiber optics and least amount of losses. These parameters can be porosity, D_{core} and frequency. From the cross-sectional view of the designs, the core and/or cladding can be categorized into hexagonal, octagonal, decagonal, circular, and hybrid. Since our designs are based on hexagonal, circular and hybrid cores and decagonal, octagonal and circular cladding, these variations are explained below.

2.2 Hexagonal Core

Based on hexagonal cladding, the core designs are categorized according to hexagonal (symmetric/ asymmetric), hollow, circular, hybrid, array, penta hole elliptical, hexagonal slotted, rectangular slots, rhombic, octagonal and diamond.

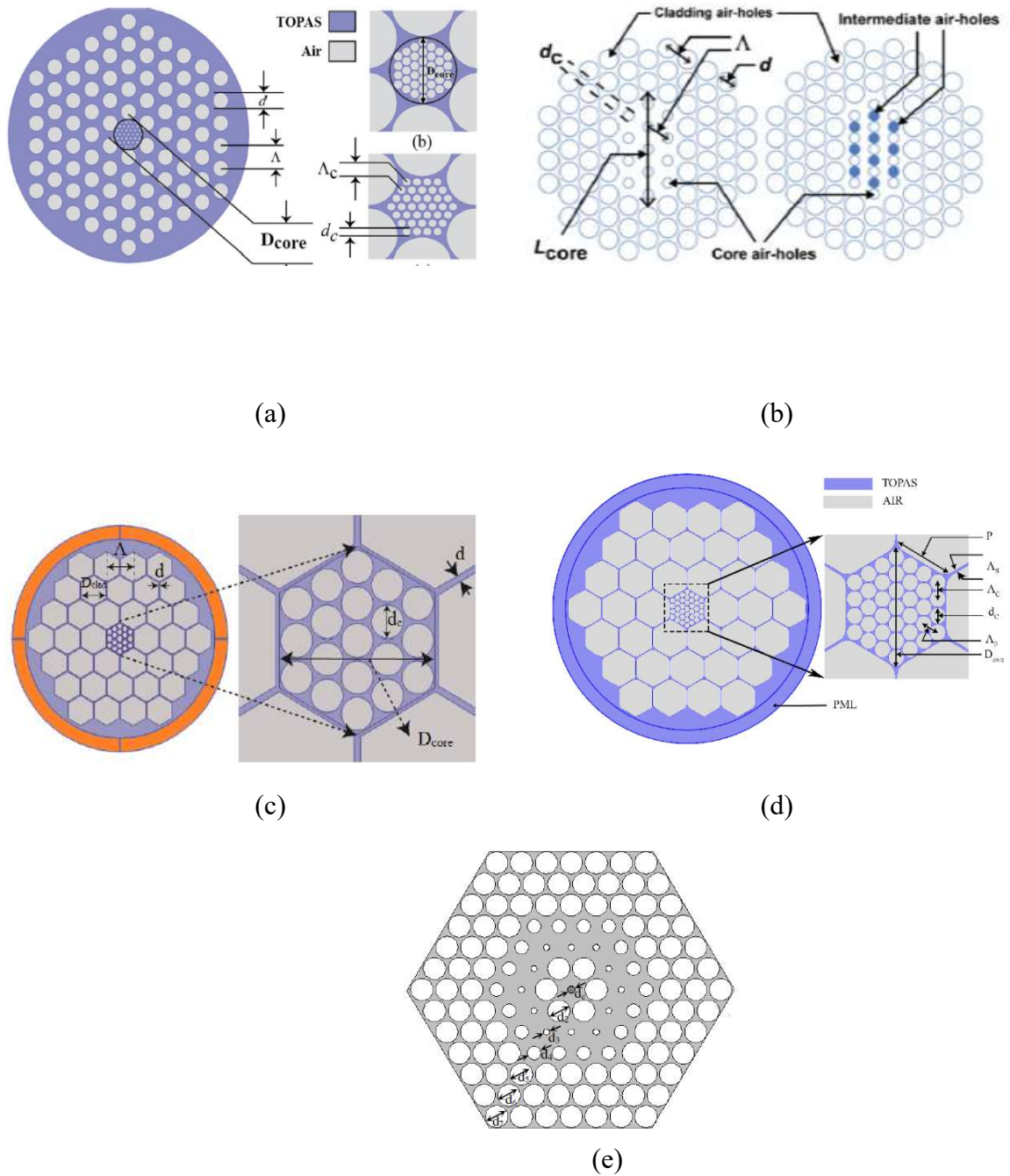


Fig. 2.1 Cross-sectional view of (a) rotated hexagonal porous core hexagonal PCF, (b) PCF is anti-symmetric inside core and cladding, (c) PCF having hexagonal air holes inside the dense cladding area encircled by circular air holes and a PML in the core, (d) dispersion flattened porous-core honeycomb lattice, (e) dual-core microstructured optical fiber design.

In 2015 [69], the author have proposed a low-loss PC-PCF hexagonal single-mode fiber, shown in Fig. 2.1(a), in the THz regime. In their literature, within a frequency span of 0.5–1.08 THz, a dispersion of 1.06 ± 0.12 ps/THz/cm was noted ,what is more, a very low EML (0.066 cm^{-1}) and low confinement loss ($4.73 \times 10^{-4} \text{ cm}^{-1}$) at the operational frequency $f = 1$ THz had attained. At 60% porosity, single mode operation was affirmed when the core diameter was less than $390 \text{ }\mu\text{m}$ and frequency less than 1.3 THz. It was also noted when frequency, $f = 1$ THz, 60% porosity and core diameter $300 \text{ }\mu\text{m}$, power fraction obtained was 47% whereas EML was only 38% of the bulk material absorption loss (0.066 cm^{-1}). The structure can be fabricated straightforwardly utilizing the stack and draw method [69]. A porous core photonic fiber in Fig. 2.1 (c) having large hexagonal air holes in the cladding region and a porous core including smaller circular air holes, was presented by Shekh Farhad Uddin Ahmed et al. where an EML of $\sim 0.028 \text{ cm}^{-1}$ was achieved at the operating frequency, f , of 1 THz. Furthermore, the confinement loss of about 0.0005 cm^{-1} was reached at 1 THz, which was small compared to 0.196 ± 0.183 ps/THz/cm flat dispersion profile. The ideal value for core diameter was taken as $450 \text{ }\mu\text{m}$ where the fraction of power in air-holes of core gets above 50% and was suitable for long distance THz wave transmission [70]. Md. Shariful Islam et al. in 2017, suggested the design of a porous-core honeycomb lattice photonic crystal fiber (PH-PCF) with a very low loss and flattened dispersion for guiding terahertz (THz) wave. The design contained three cladding rings of large hexagonal air holes, shown in Fig. 2.1(d). The circular air holes were suitably housed within the hexagonal core to offer the required porosity and at high porosities brilliant confinement was observed. Bulk material absorption loss of TOPAS was decreased by 88.87% using the layout suggested. EML was as small as 0.02227 cm^{-1} , confinement loss of 8.4×10^{-4} at frequency 1 THz and dispersion achieved was 0.15 ps/THz/cm over frequency of 1.5 THz [74]. Raonaqul Islam et al. introduced an optical fiber, displayed in Fig. 2.1(b), having an asymmetry in both the porous core and cladding of the structure. The hexagonal lattice structure consisted of five rings of air holes. A birefringence of ~ 0.045 and EML of 0.08 cm^{-1} were found during the simulation for an operating frequency of 1 THz. For x-polarization mode dispersion achieved was 0.9 ± 0.26 ps/THz/cm and for y-polarization dispersion achieved was 0.98 ± 0.39 ps/THz/cm [75].

The authors have [76] suggested three models for chromatic dispersion compensation of microstructure optical fibers in Fig. 2.1(e). Dispersion of -3500 , -25000 , and -135000 ps/nm/km were achieved using FWHM of ~ 30 nm, ~ 6 nm, and ~ 2 nm, respectively. The designs included a center-core hole that was selectively filled with liquid or polymer to achieve very elevated negative dispersion; not only that, the filled central hole add an extra non-geometric controllability for the procedure to tune the maximum negative dispersion at ~ 1.55 μm . Very high negative dispersion could be achieved enabling the dispersion compensating fiber length to be reduced significantly.

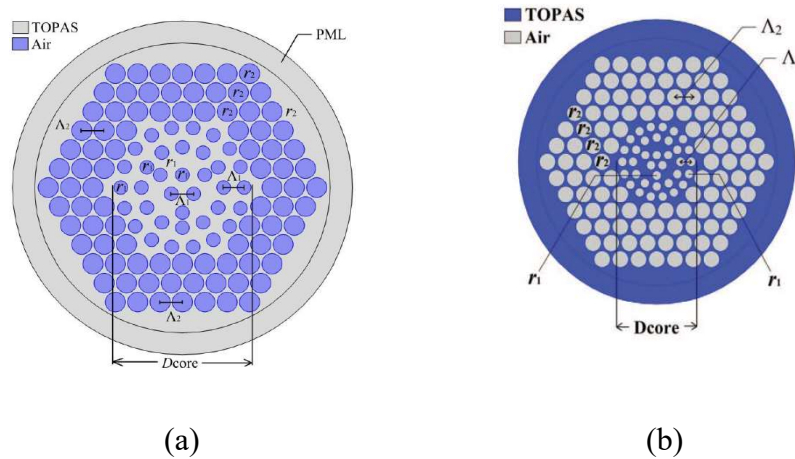


Fig. 2.2 Cross-sectional diagram of (a) hybrid porous core structure having triangular air hole arrangements, (b) PCF having hybrid air hole configuration inside core accompanied hexagonal cladding.

2.3 Hybrid Core

The authors have [77] delineated the effects of rotating the air-hole configuration of a hybrid porous core structure, shown in Fig. 2.2(a). To assess the effects on various waveguide characteristics, the triangular core was rotated in an anticlockwise direction (30° , 60° , 90°). The result showed a low flat change in EML of ± 0.000416 cm^{-1} from 1.5 to 5 terahertz (THz) range, dispersion of 0.4 ± 0.042 ps/THz/cm from 1.25 to 5.0 THz with core diameter 2450 μm and porosity 33.32%. At frequency 1 THz, the EML obtained was 0.1875 cm^{-1} . In the core area, the porous fiber showed a hybrid structure that involved circular rings with the central structure of a triangular air hole. In another work of same authors [77], they represented a PCF, shown in Fig. 2.2(b), having a hybrid air

hole preparation at the core region with hexagonal cladding. The simulation result showed a low EML of 0.425 dB/cm at 0.7 THz frequency with insignificant ($< 10^{-2} \text{ dB/cm}$) confinement loss and bending losses for the proposed porous fiber. Numerical results also showed a near-zero flat dispersion band of 0.46 THz at $0.9 \pm 0.05 \text{ ps / THz / cm}$ and an optimum porosity of 47% . The core diameter was taken $550 \mu\text{m}$ and PML was 13% .

2.4 Circular Core

The authors have [78] introduced a hexagonal cladding with a circular core in Fig. 2.3(a). The result showed an EML of 0.063 cm^{-1} at 1.0 THz , bending loss of $1.07 \times 10^{-11} \text{ cm}^{-1}$, confinement loss of $6.9 \times 10^{-3} \text{ cm}^{-1}$ and dispersion of $1.3 \pm 0.55 \text{ ps/THz/cm}$ between the frequency ranging from 0.7 to 1.2 THz . The core diameter taken was $300 \mu\text{m}$. Circular type core was selected in the core province because it offered circular polarization and a big amount of air holes could be implemented. Since EML decreases with the increase of core porosity for a specific value of core diameter, the proposed fiber offered the lowest EML of 0.057 cm^{-1} at core diameter of $200 \mu\text{m}$. However, since power fraction got lowered this was not taken as optimum value. Nearly 45% of the complete power travelled through the core air holes.

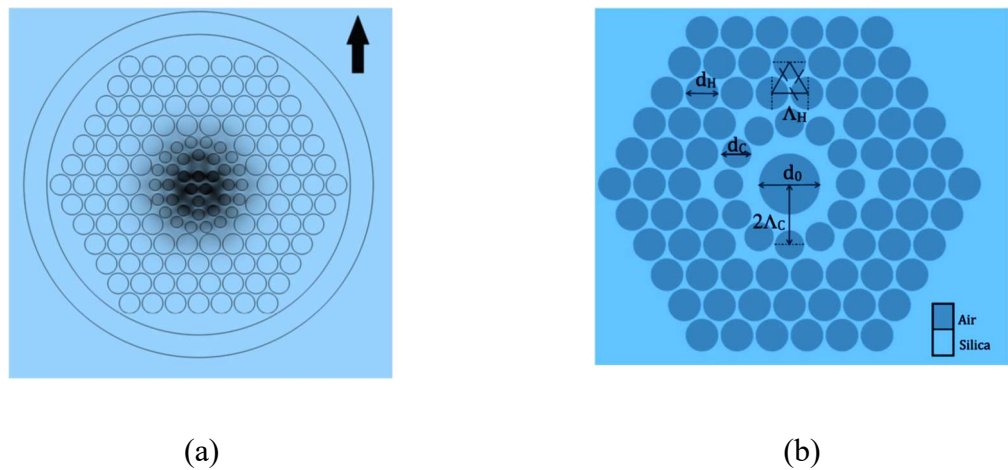


Fig. 2.3 Cross-sectional view of (a) porous core PCF, (b) ring-core PCF geometry.

In [79] the authors have proposed a novel ring-core photonic crystal fiber that supported four groups of orbital angular momentum modes accompanied 2.13×10^{-3}

minimum difference of effective refractive indices at 1550 nm. The acknowledged fiber, shown in Fig. 2.3(b), was foreseen to be an incredible transmission stage for OAM mode. The structure that was proposed was a mixture of hexagonal and circular symmetry cladding around a ring with an air hole. The first ring made it possible to achieve a close-to-circular symmetry favourable to the stability of OAM modes. The three extra rings, used to boost light confinement in the ring core, had a hexagonal symmetry, which was easier to manufacture. The first ring consisted of 12 air holes with diameter $d_C = 2.6 \mu\text{m}$ and $\Lambda_C = 2.7 \mu\text{m}$. The outer Hexagonal rings consisted of air holes with a diameter $d_H = 2.9 \mu\text{m}$ together with a pitch = $3.04 \mu\text{m}$. Confinement losses were all most non-existent across the entire wavelength span (from 1250 nm to 2000 nm); the biggest calculated value was about $2 \times 10^{-5} \text{ dB / km}$. The fiber guides 10 vector modes with an efficient index of $1.55\mu\text{m}$ which were very well separated.

2.5 Others (Hexagonal Slotted, Rectangular slotted, Rhombic, Octagonal, Diamond shaped, Elliptical cores)

In [80], the authors have launched an extremely birefringent PCF with nearly zero dispersion characteristics through the implementation of elliptical air holes in the core region. The core area in Fig. 2.4(a) , presenting asymmetry between x and y polarization modes, resulted in very large birefringence. Also, most of the valuable power are confined inside dense geometry of the traditionall hexagonal structure inside cladding. Output simulation showed a high birefringence of 0.086 and a dispersion of $0.53 \pm 0.07 \text{ ps/THz/cm}$ in a wide frequency range. The practical application of the suggested fiber is possible adaptingcurrent manufacturing methods.

The authors have introduced a slotted-core PCF [72] and were marked for polarization maintaining 1 THz wave guidance in Fig. 2.4(c). It had a hexagonal cladding structure with nine rectangular slots and five rings of air-holes in the core. The main elements of the structure were its ultra-high birefringence (0.08), small EML (0.08 cm^{-1}) and periodic hexagonal cladding that made the structure further convenient. In addition, an adequate quantity of mode power was transferred through the core resulting in a very small loss of leakage. Throughout the simulations, the slot width was varied while the slot lengths were kept fixed. Birefringence decreased when porosity was increased and

stayed almost continuous with regard to porosities above 35%. Because of the rectangular slots, it was not possible to make the proposed porous fiber by stacking or drilling mechanism.

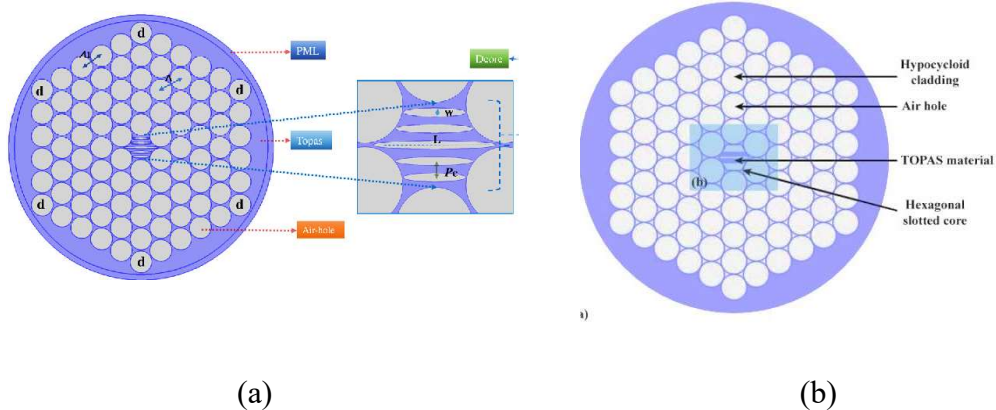
The authors have showed [81] that it was feasible to achieve very small bending losses of $3.04 \times 10^{-11} \text{ cm}^{-1}$ at optimum frequency of 1.0 THz by presenting a rhombic-shaped core composed of circular air holes within the standard hexagonal cladding which is shown in Fig. 2.4(e). In addition to that, negligible confinement loss of $1.17 \times 10^{-3} \text{ dB/cm}$ and low EML of 0.089 cm^{-1} were found for ideal design parameters. The numerically controllable drilling technique can be used to manufacture the suggested structure. Not only that the technique offered very smooth finishing with surface roughness being decreased.

In 2016, the authors [82] have investigated a novel PCF, having a diamond core structure, with high birefringence in the THz region. The suggested fiber, shown in Fig. 2.4(d) displayed a birefringence of 10^{-2} within 0.48-0.82 THz at optimum parameters and an EML of $\sim 0.07 \text{ cm}^{-1}$ for X and Y polarization modes respectively. The three significant characteristics of the diamond-core structure were its exceptional easiness, high-birefringence around ($\sim 0.34 \text{ THz}$) and negligible polarization reliant loss. The PC-PCF would have a notable role to the polarization that maintains THz transmission with adequate usage [83].

The authors [83] have delineated a diamond-core optical crystal fiber, shown in Fig. 2.4 (g). The hexagonal cladding consisted of square air holes and the diamond core consisted of circular air holes. The entire PCF was based on cyclic-olefin copolymer (COC), which is also known as TOPAS. It was also shown that the constructed PCF resulted in an ultra-high birefringence of the order 10^{-3} . Birefringence was an increasing function with an increase in the core air-filling proportion; increasing the air filling ratio resulted less confinement loss. The y-polarization direction of the effective refractive index was greater than the x-polarization direction of the effective refractive index because of the implementation of two large air holes, making it simpler to extend the x-polarization mode to the cladding.

In [84] the researchers have introduced a porous core photonic crystal fiber that had an octagonal core encircled in a hexagonal cladding, shown in Fig. 2.4 (f). EML achieved was 73.8 % lower than the loss of bulk material absorption at the working frequency of 1.0 THz. Additionally, confinement loss of $7.53 \times 10^{-5} \text{ cm}^{-1}$ and dispersion of $1.0823 \pm 0.06 \text{ ps/THz/cm}$ within 0.7–1 THz were achieved using design parameters that were selected. The lowest EML of approximately 0.03 cm^{-1} was achieved at $200 \mu\text{m}$ and 63 % porosity, while the largest EML of approximately 0.085 cm^{-1} was achieved at $400 \mu\text{m}$ and 50% porosity.

The authors in [85] have proposed a hexagonal slotted porous core lattice tube cladding photonic crystal fiber to get a very large birefringence and a very small loss of transmission at the same time. The suggested SPC-TLC-PCF, which is shown in Fig. 2.6(b), provided a birefringence of 9.06×10^{-1} and an effective material loss of 0.047 cm^{-1} at the frequency of 1 THz. The main distinctive characteristic of the suggested design was steady birefringence over a broad frequency region. The fiber worked solely in fundamental mode and displayed a little favourable dispersion of less than 1.6 ps/THz/cm over a band of 250 GHz (0.85 THz to 1.1 THz). In addition, bending loss was about $1.6 \times 10^{-7} \text{ cm}^{-1}$ at 1 THz, and confinement loss was also reasonably low. These favourable characteristics endorse this very helpful SPC-TLC-PCF for polarization maintaining as well as sensing applications in the THz system. The suggested design is comparatively easier accompanied by two-size circular air holes, that predicts that fiber manufacturing is possible when using verified methods.



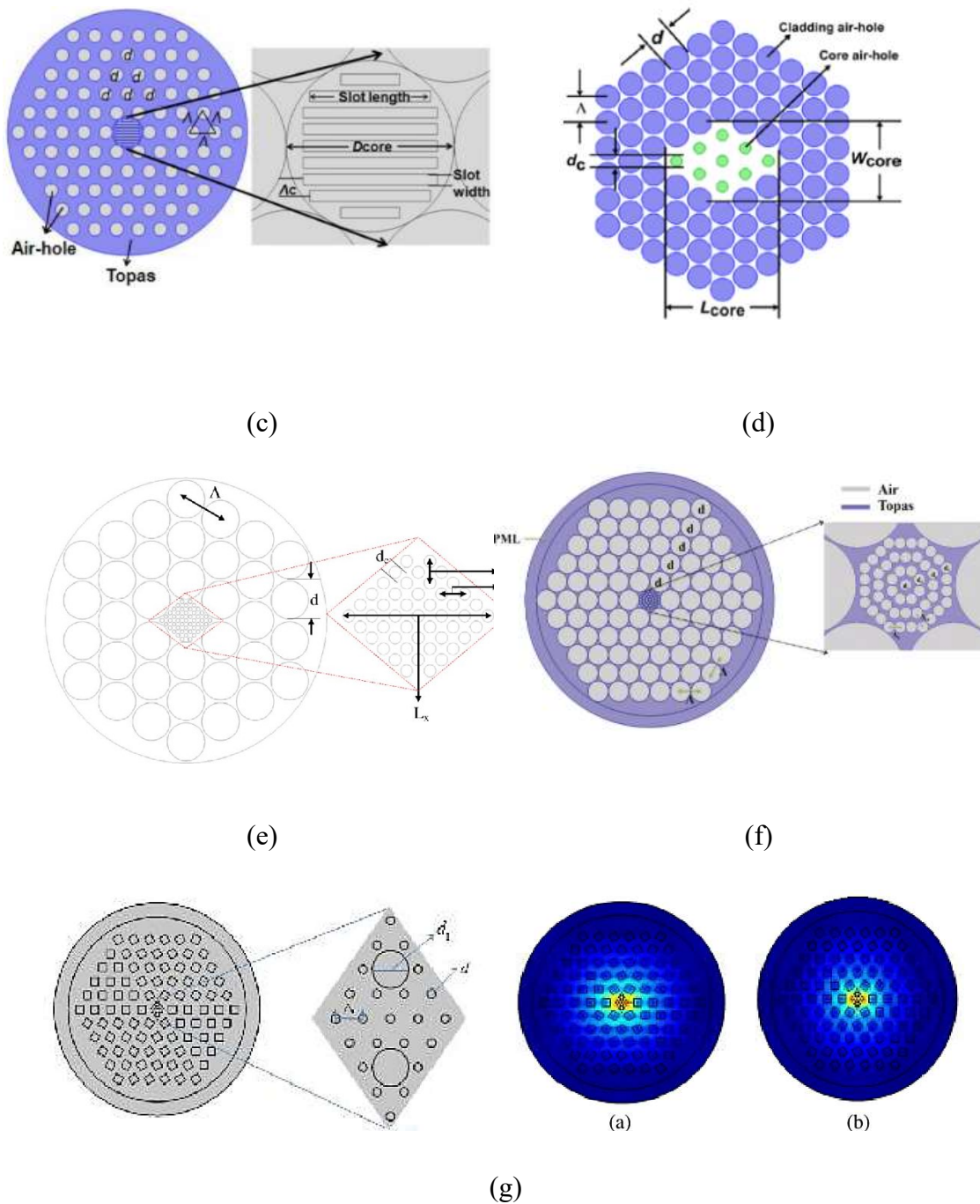


Fig. 2.4 Cross-sectional view of (a) Topas based PCF having of a conventional hexagonal cladding and a penta-hole elliptical structure in the core, (b) slotted porous core fiber, (c) slotted-core PCF having a hexagonal cladding., (d) diamond-core porous fiber, (e) rhombic-shaped porous-core PCF(f) PC-PCF comprising of a regular octagonal core, (g) COC based diamond-core PCF.

2.7 Octagonal cladding

The authors in reference [89, 90, and 68] have proposed octagonal cladding base PCFs. They have reported some important modal parameters like confinement loss (CL), EML, dispersions and core power fractions. Among these designs (in Fig. 2.6) reference [68] operates in THz regime (1 to 10 THz). In the design they only reported EML of 0.07 cm^{-1} using topas as background material. In [89] the authors have proposed silicon based octagonal claddings with hollow core and the design operates around 215THz. They have reported only CL of 10^{-5} cm^{-1} . The authors have presented dispersion property of the silicon base PCF in reference [90]. They have reported dispersion 11.3 ps / nm.km and CL of 0.45 cm^{-1} at operating frequency near about 217 THz.

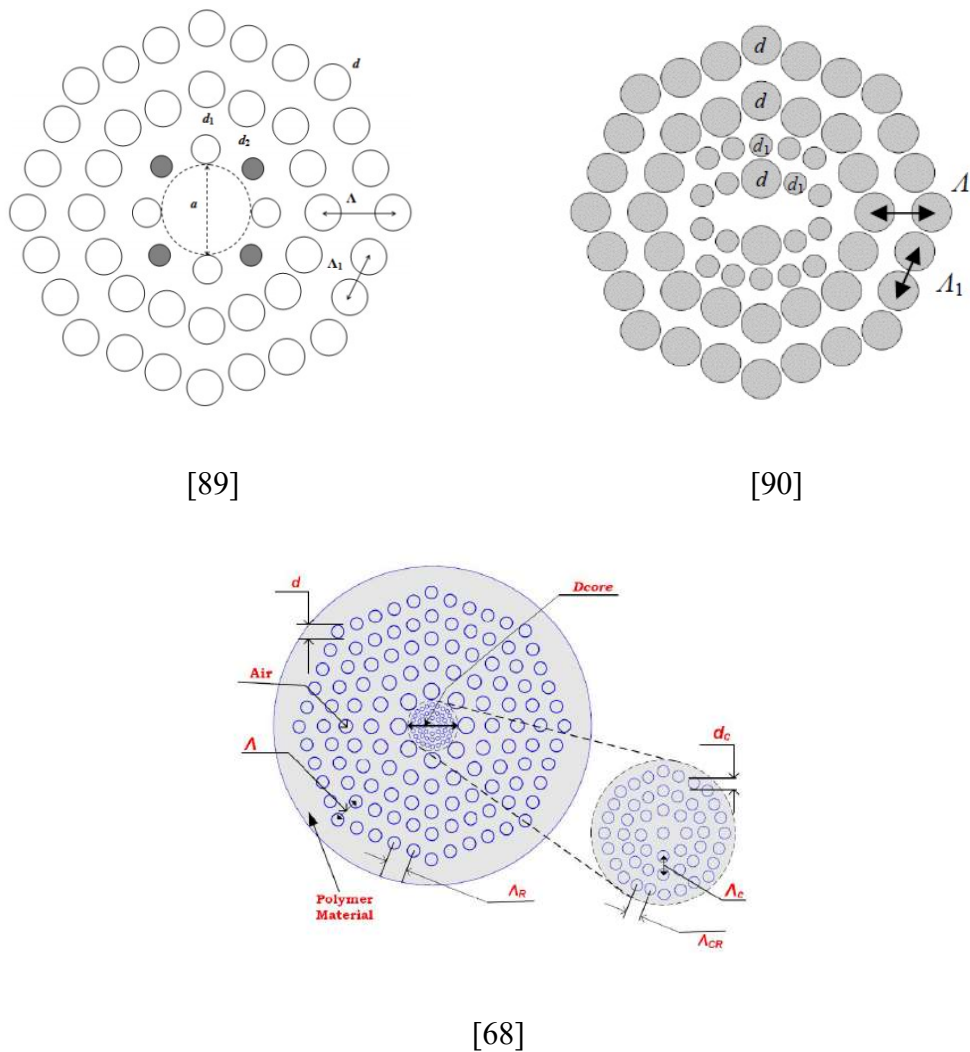
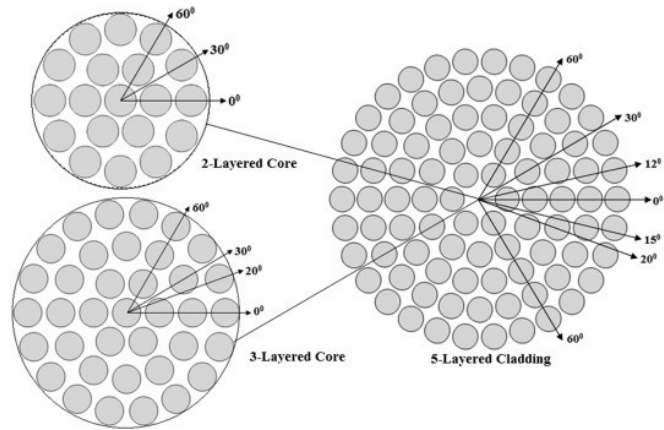
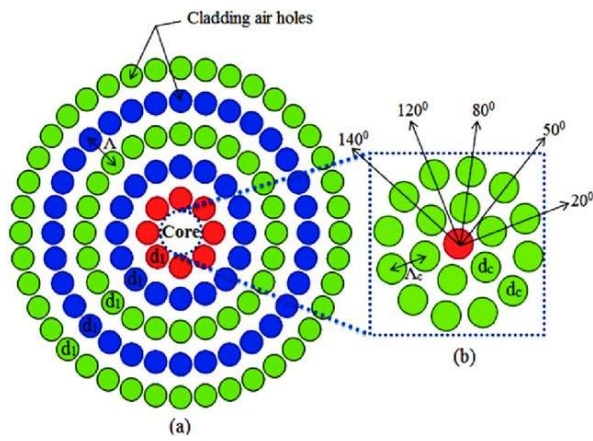


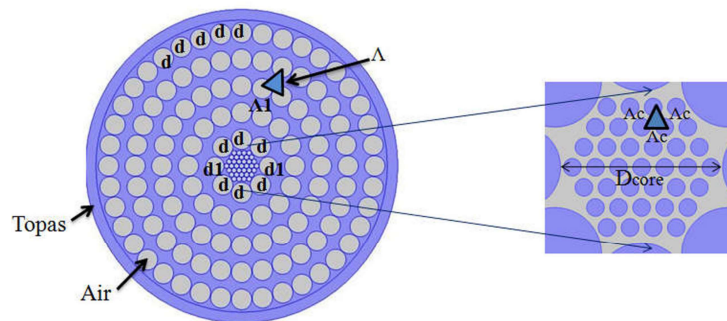
Fig. 2.6 Cross sectional view of Octagonal PCFs



[86]



[87]



[71]

Fig. 2.7 Cross sectional view of Circular PCFs

2.8 Circular cladding

The circular cladding is more fabrication friendly among all PCFs. The authors have proposed several PCFs recently in reference [71, 91, and 92]. In [92] the authors have proposed five layered circular PCF operating around 220THz and achieved low confinement loss of 10^{-8} cm^{-1} . But they did not report other modal parameters. In [91], the authors have reported ultra-low loss circular hollow PCF which operates around 1THz. They have achieved higher core power fractions of 51% with EML of 0.04 cm^{-1} . They have also presented CL of 10^{-3} cm^{-1} . From operating frequency 0.9 to 1.3THz, the authors have proposed [71] circular PC-PCF with EML of 0.043 cm^{-1} . They used topas as background material. They have also reported core power fraction of 47% along with CL of $10^{2.5} \text{ cm}^{-1}$ at 81% porosity.

Finally, the leading complication in designing geometry of a terahertz structure is the elevated material absorption loss of the host material. This is one of the main focuses of the research work. It is likely to decrease the loss by rising the core power fraction, porosity and preserving compact confinement between the air holes of the core which has been investigated in this thesis.

2.9 Summary of the Chapter

In the chapter, the author has presented literature review of related papers. The next chapter discusses about methods of analysis, Maxwell's and wave equations, and the simulation technique and finite element method.

CHAPTER 3

METHODS OF ANALYSIS

3.1 Introduction

The optical characteristics of a device will have a significant subject in selecting the correct structure in order to achieve a real-life application. For fiber optic geometric structure, the measurement of resources like time and money to deliver a device is a noteworthy factor considering total expense of the device. If the structure does not go through appropriate analysis, then design will not be able to meet the target requirements. This experimental design method is normally constrained by the asset availability [93]. Therefore, there is a necessity to examine and anticipate the attributes of a device before it is produced. In engineering, computational techniques have been created and utilized to validate simulation techniques. Also, massive computational techniques encourage the researchers for investigating the structure of fiber optic.

The computational simulation has achieved enormous development in computational performance. As a result, cost and time that are required to make an optical waveguide or device can be significantly minimized. The method needs basic computational simulation for testing the prototype design. After performing the simulation, the achieved results are further analyzed to meet the design goal. There could be iterations of design until they meet the requirements.

The author of the thesis has presented numerical design simulation of porous core photonic crystal fiber and their light guiding properties. The simulation method has been adapted for this thesis is the finite element method (FEM). It has adapted due to its interpolation functions can present any arbitrary refractive index profile with precision. Further, FEM can produce results more accurately than other numerical methods in the frequency domain as well.

3.2 Introduction to Electromagnetism

As light is an electromagnetic radiation, the behavior of an electromagnetic signal needs to be understood by Maxwell's equations. The differential form of Maxwell's equations will be discussed and the boundary condition will be imposed. After that wave

equation will be derived. The solution to the wave equation will lead us to propagation characteristics of the guided mode in the waveguide.

3.2.1 Maxwell's Equations

The differential equations for Maxwell's equations are given below. The equation demonstrates how the electric and magnetic field travels in the medium together. They are from equation (3.1) to (3.4) [94].

$$\nabla \times \mathbf{E} = -\frac{\partial \mathbf{B}}{\partial t} \quad (3.1)$$

$$\nabla \times \mathbf{H} = \frac{\partial \mathbf{D}}{\partial t} + \mathbf{J} \quad (3.2)$$

$$\nabla \cdot \mathbf{D} = \rho \quad (3.3)$$

$$\nabla \cdot \mathbf{B} = 0 \quad (3.4)$$

where \mathbf{E} denotes electric field intensity in *volt/meter* (V/m), \mathbf{B} denotes magnetic flux density *weber/meter²* (Wb/m^2), \mathbf{H} is magnetic field intensity *ampere/meter* (A/m), \mathbf{D} denotes electric flux density *coulomb/meter²* (C/m^2), \mathbf{J} denotes electric current density *ampere/meter²* (A/m^2), and ρ is electric charge density *coulomb/meter³* (C/m^3).

The constitutive relations between electric flux density, electric field intensity in terms of permeability of the medium (μ) given in equation 3.5 [94]. The relations between magnetic flux density, magnetic field intensity with permeability of the medium (μ) presented in equation (3.6) [90]:

$$\mathbf{B} = \mu \mathbf{H} = \mu_0 \mu_T \mathbf{H} \quad (3.5)$$

$$\mathbf{D} = \varepsilon \mathbf{E} = \varepsilon_0 \varepsilon_T \mathbf{E} \quad (3.6)$$

Where $\mu_0 = 4\pi \times 10^{-7} (H/m)$ and $\varepsilon_0 = 8.854 \times 10^{-12} (F/m)$ are permeability and permittivity of vacuum, μ_T along with ε_T are the relative permeability and permittivity, correspondingly.

3.2.2. Boundary Conditions

The unique solution of Maxwell's equations for physical dimension considering boundary continuing condition at the interfaces (in Fig. 3.1) where the surface current and charge is zero can be obtained [93]. If the two different mediums are denoted by subscript 1 and 2 respectively and \hat{n} is the unit vector that is perpendicular to the at the interface of two medium then the electric and magnetic fields tangential component have to be continuous shown from equation (3.8) and (3.9) respectively.

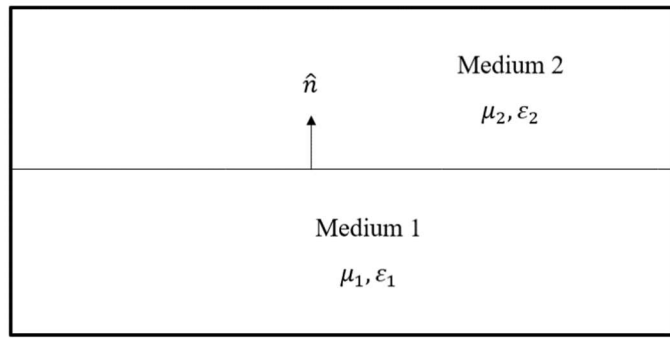


Fig. 3.1 Mediums with interfaces

$$\hat{n} \times (\mathbf{E}_1 - \mathbf{E}_2) = 0$$

$$\therefore \mathbf{E}_{t1} = \mathbf{E}_{t2} \quad (3.8)$$

For the magnetic field,

$$\hat{n} \times (\mathbf{H}_1 - \mathbf{H}_2) = 0$$

$$\therefore \mathbf{H}_{t1} = \mathbf{H}_{t2} \quad (3.9)$$

the accuracy of the physical dimensions, perpendicular component of electric and magnetic flux density should be continuous as well has found in equation (3.10) and (3.11) [89].

$$\hat{n} \cdot (\mathbf{D}_1 - \mathbf{D}_2) = 0$$

$$\therefore \mathbf{D}_{n1} = \mathbf{D}_{n2} \quad (3.10)$$

For magnetic flux density, boundary condition is,

$$\hat{n} \cdot (\mathbf{B}_1 - \mathbf{B}_2) = 0$$

$$\therefore \mathbf{B}_{n1} = \mathbf{B}_{n2} \quad (3.11)$$

According to equation (3.6), and the variation of permittivity between two medium

($\epsilon_1 \neq \epsilon_2$), the equation should be,

$$\begin{aligned}\epsilon_1 \mathbf{E}_{n1} &= \epsilon_2 \mathbf{E}_{n2} \\ \therefore \mathbf{E}_{n1} &\neq \mathbf{E}_{n2}\end{aligned}\quad (3.12)$$

According to equation (3.5), and for non-magnetic materials permeability is found 1 ($\mu_1 = \mu_2 = 1$),

$$\begin{aligned}\mu_1 \mathbf{H}_{n1} &= \mu_2 \mathbf{H}_{n2} \\ \therefore \mathbf{H}_{n1} &= \mathbf{H}_{n2}\end{aligned}\quad (3.13)$$

There are still two condition have to be satisfied in nonappearance of ρ and \mathbf{J} . One is vanishing tangential magnetic field component for perfect magnetic conductor. Another is tangential \mathbf{E} component due to being perfect magnetic conductor. The equation are (3.14) and (3.15) [95].

$$\mathbf{n} \times \mathbf{E} = 0 \text{ or } \mathbf{n} \cdot \mathbf{H} = 0 \quad (3.14)$$

$$\mathbf{n} \times \mathbf{H} = 0 \text{ or } \mathbf{n} \cdot \mathbf{E} = 0 \quad (3.15)$$

In next, the derivation of wave equation as solution to of Maxwell's equations will be derived.

3.2.3 Wave Equation Derivation

The wave equation is second order differential equation explains how wave in terms of electric and magnetic fields propagate through space. From the Maxwell's equations 3.5 and 3.1[94]. It can be written,

$$\nabla \times \mathbf{E} = -\mu \frac{\partial}{\partial t} \mathbf{H} \quad (3.16)$$

After putting curl

$$\nabla \times (\nabla \times \mathbf{E}) = -\mu \frac{\partial}{\partial t} (\nabla \times \mathbf{H}) \quad (3.17)$$

and substituting (3.2) into (3.6) we obtain,

$$\nabla \times (\nabla \times \mathbf{E}) = -\varepsilon\mu \frac{\partial^2}{\partial t^2} \mathbf{E} \quad (3.18)$$

For frequency domain, The phasor form of the electric field component in terms of angular frequency ω [95]:

$$\mathbf{E}(x, y, z, t) = \mathbf{E}(x, y, z) e^{j\omega t} \quad (3.19)$$

The phasor form allows the alternation of time-derivative $j\omega$ presented in below [90].

$$\therefore \frac{\partial e^{j\omega t}}{\partial t} = j\omega e^{j\omega t} \quad (3.20)$$

$$\therefore \frac{\partial}{\partial t} = j\omega \quad (3.21)$$

From equation (3.4) and (3.18)

$$\nabla \times (\nabla \times \mathbf{E}) = \omega^2 \varepsilon\mu \mathbf{E} \quad (3.22)$$

The above equation is for electric field component. In the same way for the magnetic field,

$$\nabla \times \frac{1}{\varepsilon} (\nabla \times \mathbf{H}) = \omega^2 \varepsilon\mu \mathbf{H} \quad (3.23)$$

According to the curl vector relation,

$$\nabla \times (\nabla \times \mathbf{E}) = \nabla (\nabla \cdot \mathbf{E}) - \nabla^2 \mathbf{E} ,$$

After reorganization of above equation on relation

$\nabla (\nabla \cdot \mathbf{E}) = -\nabla (\ln \varepsilon) \cdot \mathbf{E}$, putting in Equation (3.22) and reorganize to get the wave equation for electric field:

$$\nabla^2 \mathbf{E} + \omega^2 \varepsilon\mu \mathbf{E} = -\nabla (\ln \varepsilon) \cdot \mathbf{E} \quad (3.24)$$

Similarly, for the magnetic field:

$$\nabla^2 \mathbf{H} + \omega^2 \varepsilon\mu \mathbf{H} = -\nabla (\ln \varepsilon) \times \nabla \times \mathbf{H} \quad (3.25)$$

The above equations are vector wave equation for the electric and magnetic field respectively [93]. The above equation in scalar form are presented below.

$$\nabla^2 E = \omega^2 \varepsilon\mu E \quad (3.26)$$

In the same way, magnetic field scalar equation is obtained.

$$\nabla^2 H = \omega^2 \varepsilon\mu H \quad (3.27)$$

The vectoral form has been adapted to explain for the modes of the optical waveguide's simulation will be discussed next.

3.3 Numerical Technique

The optical wave propagation analysis is a complex mathematical process to derive an analytical solution accurately. This process requires huge time. Using computational process, the time can be saved significantly. Also, this numerical analysis allows us to examine and analyse the results properly. Recently, the advanced efficient algorithm and computational performance enables to investigate optical modal characteristic accurately [96]. Currently, there are some numerical analysis techniques have developed. They are methods of moments (MOM), method of lines (MOL), finite difference method (FDM), finite-time finite-domain method (FDTD), and finite element method (FEM). In this thesis, FEM has been adapted for numerical investigations. So, the steps involve in FEM will be discuss next.

3.4 Finite Element Method

The researchers were made proposal for FEM in late nineteen forty. In 1960s, its applications were developed for various areas of science and engineering [93]. Still FEM is using in computational method for solving complex geometric structures specially in more advanced PCFs design. COMSOL Multiphysics is one of them [93].

In FEM analysis sub-domains are created equally from a domain. This sub-domain is also called element. In this method, each element values are approximated using basis function. The basis functions are polynomials [94]. This function has non-zero value in each sub-domain and put zero otherwise. The basis function utilizes interpolation function which is continuous inside sub-domains. If each sub-domain has interpolation function, Ψ , m being the number of nodes for each discrete domain and ψ_i is specific interpolation function for the field value then according to [93] it can be written

$$\Psi^e = \sum_{i=1}^m N_i \Psi_i \quad (3.28)$$

As FEM can solves initial value problem in both time and frequency domain, solution of those values can be achieved using two method. The first one is variational method also known as Rayleigh-Ritz method. The other one is weighted method or also called

Galerkin method. Using above mention methods, boundary value problem and their solution is minimized by FEM to matrix equation involving eigenvalue [97].

The stages to yield magnetic field formula considering the variational method are derived next.

Equivalent eigenvalue equation from wave equation (3.23) is given as:

$$L\mathbf{H} - \lambda M\mathbf{H} = 0 \quad (3.29)$$

The operators $M = \mu$ and self-joining operator $L = \nabla \times \epsilon^{-1} \nabla$, and the eigenvalue is $\lambda = \omega^2$.

The L operator denotes $\langle L\phi, \psi \rangle = \langle \phi, L\psi \rangle$ after reducing or maximizing required functional provides [162]:

$$F(\tilde{H}) = \frac{1}{2} \langle L\tilde{H}, \tilde{H} \rangle - \frac{\lambda}{2} \langle M\tilde{H}, \tilde{H} \rangle \quad (3.30)$$

Here, the symbol $\langle \rangle$ is the inner product and $*$ means conjugate then:

$$\langle f, g \rangle = \int g^* \cdot f dV \quad (3.31)$$

The stationary value of the functional has found, $F(\tilde{H}) = 0$

Therefore,

$$\lambda = S.V. \frac{\langle L\mathbf{H}, \mathbf{H} \rangle}{\langle M\mathbf{H}, \mathbf{H} \rangle} \quad (3.32)$$

here $S.V.$ denotes stationary value. So, the full vectoral magnetic field component gained according to the Rayleigh-Ritz method [84]:

$$\omega^2 = S.V. \frac{\int \int (\nabla \times \mathbf{H})^* \cdot \epsilon^{-1} (\nabla \times \mathbf{H}) dV}{\int \int \mathbf{H}^* \cdot \mu \mathbf{H} dV} \quad (3.33)$$

The reduction formula found as an eigenvalue problem

$$[A]\mathbf{x} = \lambda[B]\mathbf{x} \quad (3.34)$$

Here A denotes the mass matrix, B indicates the stiffness matrix, \mathbf{x} denotes eigenvector and λ denotes the eigenvalue. Matrices created by the technique is symmetric. This technique shortens the numerical computation [93].

The substitute of variational process is the weighted method that do not need information of functional [93]. It can be obtainable as following:

$$Lu = v \quad (3.35)$$

L denotes differential Laplace operator, v denotes source of excitation and u the unidentified quantity.

The unidentified function is found by increasing this unidentified functional accompanied by some identified basis functions with unidentified coefficients. The coefficients have selected for reducing residual error, from equation 3.36, and enforced to 0 [94].

$$R(s) = Lu - v \quad (3.36)$$

The matrix form of above equation:

$$[L][u] = [v] \quad (3.37)$$

According to electromagnetism, the unknown quantity u denotes magnetic field, the operator $L = \nabla \times \varepsilon^{-1} \nabla \times (-\omega^2 \mu)$, as well as source $[v] = 0$.

The natural boundary conditions require additional attention because boundary condition does not straightforwardly fulfil as does in the variational method [93]. While any one of these above approaches might be pragmatic to utilize FEM. Here in this work, Rayleigh-Ritz method has been applied. Vector as well as scalar preparations of FEM have presented in following section.

3.4.1 Scalar Formulation

The vector as well as scalar wave equations can be solved by FEM. The wave equations for electric and magnetic fields derived in (equation (3.24) and (3.25)) can be ignored if the index difference is insignificant.

The confined fields in the optical waveguides neither truly transverse electric nor transverse magnetic. Then the confined fields are actually quasi-transverse electric (TE) or quasi-transverse magnetic (TM). (E_x) is the dominant TE and TM modes in scalar form presented in equation (3.38) and (3.39) respectively [94].

$$L = \iint_{\Omega} \left[\left(\frac{\partial E_x}{\partial x} \right)^2 + \left(\frac{\partial E_x}{\partial y} \right)^2 - k_0 n^2 E_x^2 + \beta^2 E_x^2 \right] d\Omega \quad (3.38)$$

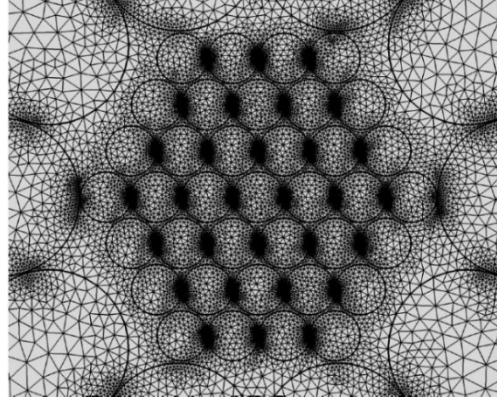


Fig. 3.2a Shape of the elements and mesh size

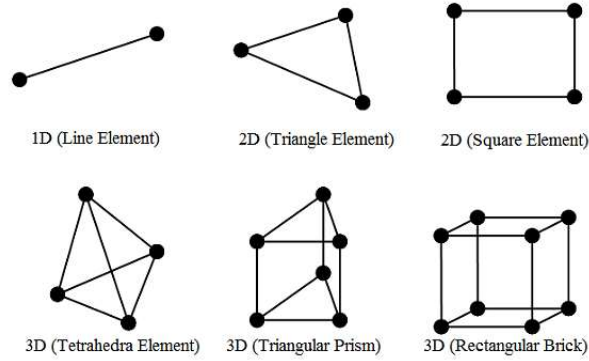


Fig. 3.2b Shape of elements for one, two and three dimensions [93]

Here Ω denotes cross-section area of a waveguide and L is Laplacian operator.

In Equation (3.38) β^2 represent eigenvalue of k_0 and in equation (3.39) k_0^2 indicates eigenvalue for β .

$$L = \iint_{\Omega} \left[\frac{1}{n^2} \left(\frac{\partial H_x}{\partial x} \right)^2 + \frac{1}{n^2} \left(\frac{\partial H_x}{\partial y} \right)^2 - k_0 n^2 H_x^2 + \frac{1}{n^2} \beta^2 E_x^2 \right] d\Omega \quad (3.39)$$

The above two equation have continuity of $\frac{\partial E_x}{\partial \hat{n}}$ and $\left(\frac{1}{n^2}\right)\left(\frac{\partial H_x}{\partial \hat{n}}\right)$ for the boundary condition, correspondingly. In next section, the domain would be discretized to sub-domain or element to apply FEM [94].

3.4.2 Elements Formation in Finite Element Method

One of the crucial phases in FEM is meshing or discretization of domain. The meshing determinises the resource allocation needed for computations. These resources are mainly the primary memory as well as processing speed. In this literature in chapter four, the proposed design of decagonal structure has around 1.2 million elements which demands huge computation resources in an acceptable time shown in Fig. 3.2a. During the meshing process, the sub-domain must not overlap with neighbours. During the FEM process various types of element shape is possible. These elements are line elements for one dimensional problem, triangular and square elements for two-dimensional problem and for third dimensional problem the shape of the elements can be found in Fig. 3.2b [93].

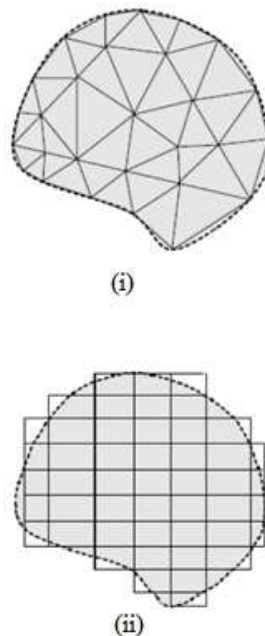


Fig. 3.3 Meshing at the boundary edge (i) triangular (ii) rectangular elements [93]

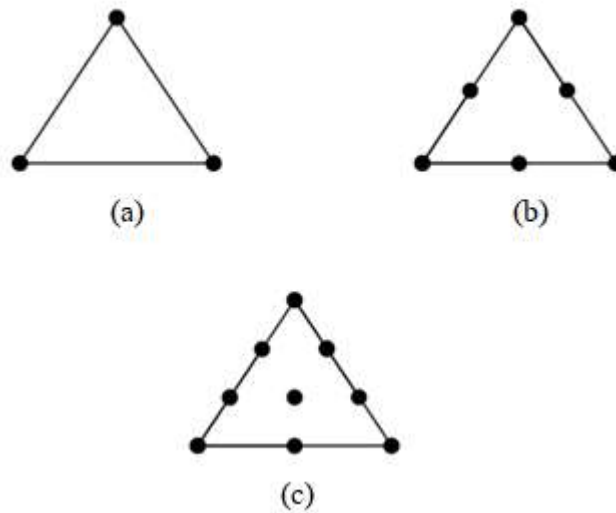


Fig. 3.4 (a) First order, (b) second and (c) third order element [94]

Line elements for one dimensional problem must have two end point called node. In case of solving two dimensional the sub-domain must be either triangular or square shape can be also seen in Fig. 3.2b. The triangular and square elements have three and four nodal point respectively. From the Fig. 3.3, it can be observed that the mapping of complex domain including boundary area covered by triangular shape element more accurately than square elements [93].

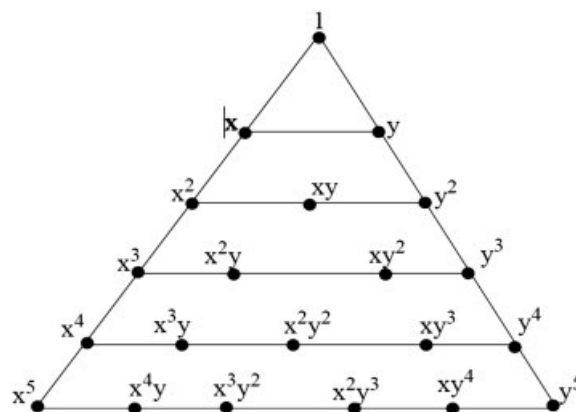


Fig. 3.5 View of polynomial in Pascal triangle [94]

Nodal point of first, second and third order elements has been depicted in Fig. 3.4. The approximation of nodal points depends on interpolation function. The interpolation

function describes each nodal point as polynomial. The polynomial must have one copy only. A complete polynomial with unique nodal point shown in Fig. 3.5. Here, the polynomial has been described by Pascal's triangle.

The shape function assign values to these generated nodal points. A shape function is collection of polynomials. For the first order triangle mesh, the polynomial is given by [92] is $(a + bx + cy)$.

Elements in the field (ϕ_e) is well-defined by,

$$\phi_e(x, y) = a + bx + cy \quad (3.48)$$

where a, b, c are constants and nodal point are :

$$\phi_e(x_i, y_i) = \phi_i ; i=1,2,3 \quad (3.49)$$

Then, for three nodal points it can be written

$$\begin{aligned} \phi_1 &\equiv \phi_e(x_1, y_1) = a + bx_1 + cy_1 \\ \phi_2 &\equiv \phi_e(x_2, y_2) = a + bx_2 + cy_2. \\ \phi_3 &\equiv \phi_e(x_3, y_3) = a + bx_3 + cy_3 \end{aligned} \quad (3.50)$$

The above equation in matrix form

$$\begin{Bmatrix} \phi_1 \\ \phi_2 \\ \phi_3 \end{Bmatrix} = \begin{bmatrix} 1 & x_1 & y_1 \\ 1 & x_2 & y_2 \\ 1 & x_3 & y_3 \end{bmatrix} \begin{Bmatrix} a \\ b \\ c \end{Bmatrix} \quad (3.51)$$

The a, b, c can be represent as below

$$\begin{aligned} a &= \frac{1}{2A_e} [\phi_1(x_2y_3 - x_3y_2) + \phi_2(x_3y_1 - x_1y_3) + \phi_3(x_1y_2 - x_2y_1)] \\ b &= \frac{1}{2A_e} [\phi_1(y_2 - y_3) + \phi_2(y_3 - y_1) + \phi_3(y_1 - y_2)] \end{aligned}$$

$$c = \frac{1}{2A_e} [\phi_1(x_3 - x_2) + \phi_2(x_1 - x_3) + \phi_3(x_2 - x_1)] \quad (3.52)$$

where A_e is the area of the triangle element and expression is [93]:

$$A_e = \frac{1}{2} \begin{vmatrix} 1 & x_1 & y_1 \\ 1 & x_2 & y_2 \\ 1 & x_3 & y_3 \end{vmatrix} = \frac{1}{2} [(x_2y_3 - x_3y_2) + (x_3y_1 - x_1y_3) + (x_1y_2 - x_2y_1)] \quad (3.53)$$

Replacing Equation (3.52) into Equation (3.48) and reshuffling

$$\phi_e(x, y) = N_1(x, y) \cdot \phi_1 + N_2(x, y) \cdot \phi_2 + N_3(x, y) \cdot \phi_3 \quad (3.54)$$

$$\phi_e(x, y) = [N] \{ \phi_e \}$$

Where $\{N\}^T$ denotes shape functions and expressed as:

$$\{N\}^T = \begin{bmatrix} N_1 \\ N_2 \\ N_3 \end{bmatrix} = \frac{1}{2A_e} \begin{bmatrix} x_2y_3 - x_3y_2 & y_2 - y_3 & x_3 - x_2 \\ x_3y_1 - x_1y_3 & y_3 - y_1 & x_1 - x_3 \\ x_1y_2 - x_2y_1 & y_1 - y_2 & x_2 - x_1 \end{bmatrix} \begin{bmatrix} 1 \\ x \\ y \end{bmatrix} \quad (3.55)$$

The shape function matrix also expressed as:

$$\{N\}^T = \begin{bmatrix} N_1 \\ N_2 \\ N_3 \end{bmatrix} = \frac{1}{2A_e} \begin{bmatrix} a_1 + b_1x + c_1y \\ a_2 + b_2x + c_2y \\ a_3 + b_3x + c_3y \end{bmatrix} \quad (3.56)$$

a_i, b_i, c_i and $i = 1, 2, 3$ are found as:

$$\begin{aligned} a_1 &= x_2y_3 - x_3y_2 \\ b_1 &= y_2 - y_3 \\ c_1 &= x_3 - x_2 \end{aligned} \quad (3.57)$$

Also, a_2, b_2, c_2, a_3, b_3 and c_3 will be calculated by cyclical exchange of $1 \rightarrow 2 \rightarrow 3$ in Equation 3.57. The shape function N_i has a value of 1 at node i and 0 elsewhere [93].

The subsequent phase is construction of global and element matrices. The construction of these matrices is discussed in next.

3.4.3 Global Matrices Formation

The eigenvalue equation is found from wave equation. This eigen value equation can be converted to matrix equation. This element matrix is generated from the eigen matrix. They are the global and element matrices. The magnetic field magnitude for all three direction can be expressed as [93],

$$\{H\}_e = \left[\{H_x\}_e \{H_y\}_e \{H_z\}_e \right]^T \quad (3.58)$$

and

$$[N]^T = \begin{bmatrix} \{N\} & \{0\} & \{0\} \\ \{0\} & \{N\} & \{0\} \\ \{0\} & \{0\} & j\{N\} \end{bmatrix} \quad (3.59)$$

Here $\{N\} = [N_1 N_2 N_3] T$ as well as $\{0\}$ is empty vector.

By combining Equation 3.58 into 3.59 then,

$$\{H\}_e = \begin{bmatrix} N_1 & N_2 & N_3 & 0 & 0 & 0 & 0 & 0 & 0 \\ 0 & 0 & 0 & N_1 & N_2 & N_3 & 0 & 0 & 0 \\ 0 & 0 & 0 & 0 & 0 & 0 & jN_1 & jN_2 & jN_3 \end{bmatrix} \begin{Bmatrix} H_{x1} \\ H_{x2} \\ H_{x3} \\ H_{y1} \\ H_{y2} \\ H_{y3} \\ H_{z1} \\ H_{z2} \\ H_{z3} \end{Bmatrix} \quad (3.60)$$

The global matrices $[A]$ and $[B]$ can be written as [93]:

$$(\nabla \times \mathbf{H})_e = [\nabla \times][N]^T \{H\}_e = \begin{pmatrix} 0 & -\partial/\partial z & \partial/\partial y \\ \partial/\partial z & 0 & \partial/\partial x \\ -\partial/\partial y & \partial/\partial x & 0 \end{pmatrix} \quad (3.61)$$

Above equation can be reduce to,

$$(\nabla \times \mathbf{H})_e = [Q]^T \{H\}_e \quad (3.62)$$

Here $[Q]$ is

$$[Q] = \begin{bmatrix} \{0\} & j\beta\{N\} & \partial\{N\}/\partial y \\ -j\beta\{N\} & \{0\} & \partial\{N\}/\partial x \\ -\partial\{N\}/\partial y & \partial\{N\}/\partial x & \{0\} \end{bmatrix} \quad (3.63)$$

Therefore, mass matrix, A is specified as per

$$A = \sum_e [A]_e = \sum_e \iint_{\mathcal{E}_e} \frac{1}{\epsilon_e} [Q]^* [Q]^T dx dy \quad (3.64)$$

$$A = \begin{bmatrix} A_{xx} & A_{xy} & A_{xz} \\ A_{yx} & A_{yy} & A_{yz} \\ A_{zx} & A_{zy} & A_{zz} \end{bmatrix} \quad (3.65)$$

and

$$[A_{xx}] = \iint_e \left[\beta^2 \{N\} \{N\}^T + \frac{\partial\{N\}}{\partial y} \frac{\partial\{N\}^T}{\partial y} \right] dx dy \quad (3.66)$$

$$[A_{xy}] = \iint_e -\frac{\partial\{N\}}{\partial y} \frac{\partial\{N\}^T}{\partial x} dx dy \quad (3.67)$$

$$[A_{xz}] = \iint_e \beta\{N\} \frac{\partial\{N\}^T}{\partial x} dx dy \quad (3.68)$$

$$[A_{yy}] = \iint_e \left[\beta^2 \{N\} \{N\}^T + \frac{\partial\{N\}}{\partial x} \frac{\partial\{N\}^T}{\partial x} \right] dx dy \quad (3.69)$$

$$[A_{yz}] = \iint_e \beta\{N\} \frac{\partial\{N\}^T}{\partial y} dx dy \quad (3.70)$$

$$[A_{zz}] = \iint_e \left[\frac{\partial\{N\}}{\partial y} \frac{\partial\{N\}^T}{\partial y} + \frac{\partial\{N\}}{\partial x} \frac{\partial\{N\}^T}{\partial x} \right] dx dy \quad (3.71)$$

Stiffness matrix, B as [93]:

$$B = \sum_e \iint_e [N]^* [N]^T dx dy \quad (3.72)$$

$$B = \begin{bmatrix} [B_{xx}] & [0] & [0] \\ [0] & [B_{yy}] & [0] \\ [0] & [0] & [B_{zz}] \end{bmatrix} \quad (3.73)$$

$$[B_{xx}] = [B_{yy}] = [B_{zz}] = \sum_e \iint_e [N]^* [N]^T dx dy \quad (3.74)$$

Stiffness matrix, A as well as mass matrix, B are the universal form of global matrices for two-dimensional problem. Here, the first order nodal matrix in terms of triangular shape has been constructed. The matrix size is 9×9 . Again, after few steps of simplification following matrix can be derived

$$B_e = \begin{bmatrix} \frac{A}{6} & 0 & 0 & \frac{A}{12} & 0 & 0 & \frac{A}{12} & 0 & 0 \\ 0 & \frac{A}{6} & 0 & 0 & \frac{A}{12} & 0 & 0 & \frac{A}{12} & 0 \\ 0 & 0 & \frac{A}{6} & 0 & 0 & \frac{A}{12} & 0 & 0 & \frac{A}{12} \\ \frac{A}{12} & 0 & 0 & \frac{A}{6} & 0 & 0 & \frac{A}{12} & 0 & 0 \\ 0 & \frac{A}{12} & 0 & 0 & \frac{A}{6} & 0 & 0 & \frac{A}{12} & 0 \\ 0 & 0 & \frac{A}{12} & 0 & 0 & \frac{A}{6} & 0 & 0 & \frac{A}{12} \\ \frac{A}{12} & 0 & 0 & \frac{A}{12} & 0 & 0 & \frac{A}{6} & 0 & 0 \\ 0 & \frac{A}{12} & 0 & 0 & \frac{A}{12} & 0 & 0 & \frac{A}{6} & 0 \\ 0 & 0 & \frac{A}{12} & 0 & 0 & \frac{A}{12} & 0 & 0 & \frac{A}{6} \end{bmatrix} \quad (3.75)$$

These matrices are implemented in COMSOL to solve for a mode.

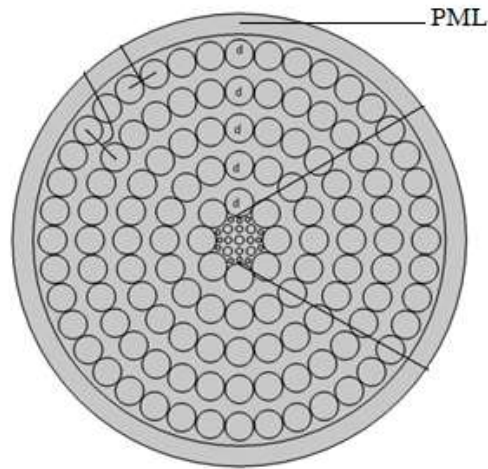


Fig. 3.6 Perfectly Matched Layer

3.5 Perfectly Matched Layer

In the space, the physical dimension of geometric structure is endless. Side by side, the computational properties are restricted. Hence, the endless physical geometric structure needs to build on a computer. The diagram of PML shown in Fig. 3.6. So, the domain must reduce to finite limit via inserting borders. This border or boundary known as PML. PML is an artificial boundary. It perfectly absorbs incident electric field. Also, due to PML no fields from outside the computational can come in [98]. This layer also helps during the computation of effective mode index. For this thesis, the cylindrical PML has been adopted due to COMSOL Multiphysics and it is chosen in between 7 to 10 percent of the total diameter of the geometric structure of the PC-PCF.

The pulse at the borders can reflect and result in non-physical radiation to the structure of geometry. So, there are two methods used in defining the border which is used to cut the domain to finite. The first method is mathematical in which an operator can be defined: either global or local. The global mathematical method fallouts in a fully occupied matrix which is a disadvantage and cannot be employed in large meshes. The local mathematical method [93] states the local operator which abandons the field at the borders. Its disadvantage is that it needs trial and error to figure out the boundary location which cannot be placed near the foundation [93]. The other technique is to place artificial layer. Berenger has proposed the concept of PML in 1994 [93] and since then it has been implemented in numerical methods in FDTD and FEM. The idea of PML is to insert an absorbent layer with permittivity like the material in the core domain. The impedance of

both is identical thus no reflection occurs at interface. The PML boundary absorbs pulse traveling outwards from the main domain at any angle and frequency. The magnitude of the pulse declines exponentially inside PML boundary. Also, the EM radiation is reflected to the domain [93].

The first proposed PML was proposed for FDTD and it cannot be easily implemented in unstructured meshes which are used in FEM. The PML is implemented as stretching of the complex coordinate in FEM [93].

$$x \rightarrow \tilde{x} = \int_0^x s_x(x') dx' \quad (3.76)$$

$s_x(x)$ is complex stretching variable.

This results in a change in the nabla operator, ∇ , which is written as:

$$\nabla \rightarrow \tilde{\nabla} = \hat{x} \frac{\partial}{\partial \tilde{x}} + \hat{y} \frac{\partial}{\partial \tilde{y}} + \hat{z} \frac{\partial}{\partial \tilde{z}} = \hat{x} \frac{1}{s_x} \frac{\partial}{\partial x} + \hat{y} \frac{1}{s_y} \frac{\partial}{\partial y} + \hat{z} \frac{1}{s_z} \frac{\partial}{\partial z} \quad (3.77)$$

Then the Maxwell's equations can be written with $\tilde{\nabla}$ instead of ∇ , and the time derivative $\partial/\partial t$ is replaced with $j\omega$

$$\tilde{\nabla} \times \mathbf{E} = -j\omega \mathbf{B} \quad (3.78)$$

$$\tilde{\nabla} \times \mathbf{H} = j\omega \mathbf{D} \quad (3.79)$$

$$\tilde{\nabla} \cdot \mathbf{D} = \rho \quad (3.80)$$

$$\tilde{\nabla} \cdot \mathbf{B} = 0 \quad (3.80)$$

This leads to a modification of equation (3.23).

Finally, PML absorbs unwanted radiation and helps to measure confinement loss of the fiber geometry

3.6 Summary of the Chapter

The chapter started with Maxwell's law. The scalar and vector wave equation have been showed. For optical waveguide boundary condition has been described. Afterward, meshing and development of element matrices was described. Lastly, the PML was

discussed. In following chapters these analyses will be applied to our proposed designs using FEM solver called COMSOL multiphysics.

In the next chapter, the first proposed PC-PCF design having decagonal cladding and hexagonal core will be presented along with its mesh size and PML.

CHAPTER 4

DECAGONAL CLADDING-HEXAGONAL CORE PC-PCF

In this chapter, decagonal cladding with hexagonal core has been proposed. The researchers have reported some promising decagonal structures [86,87] recently. The wave guiding parameters like core diameter (D_{core}), air filling fraction (d/A), air hole diameter for core and cladding are d_c and d respectively. The distance between two air holes in the same ring and adjacent ring (cladding pitch) in cladding is A_1 and A respectively. Distance between two adjacent air holes in the core is called core pitch (A_c). The proposed design optimized numerically to set the photonic band gap near 1 THz. So that the maximum power can propagate through the PC-PCF core air holes. In following sections, the geometry design and results will be discussed.

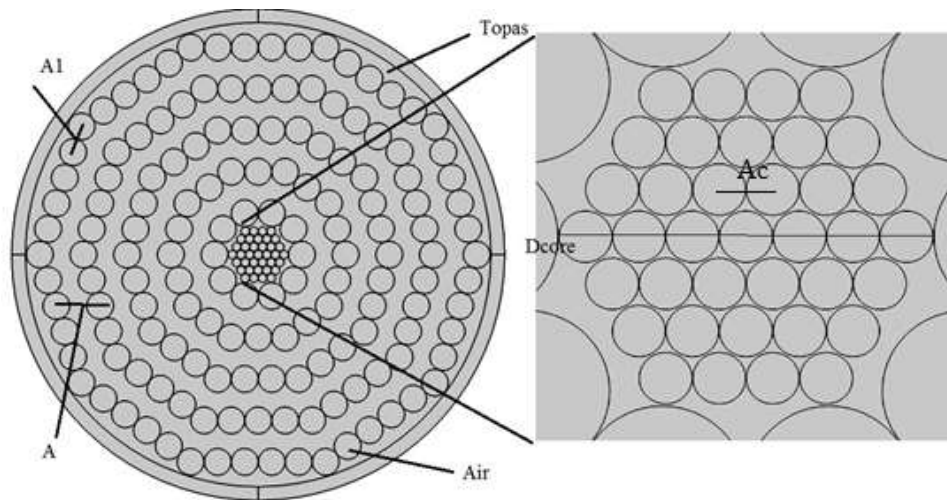
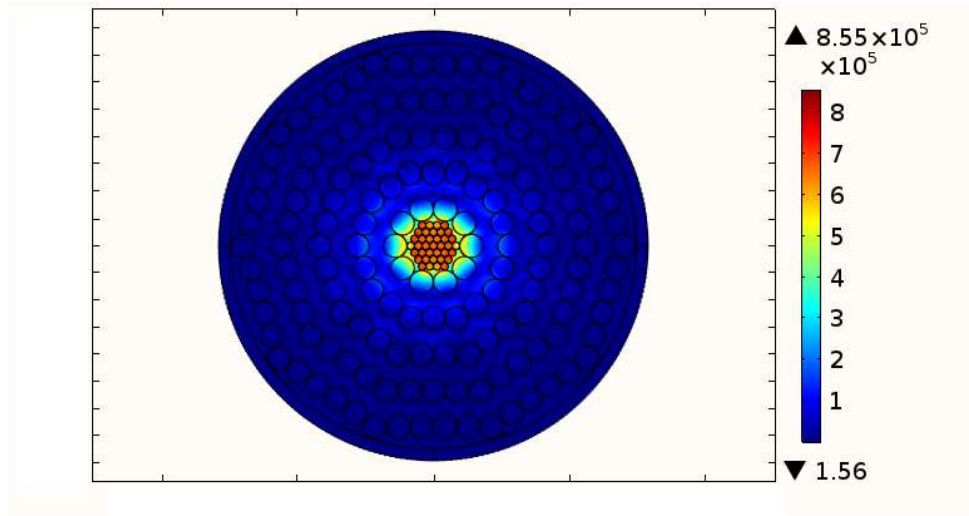


Fig. 4.1 Geometry area of the proposed PC-PCF accompanied by zoomed view of porous core

4.1 Introduction

To make the guided transmission more efficient and reliable in case of terahertz wave, a porous core hexagonal porous core photonic crystal fiber with decagonal cladding structure is presented with theoretical and simulation results. The finite element method (FEM) as well as perfectly matched layer border condition has been adapted to investigate the transmission characteristics of the fiber.



Full View

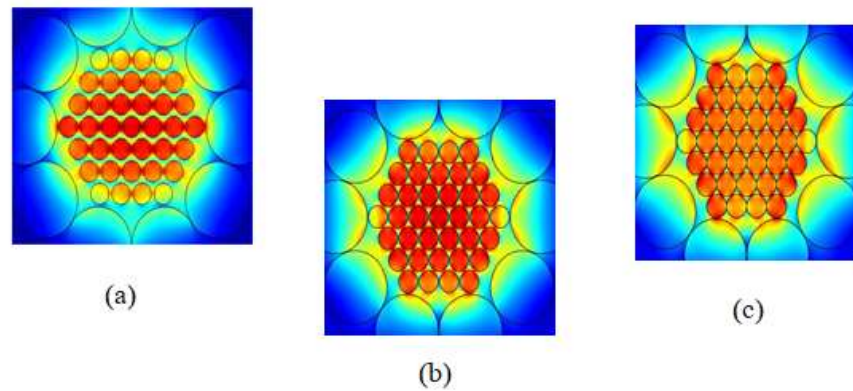


Fig. 4.2 Modal field of the proposed geometry structure full view (81% porosity) and zoomed (a) 61.5%porosity (b) 71.5%porosity (c) 81.5%porosity

The proposed design gives an extremely lower effective material loss of 0.049cm^{-1} while maintaining higher percentages core power 43% for an operating frequency of 1 THz. Also, the confinement loss was achieved is 0.00135cm^{-1} . So, the total loss is found 0.504cm^{-1} . Other important design parameters including single mode condition, confinement loss, as well as dispersion are also discussed. The proposed design is anticipated to be fabricated using the modern fabrication method uniting the capillary stacking as well as sol-gel techniques. It is expected that designed structure can be engage in application such as long-distance fiber optics communications.

Table 1: Optimized Parameter for Decagonal PC-PCF at 1 THz

| Parameter | Value |
|---|-------------------|
| Total Number of Air holes (Cladding+Core) | 177(140+37) |
| Radius of core | 280 μm |
| Cladding air-hole radius | 86 μm |
| Core air-hole radius | 20 μm |
| AFF | 0.766 |
| PML | 7.8% |
| Number of elements | 1,67,505 |

4.2 Design Methodology of Proposed Decagonal- Hexa Core PC- PCF

The air hole arrangement of cladding made of decagonal structure and the air holes in the core are in hexagonal structure. Decagonal structure for the cladding is chosen because of its better confinement. The structure is chosen to have a pitch of $A= 225\mu\text{m}$ and hole-to-pitch ratio of $d/A= 0.776$, as this results in a fundamental bandgap near 1 THz. The term porosity which depends on the air hole size of the core is denoted as the fraction of the air hole area to the total area of the fiber core. If porosity is reduced, then most of the power will be spread into cladding. As the air holes in the core perform as a low index material and dry air, $\alpha_{mat}=0$ is transparent in the terahertz frequency range, the absorption loss of material can be significantly decreased. The cross section of the proposed fiber with zoomed form of the core has shown in Fig. 4.1. The distance between two adjacent air holes on the same ring in the cladding is A_l that is related to A by $A_l = 0.766*A$. The distance between air holes on the adjacent ring of the porous core is A_c which is related to A by $A_c= 0.245*A$. The core diameter, $D_{core} = 2(A-d/2)$ has been changed while the air filling fraction ($AFF=d/A$) was preserved fixed at 0.76 throughout the whole simulation. Here, d denoted as the diameter of cladding air holes and A is the

outer pitch. Such higher AFF helps to increase the core confinement and reduces the EML. AFF cannot be increased further because it causes overlapping the air holes in the cladding and hence fabrication will be challenging. For all the simulation, five rings of air holes in cladding and three rings of air holes in the core is utilized so that more of the light can be passed through the core and thus confinement is gained. Also, details parameters are shown in table 1.

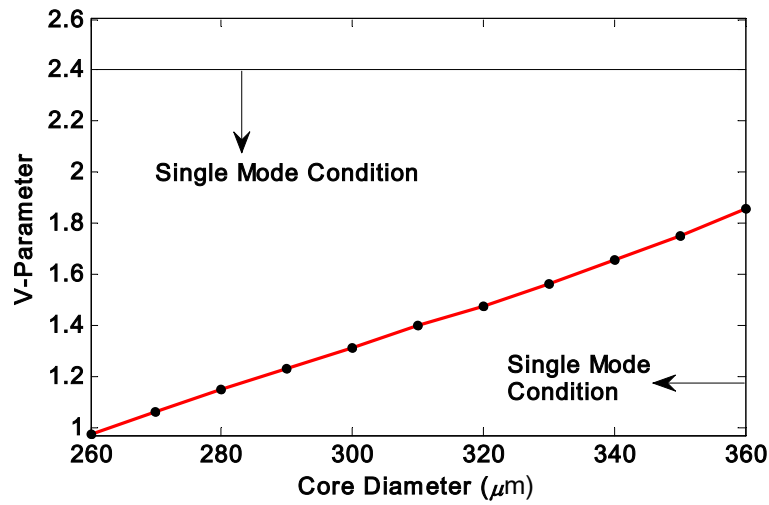


Fig. 4.3 V- parameter and D_{core} at $f = 1$ THz

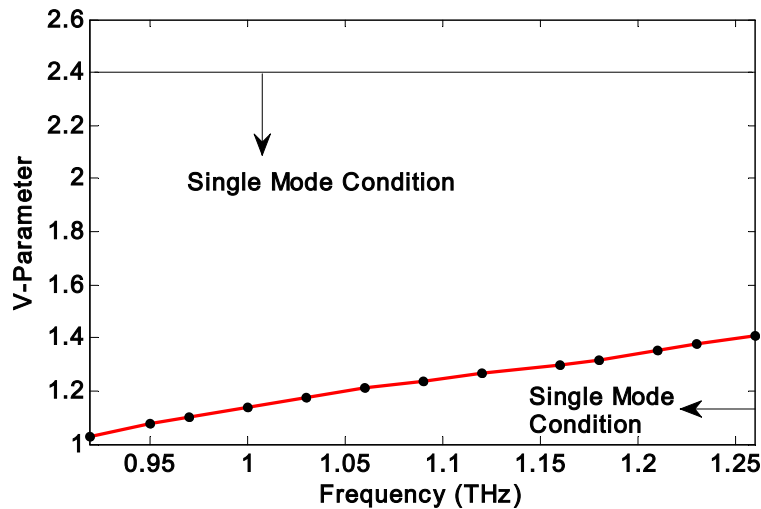


Fig. 4.4 V- parameter and frequency for $D_{\text{core}} = 280 \mu\text{m}$

In the proposed design, TOPAS is used as the background material which is mainly Cyclic-olefin copolymer (COC). The reason why we choose this material as the background is that its lower absorption loss, about 0.1-0.2 dB cm⁻¹. It has a lower EML [$\alpha_{mat} = 0.2 \text{ cm}^{-1}$] at $f=1$ THz. It has constant refractive index, $n=1.53$ over the frequency range 0.1-1.5 THz almost zero material dispersion in this range [72]. Moreover, it offers low confinement loss, less dispersion and guard against water vapor absorption.

4.3 Results and discussions of the Proposed PC-PCF

The simulation of proposed geometry structure has done using the full vector finite element method (FEM) based software COMSOL. For the representation of the structure, a perfectly matched layer (PML) is introduced and the thickness of the PML region used for the numerical investigation is around 7.8% of the total fiber radius. During the simulation, solved mesh elements were 167505 along with 13627 numbers of boundary elements. The calculation is done for different porosities. The porosities are taken as 61.5%, 71.5% and 81.5%. The modal power distribution at various porosities has presented in the Fig. 4.2. It can be described from the Fig., while core porosity rises the amount of optical power confined in core region. Unfortunately, some of the researchers [80-82] put less focus to analyze the condition for single mode fiber that is one of the most important factors for terahertz signal application.

The core is porous core that is why its refractive index should be equal to the effective refractive index, n_{eff} . For the existence of the single mode condition, the value of normalized frequency V-parameter must be equal to or less than 2.405. The alternation of the V-parameter changes with various values of D_{core} and f is presented in the Fig. 4.3 and 4.4 correspondingly.

Before starting the design, our prime mindset was to reduce the EML and to get a maximum threshold value of the core power fraction. To reduce the EML, more focus is given to reduce the TOPAS material in the core. EML mostly rely on the quantity of host material in the core region well as the material in the core relay on core porosity. As the core porosity rises the amount of air increases at the same time the amount of material reduces and therefore the EML decreases.

Fig. 4.5 displays the EML with respect to D_{core} for various core porosity at set frequency of 1.0 THz. It has been realized from the Fig. that for fixed values of D_{core} , as the porosity increases the EML decreases. Porosity increases means filling more air into the core and it results less amount of material which is responsible for the reduction of the EML. It is obvious from the Fig. that at core porosity 81.5% material absorption loss is 0.049 cm^{-1} for core diameter of $280 \mu\text{m}$. This is since the guided mode undergoes reduce material and the core air holes bearing majority of the power.

Another important parameter that must be considered before designing a standard terahertz waveguide is the percentages total optical power travels along the fiber core air holes. For designing a standard fiber, it is required to increase the optical power flow along the fiber-core air holes. Fig. 4.6 describes the changing of EML and fraction of mode power together with respect to change in the frequency. If the frequency is tunes to higher values, then the EML increased. On the contrary, the core power fraction decreases while the frequency increase. The reason is the wave frequency is found relative to EML. Therefore, in proportion to the observed formula: $\alpha(\nu) = V^2 + 0.63V - 0.13 \text{ [dB/cm]}$ [92], it is practically determined that, the bulk material absorption loss is a function of frequency changes.

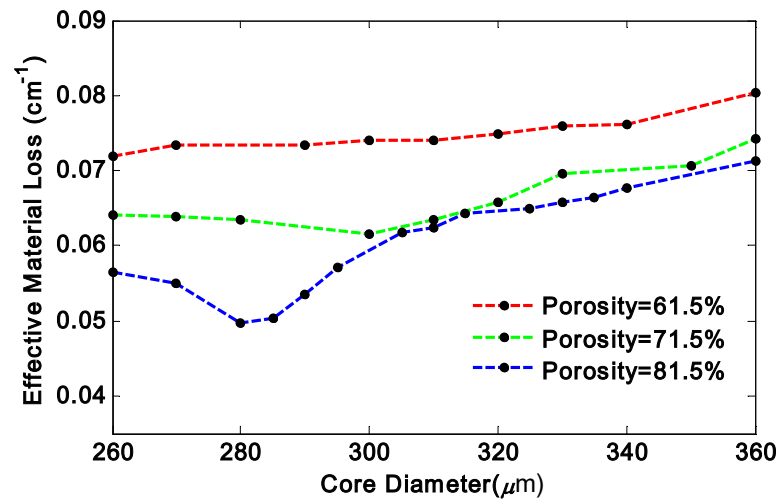


Fig. 4.5 EML versus core radius at different porosities

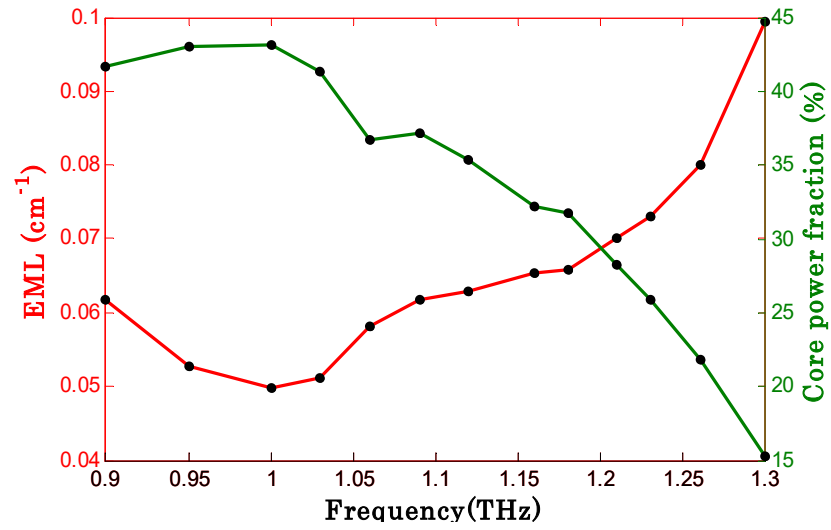


Fig. 4.6 Characteristics of EML, core power fraction and Frequency at $D_{\text{core}} = 280 \mu\text{m}$

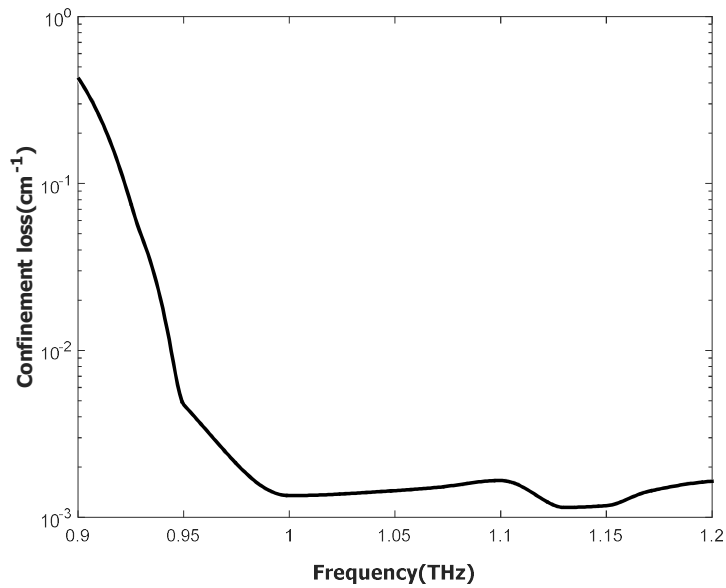


Fig. 4.7 Calculated confinement versus frequencies at $D_{\text{core}} = 280 \mu\text{m}$

Confinement loss represents the capability of a fiber to control light with tiniest loss. It is because of the inadequate amount of periodic air hole cladding. It can be found using the imaginary part of the complex refractive index. It determines by the number of air holes in the cladding. The more the number of air holes in the cladding, the less the confinement loss will be. Fig. 4.7 displays the confinement loss with respect to

frequency. At 1 THz it is found 0.00135 cm^{-1} . As the frequency increases the confinement loss constantly decreases which is much lesser than the EML. That is why the confinement loss can be neglected. While calculating the confinement loss, the single mode condition must be carefully examined. With the aim of lowering the confinement loss even more, the number of air holes in the cladding should be increased.

Dispersion plays a vital role in terahertz spectrum wave propagation. The transmission of the wideband signal, it is expected that fiber will show flattened dispersion over the large span on frequency. TOPAS has used as the background material whose refractive index is constant over the frequency range 0.9-1.25 THz. That is why the material dispersion is neglected and the contribution of the waveguide dispersion can be taken in to account.

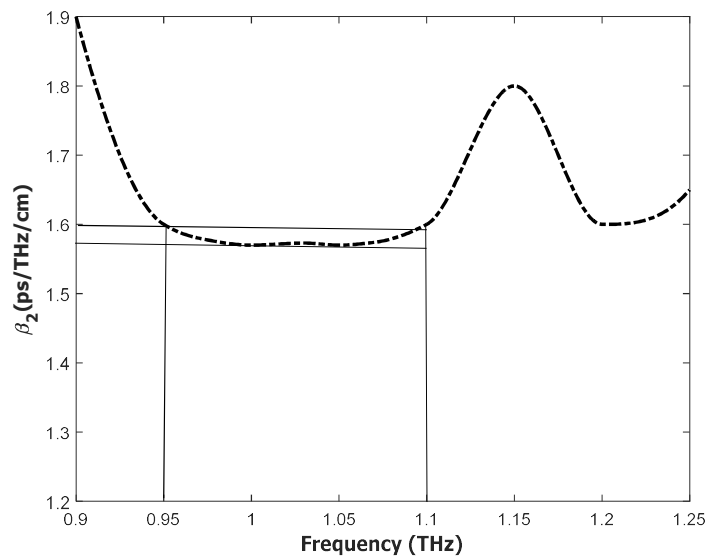


Fig. 4.8 Dispersion Characteristics of the proposed PCF versus Frequencies for $D_{\text{core}} = 280 \mu\text{m}$

It can be seen from Fig. 4.8, the changing of β_2 is less than 0.02 ps/THz/cm in the frequency spectrum 0.95-1.25 THz. Thus, it can be said that a flattened dispersion of $1.58 \pm 0.02 \text{ ps/THz/cm}$ has gained over the frequency span 0.95-1.25 THz.

Fabrication is one of the most important factors after simulating the PCF. Recently the problem with the fabrication is removed and fabrication possibilities are greatly

improved. Stack and drilling method, capillary stacking, Sol-gel technologies and Extrusion techniques are most used methods. Stack and drilling method are actually used for honeycomb and triangular lattices and is not authenticated to fabricate circular PCFs. In 2005, authors have described a sol-gel technique used in micro as well as in nano-structure manufacturing. Though Extrusion technique gives design freedom, its only limited to soft glasses. Researchers has proposed a capillary stacking technology that is appropriate and adaptable for PCF fabrication. The proposed PC-PCF can be fabricated via capillary stacking technology where the dimensions like air-hole diameter, shape and pitches can be altered properly.

4.4 Concluding Remarks of the Chapter

An extremely lower effective absorption loss, percentages of maximum optical power through the core, less confinement loss as well as near zero flat dispersion property has been introduced. In our proposed design, single mode behavior has also been satisfied and designed for terahertz wave guidance. For the first time decagonal cladding and rotate hexagonal core has been introduced which helps us to reduce the effective material loss and preferably for a margin of core power fraction. Besides, higher fractions of air filling and unique arrangement of five rings in the cladding helps to decrease the confinement loss. The primary implication of our proposed structure is its simplicity and loss minimization. Our proposed design contains attractive guiding properties which will be significant for terahertz wave application. For long distance communication of terahertz signal, our proposed design can be used relevantly.

Based on same geometric parameters, the octagonal cladding and hexagonal core PC-PCF will be discussed in next chapter, where the new proposed Octa-hexa design will be able to minimize losses and improve core power fraction.

CHAPTER 5

OCTAGONAL CLADDING-HEXAGONAL CORE PC-PCF

To minimize losses especially the EML, geometric parameters of the proposed design was optimized empirically to have the photonic bandgap around 1 THz.

5.1. Introduction

A very low loss hexagonal porous core as well as octagonally shaped circular air-hole cladding optical fiber for low loss terahertz optical wave propagation model have designed and proposed. The author has attained very low material absorption loss, moderate percentages of power through the core as well as flat dispersion characteristics in the proposed structure. To explore the communication features, finite element method adopted for the numerical investigation of the proposed PC-PCF. On the working frequency of 1 THz, the PC-PCF shows low material absorption loss of 0.045cm^{-1} while the power fraction found 58.2% setting 88% porosity. The confinement loss was found 0.00098 cm^{-1} . So, the total loss can be considered as the loss of the EML that is 0.045cm^{-1} . The proposed design displays dispersion variation of 0.225 ps/THz/cm . Similarly, this proposed structure fiber maintains single-mode condition fruitfully. It is anticipated that proposed structure of the fiber is expected to work in long distance telecommunication.

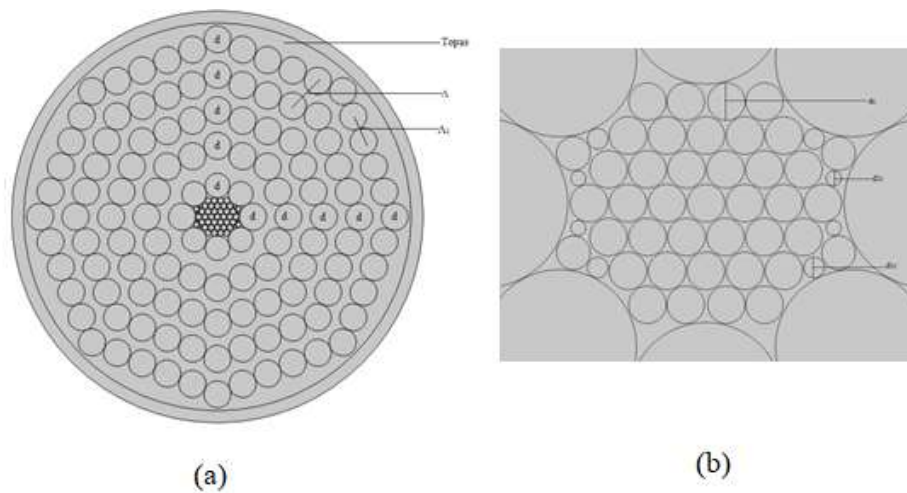


Fig. 5.1 (a) Cross section of the proposed structure (b) Zoomed core.

5.2 Proposed Geometry of Hexagonal PC-PCF

The bisecting of the geometric structure has depicted in Fig. 5.1. The air holes of the core as well as cladding of fiber geometry have organized in octagonal and hexagonal structure correspondingly that gathered 49 air holes with various radii. Five rings of air holes in the cladding have improved the confinement features lessening the effective material loss. Air holes in the core function as low index and dry air is transparent in terahertz frequency spectrum. By introducing more and more amount of air rings in the core, EML can be lowered effectively. Therefore, hexagonal structure is picked up and it has gathered 49 air rings into the core structure would be able to lower the loss.

Table 2 Optimized values for Hexagonal PC-PCF for Simulation

| Parameter | Values |
|------------------------------------|-------------------|
| No. of Air holes (cladding + core) | 169 (120+49) |
| Radius of core | 324 μm |
| Cladding air-hole radius | 98 μm |
| Core air-hole radius | 21 μm |
| AFF | 0.76 |
| PML | 9% |
| Number of mesh elements | 93,308 |

In cladding, the distance between the air holes on two adjacent rings is denoted by Λ and the distance between two adjacent air holes in the same ring is denoted by Λ_1 . The formula between these two parameters is $\Lambda_1=0.76\Lambda$. The air filling fraction has denoted here by d/Λ where d signifies the diameter of air rings. The value of AFF kept constant at 0.75 during the entire simulation. Optical mode confinement increases, and effective material loss minimized by maximizing air filling fraction. The relation between air filling fraction and core diameter is $D_{\text{core}}=2(\Lambda-d/2)$. The relation passively depends on the core porosity of the structure.

During the numerical technique porosity, frequency and core radius have varied adapting the single mode operation of the proposed structure. In the design 41 air holes are of the diameter d_c , 4 air holes of diameter d_{1c} , and 4 air holes of diameter d_{2c} have been gathered to deliver a multi radii hybrid hexagonal complex porous core. Throughout simulation the relation between d_{1c} is 0.55 times of d_c and the diameter, d_{2c} has been reduced to 0.4 times of d_c . The diameter of the cladding air holes is 4.57 times of d_c .

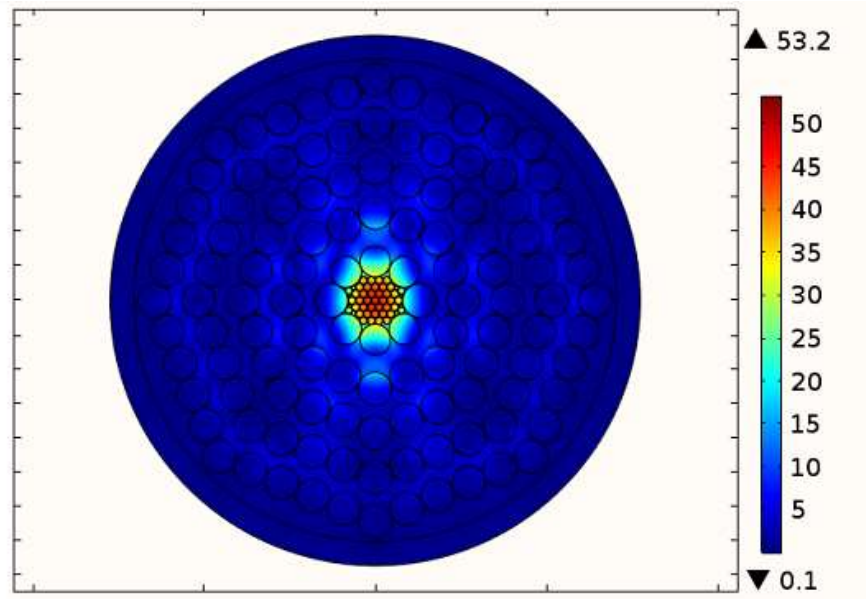


Fig. 5.2: Modal field at 81% porosity with 324 μm at 1 THz

Cyclic-olefin copolymer, Topas has been selected as host material for the proposed PC-PCF. The motive of choosing this host material over various types of polymer materials are minimum material absorption loss, high glass transition temperature and flat refractive index profile $n=1.53$ in the THz frequency spectrum. In addition, null dispersion and negligible response to humidity. Also, its ultra-violet photosensitive and decent for bio-sensing.

5.3 Simulation and Results of Proposed Design

The main optical wave confinement features of the proposed geometry had assessed involving FEM method solver COMSOL Multiphysics. During the simulation process cylindrical perfectly matched layer had been employed. The PML had set around 9% of entire radius of the total proposed PC-PCF. This PML employed due to gaining

accurateness during numerical investigations of radiating loss. During the simulation, solved mesh elements were 93630 along with 8991 numbers of boundary elements. The percentages of core power confinement presented in Fig. 5.2 while maintaining core porosity of 88% indicate that the optical mode is restricted in the geometry of the core.

In the commencement of computational investigation, V-parameter of the proposed PC-PCF had studied to confirm single mode condition of THz wave. The normalized frequency has been calculated by using the equation (1.5). Toward confirm single mode proliferation normalized frequency values expected less than or equal to 2.405. In case of fundamental mode propagation, the delivery of light power into fiber might found tough because of shrinking size of PC-PCF core radius. Thus, investigator has proposed the single mode condition for optical mode propagation.

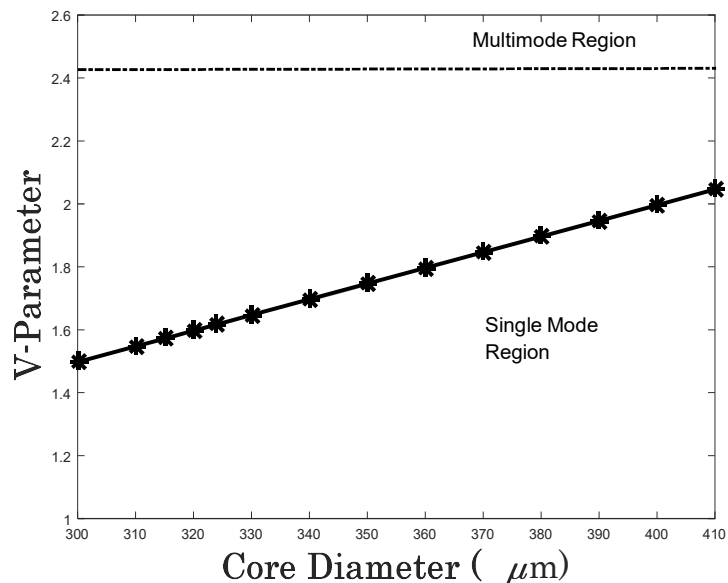


Fig. 5.3 Normalized frequency as a function of core diameter with $f=1\text{THz}$ and porosity=88%

Fig. 5.3 and Fig.5.4 displays the distinction of V - Parameter versus various values of fiber core diameter along with an operating frequency, f . From Fig 5.3 and Fig 5.4 it can be realize, normalize frequency grows as diameter of the core and frequency increases respectively.

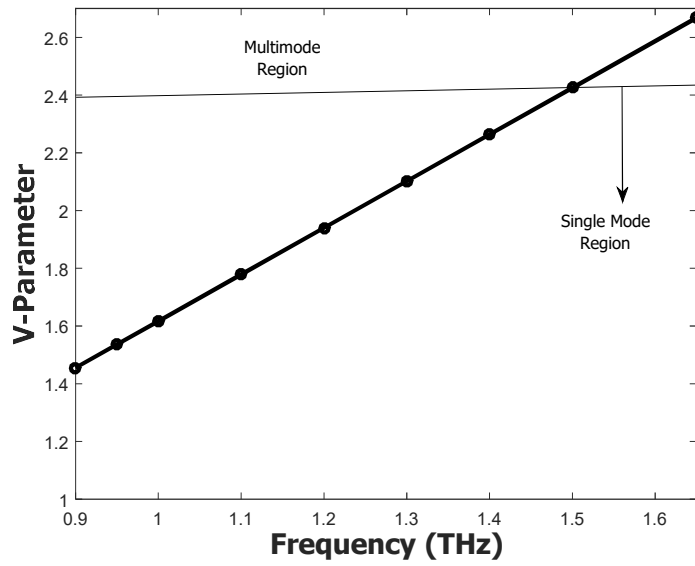


Fig. 5.4 V parameter as a function of frequency at $D_{\text{core}} = 324\mu\text{m}$ and porosity=88%.

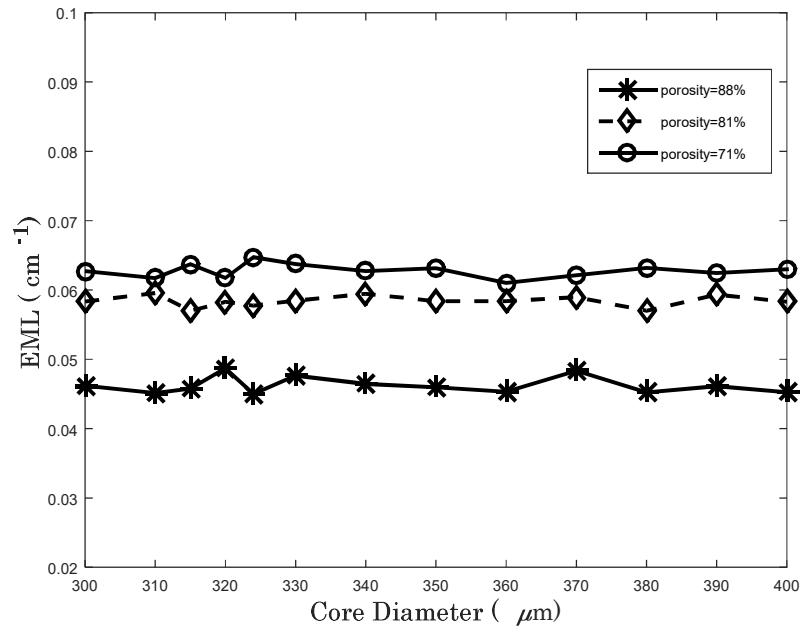


Fig. 5.5 Effective material loss as a function of core diameter at different porosities with $f=1$ THz.

Constructing a well-organized terahertz structure, the effect of losses properties needs to examine appropriately. The losses are effective material loss and confinement loss respectively. The purpose of the investigation, at beginning design phase EML can be lowered significantly. The effective material loss particularly microstructured fiber is expressed using equation 1.1.

It has been observed that the porosity declines the EML also declines. It is due to the host material reductions in the core region. Fig.5.5 depicts the the same porosity values causes notable change of material absorption loss while core diameter changes. After optimizing required parameters, the obtained result is EML 0.045 cm^{-1} at core diameter of $324\mu\text{m}$ while frequency was set to 1 THz.

The confinement loss of the crucial performance parameter in PC-PCF structure development. This parameter is function of porosity as well as total amount of air-holes designed in the cladding region. The confinement loss is achieved by considering the imaginary part of the complex refractive index profile. The confinement loss should be found by using equation 1.3.

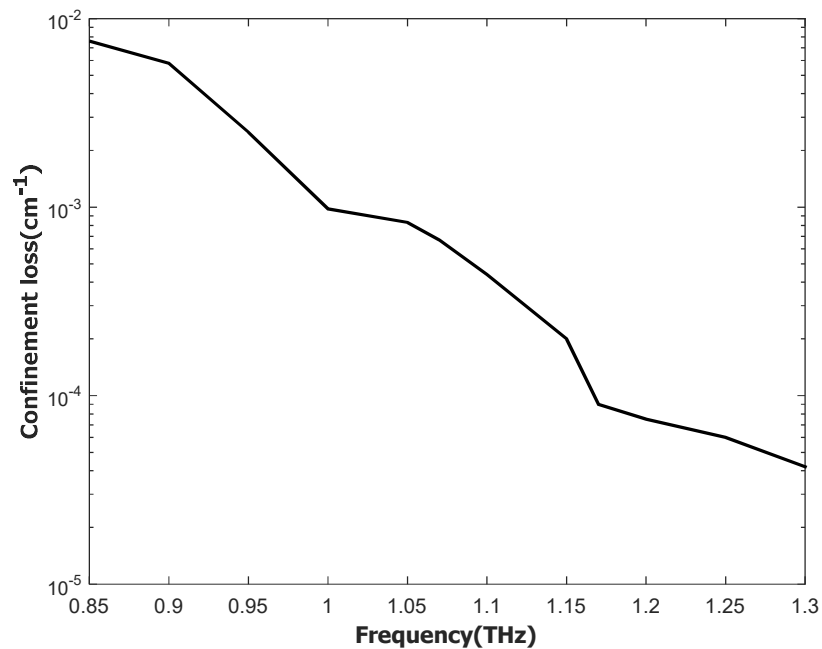


Fig. 5.6 Confinement loss versus frequency for $D_{\text{core}}=324\mu\text{m}$, porosity=88%.

From Fig. 5.6, The confinement loss found varying with changes in frequency. The Fig. validates that confinement loss declines with the escalation in frequency ranges. After numerical study at 1 THz, core diameter 324 μm and porosity of 88% confinement loss has achieved 0.00098 cm^{-1} .

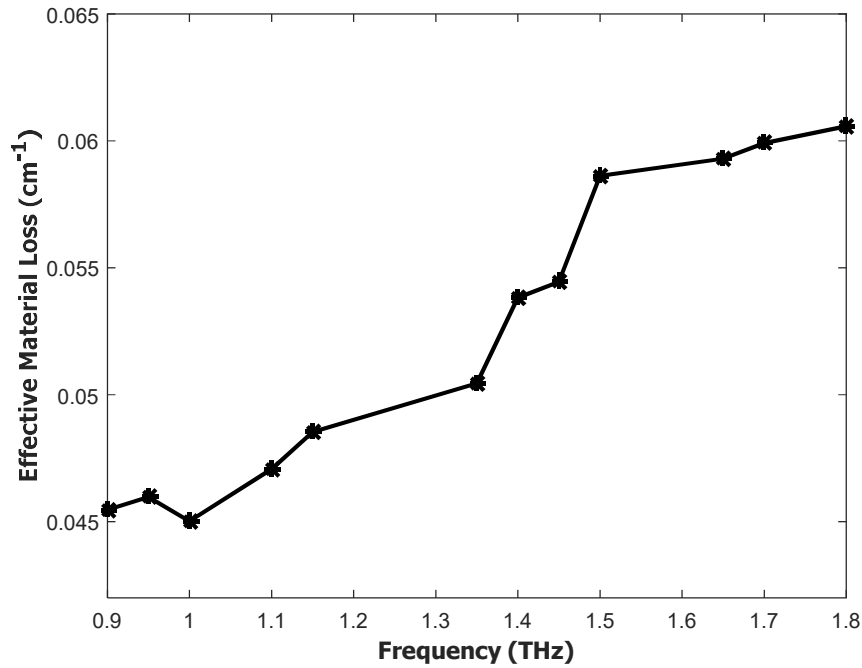


Fig. 5.7 EML versus frequency at $D_{\text{core}}=324 \mu\text{m}$, porosity=88%.

From Fig. 5.7 EML at various frequencies has been stated. The obtained finding is when the frequency increases; as a result, the EML also rises. At this point, the pragmatic the span of frequencies between 0.9 to 1.8 THz. Correspondingly, it is under single mode condition. Through seeing the above Fig., it is realized, the bulk material absorption loss of host material is changing along with the frequency span of 0.9-1.8 THz. Also, the EML is rising straightly with the frequency. Observing Figs 5.7 and Fig. 5.8, it is being understood that at 88% porosity, core diameter of 324 μm at 1terahertz of frequency, the value of material absorption loss is lowest. At the above condition EML is found 0.045 cm^{-1} as well as the core power fraction is 58.2% which is adequate for terahertz optical transmission.

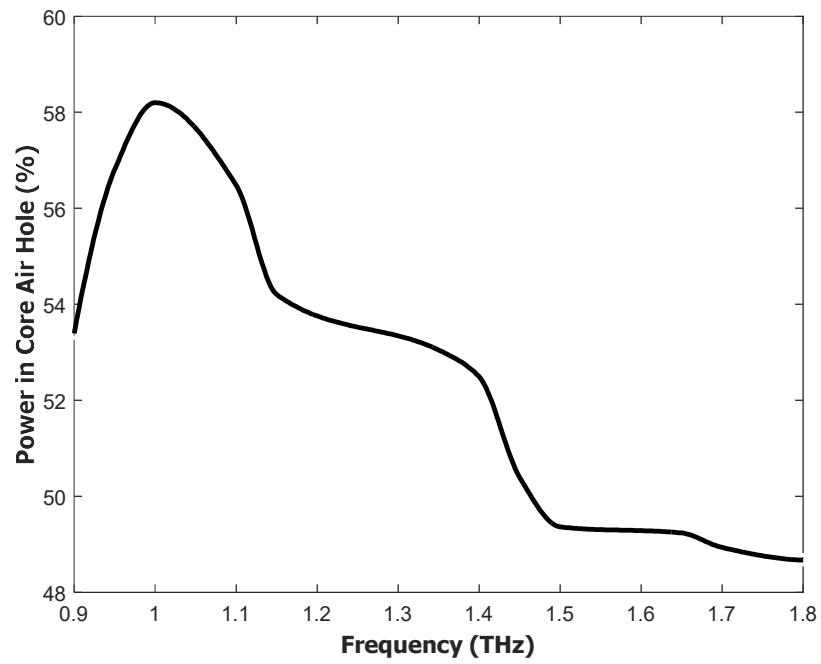


Fig. 5.8 Power fraction versus frequency at $D_{\text{core}}=324 \mu\text{m}$, porosity=88%

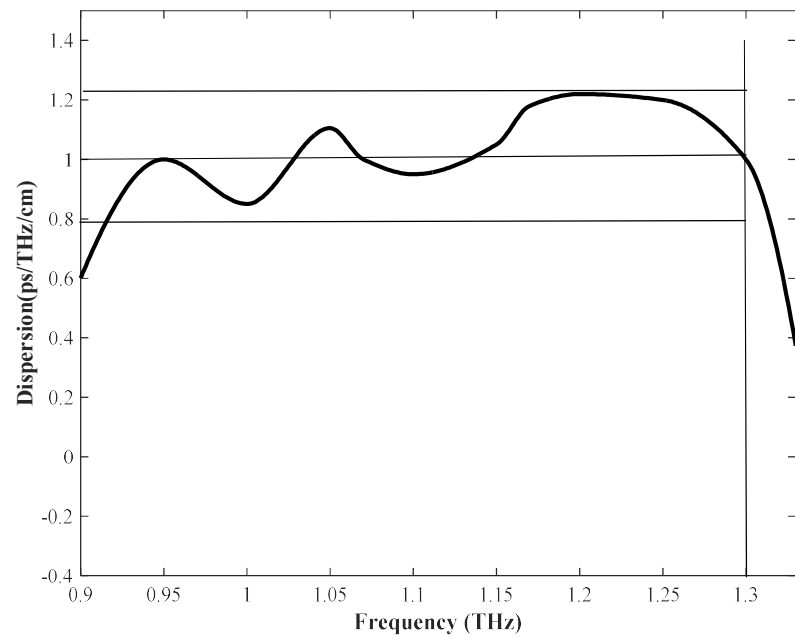


Fig. 5.9 Dispersion Characteristics at $D_{\text{core}}=324 \mu\text{m}$ and porosity=88%

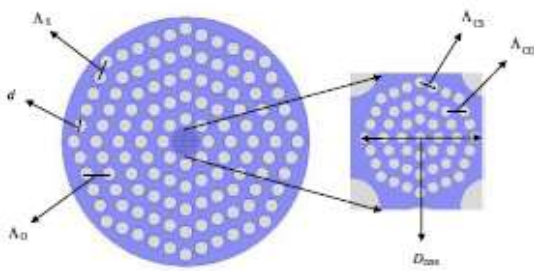
The dispersion features of the designed fiber have presented. The refractive index profile of topas has found flat in typical terahertz frequency spectrum. Therefore, material dispersion can be ignored in this spectrum. For this reason, waveguide dispersion has been adopted.

Dispersion characteristics have presented in the Fig. 5.9. It can be observed that steady dispersion has found from frequency span of 0.95 to 1.3 terahertz. Also, it is found $\beta_2 < 1.25$ ps/THz/cm and $\beta_2 > 0.8$ ps/THz/cm. Therefore, the alternation of dispersion is less than 1 ± 0.225 ps/THz/cm. The measure of dimension of β_2 for terahertz optical waveguide is in ps/THz/cm, which specifies how much signal broadens in time (ps) per unit bandwidth (THz) for the travelling distance of one centimeter. Having closely equal signal spreading designed fiber should allow multiple transmission of signal at same time is desirable.

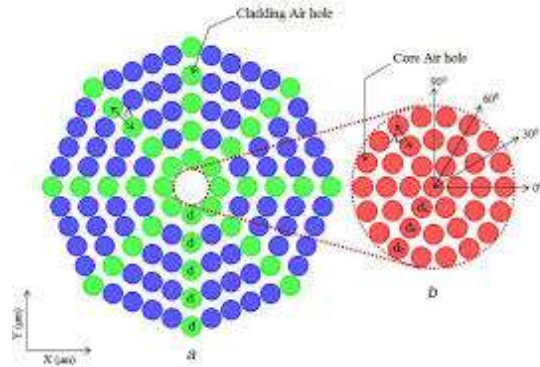
5.4 Octagonal PCF Comparisons

In this section, the proposed PCF with other reported octagonal PCFs has been compared critically in table 3.

Table 3: Octagonal PCF Comparisons

| Ref. | Design | Findings |
|------|--|---|
| [98] |  | <p>Simulation Range: 0.8 to 1.5 THz</p> <p>Material: Topas</p> <p>Core Diameter: 350μm</p> <p>Results Obtained: Porosity=60% $EML=0.045cm^{-1}$ PF=50% $CL= 10^{-4} cm^{-1}$</p> |

[99]



Simulation Range:

0.5 THz to 1.8 THz

Material: Topas

Clad. Pitch: $\Lambda_1 = 0.765 \Lambda$.

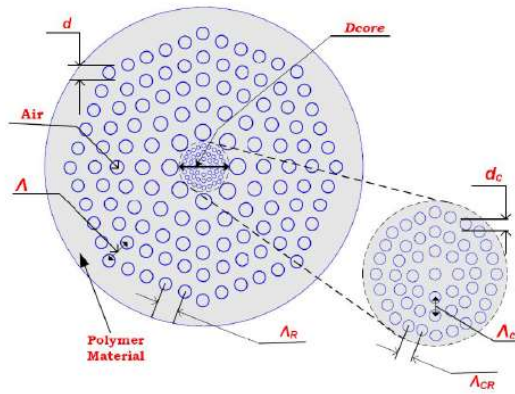
AFF= $d / \Lambda = 0.7$

Results Obtained:

EML= 0.049 cm^{-1}

PF=53.78%

[68]



Simulation Range: 0.3-1 THz

Material: Topas

AFF= $d / \Lambda = d / \Lambda = 0.68$

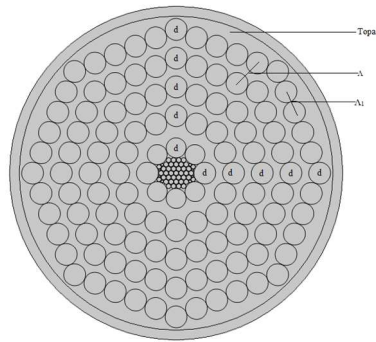
Porosity=68%

$D_{\text{core}} = 2(\Lambda - d/2) = 350 \mu\text{m}$

Results Obtained:

EML= 0.07 cm^{-1}

Proposed
Design



Simulation Range: 0.9-1.7 THz

Material: Topas

AFF= $d / \Lambda = d / \Lambda = 0.76$

Porosity=68%

$D_{\text{core}} = 2(\Lambda - d/2) = 324 \mu\text{m}$

Results Obtained:

EML= 0.045 cm^{-1}

CL= $9.8 \times 10^{-4} \text{ cm}$

Dispersion= $1 \pm 0.225 \text{ ps/THz/cm}$

It can be seen from the comparisons (table 3) that the proposed all of the designs have similar performance parameters. It can be seen that our EML is low compared to them. Finally, the proposed design is better in terms EML and power fraction than presented designs in the table 2. This is due to the structure of the proposed design.

5.5 Fabrication Method of Proposed PC-PCF

To conclude, the investigation of fabrication possibility of this proposed PC-PCF will be discussed. From the understanding of the proposed PC-PCF, as there is outstanding development in PC-PCF fabrication methods leads to in the possible scope of fabrication. Stack and drilling, capillary stacking, and sol-gel methods can be considered for PCF fabrication. In higher porosity design, the sol-gel method become effective and fabrication was precise while porosity was 87% [30]. The stack and draw method fail to create circular airhole. Drilling method does not appropriate for the proposed structure of PC-PCF as the procedure is restricted to small number of airholes. Since, the proposed structure made of a good number of micro-structured circular shape airholes, stack and draw methods are the top adoptions to fabricate where the dimension of the proposed PC-PCF can be adjusted easily.

5.6 Summary of the Chapter

A reasonably easier topas as a host material-based geometry having low loss property of 0.045 cm^{-1} , while the achieved core power fraction is 58.2% has been proposed in this chapter. Here, the proposed structure of the fiber is better compared to formerly proposed designs due to lessen value of EML, better core power fraction and easiness in the geometry. The design would be a competent candidate for the terahertz transmission.

In the next chapter a new design has been proposed (Octa-Hybrid geometry) to minimize losses and to increase birefringence to maintain polarization state of the proposed fiber. The proposed fiber will be potential candidate in the similar field.

CHAPTER 6

OCTAGONAL CLADDING –HYBRID CORE PC- PCF

In this chapter octagonal cladding and hybrid core PC-PCF has been proposed. This design has been chosen to break the symmetry of the core to achieve high birefringence to maintain polarization state of the PCF. All the parameters are optimized numerically to have band gap around 0.73 THz. The design methodology will be discussed in the following section.

6.1. Introduction

The numerical investigation of a low loss as well as highly birefringent hybrid porous core accompanied octagonal cladding geometry for terahertz optical signal direction is examined. The designed porous core photonic crystal fiber (PC-PCF) provide concurrently low effective material loss (EML) in addition to high birefringence in the THz frequency spectrum span of 0.6- 1.05 THz accompanied by single mode performance. To achieve high birefringence, the author has introduced asymmetry in the core region by employing elliptical and circular air holes respectively. The numerical outcomes gained utilizing finite element method solver. This FEM solver is COMSOL Multiphysics which ensures effective material loss of 0.044 cm^{-1} while having high birefringence of ~ 0.043 at 0.73 THz. The confinement loss $9.7 \times 10^{-4} \text{ cm}^{-1}$ was obtained. So, the total loss can be considered as the EML. Hence, the fiber is expected to be beneficial for various terahertz polarization maintaining state applications.

6.2 Design Methodology of Octa-Hybrid PC-PCF

Fig. 6.1 shows the cross-section of the proposed geometric structure. Inside the cladding region, the separation between the air-holes on two adjacent rings is meant by Λ and separation between two adjacent air-holes in the same ring is symbolized by Λ_1 . The connection between these two cladding parameters stated by $\Lambda_1=0.765\Lambda$. Two different sized air-holes having diameter d and $d1$ are exploited to fill the five layered cladding region. The diameter of $d1$ is set 0.91 times of d . The core with diameter has relation, $D_{core} = 2(\Lambda - d/2)$ has covered using air-holes of elliptical and circular shapes.

The four air holes of diameter $d1_c$ are gathered inside the core. Eight circular air holes of diameter $d2_c$, six circular holes of diameter of $d3_c$, and holes of diameter $d4_c$ are being gathered accompanied by four circular air holes and fifteen elliptical shape air holes inside the core. The core diameters $d2_c$, $d3_c$ and $d4_c$ are correlated to $d1_c$ 0.75 times, 0.1 times and 0.075 times respectively. The length of the major axis of the ellipse is twice that of the diameter of the largest circular core air hole denoted $d1_c$. The length of the minor axis is equivalent to $d1_c$. The AFF has been kept settled at 0.76 and the additional increment to this value may cause unwanted overlapping of domains. Thus, it is set to 0.76 during the entire simulation process.

Topas has been selected as host material for the proposed PC-PCF. The motive of choosing this host material over various types of polymer materials are minimum material absorption loss, high glass transition temperature and flat refractive index profile $n=1.53$ in the THz frequency spectrum. In addition, null dispersion and negligible response to humidity.

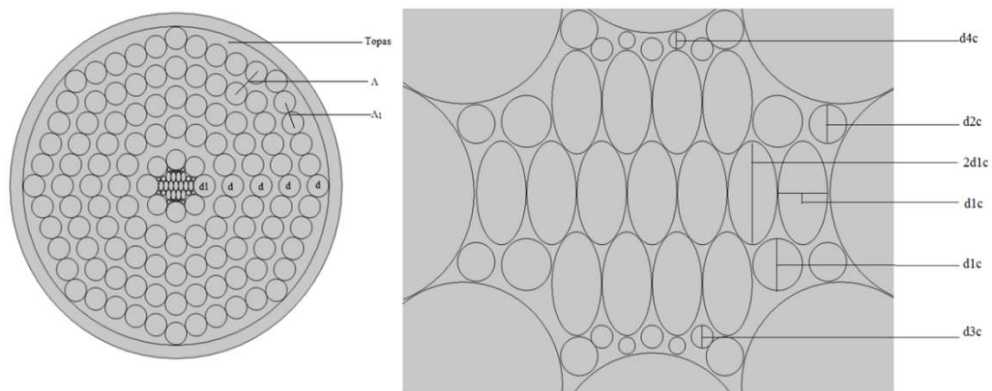


Fig. 6.1 (a) Cross section of the proposed Geometry (b) Zoomed core

6.3 Results and Discussions of the Proposed PC-PCF

The main optical wave confinement features of the proposed geometry had assessed involving FEM method solver COMSOL Multiphysics. During the simulation process cylindrical perfectly matched layer had been employed. The PML had set around 9% of entire radius of the total proposed PC-PCF. This PML employed due to gaining accurateness during numerical investigations of radiating loss. During the

numerical investigation, solved mesh elements were 109092 including 9683 numbers of boundary elements. The percentages of core power confinement presented in Fig. 6.2 while maintaining core porosity of 76% indicate that the optical mode is restricted in the geometry of the core.

Table 4 Optimize Parameter for the simulation Octa Hybrid at 0.73 THz

| Parameter | Value |
|--------------------------|-----------------------|
| No. of Air holes | 165(120+45) |
| Radius of core | 320 μm |
| Cladding air-hole radius | $9.8 \times 10^{-5}m$ |
| Core air-hole radius | $2.2 \times 10^{-5}m$ |
| AFF | 0.76 |
| PML | 9% |
| Number of elements | 109,092 |

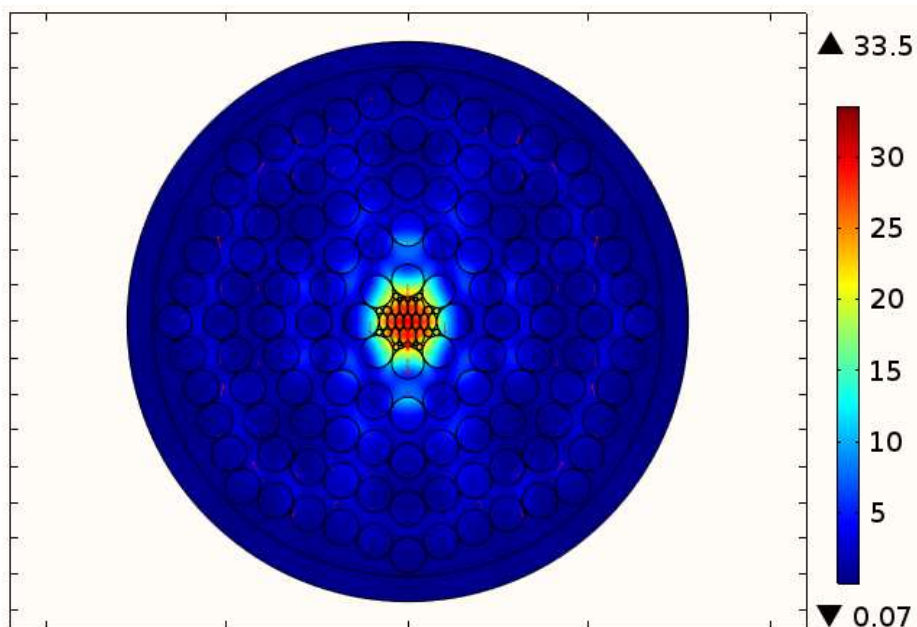


Fig. 6.2 Modal field distributions of the PC-PCF geometry at porosity 76%, $D_{\text{core}} = 320\mu\text{m}$, 0.73THz

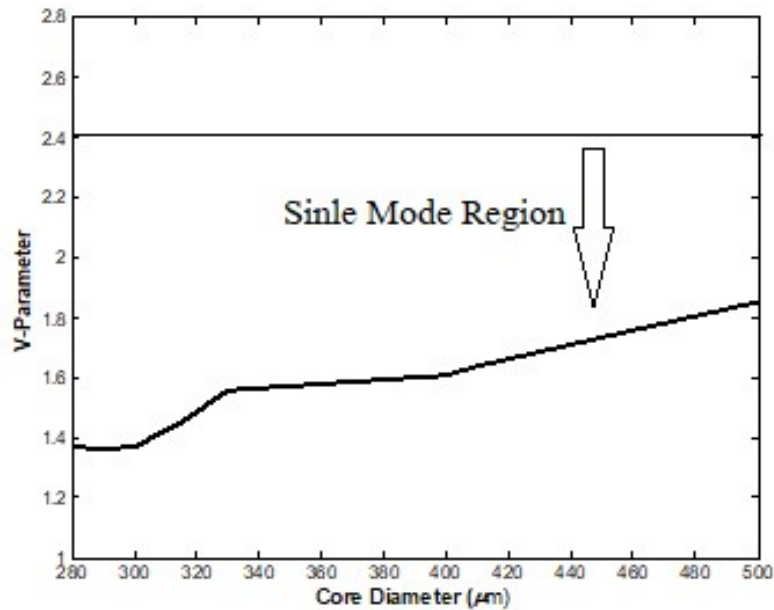


Fig. 6.3 Normalized frequency with core diameter where frequency 0.73 THz, porosity of 42%

In the commencement of computational investigation, V-parameter of the proposed PC-PCF had studied to confirm single mode condition of THz wave. The normalized frequency has been calculated by using the equation 1.5. Toward confirm single mode proliferation normalized frequency values expected less than or equal to 2.405.

The Fig. 6.3 depicts the fiber shall function in single mode condition as normalized frequency at 320 μm is 1.38 which is well underneath 2.405. In the opening of numerical investigations, normalized frequency of the proposed geometry structure has studied to confirm single mode condition of THz waveguide.

The birefringence arises from the asymmetry of the geometry of the fiber core or by breaking symmetry of the core structure intentionally. The birefringence is an absolute value signifies the difference between the refractive index of two degenerated polarization mode. They are X-polarization and Y-polarization. The linear rise and fall have observed in Fig. 6.4. During the numerical investigations of this Fig. are core diameter 320 μm, porosity 42% and frequency is 0.73 THz. The obtained value of birefringence is 0.43 which is decent value for THz applications. The rise and fall in the Fig. 6.4 due to some reason and they are the cladding pitch is lower than the

wavelength, due to Faradays effect and finally the host material is biaxial property of material. Furthermore, the complex geometric structure where the asymmetry of the core broken purposefully to achieve birefringence.

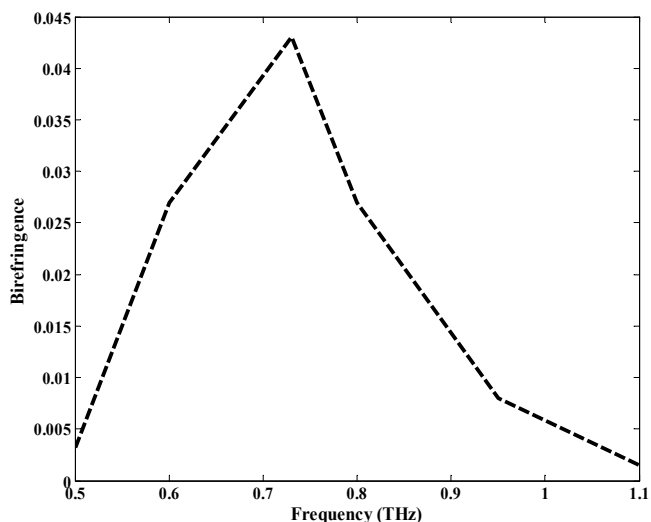


Fig. 6.4 Birefringence versus frequency in THz

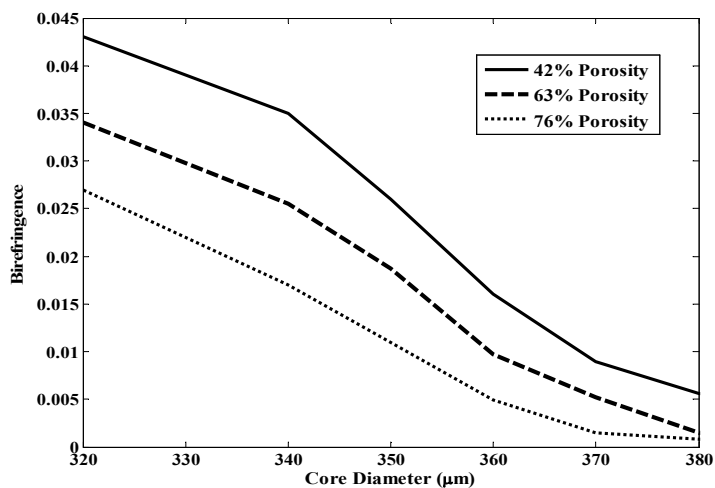


Fig. 6.5 Birefringence versus D_{core}

The characteristics of proposed birefringence for this proposed fiber geometry as a function of function of core diameter shown in Fig. 6.5. The relation between porosity and birefringence is found inverse relation. Similarly, the same relation has observed for radius of the core. The fact is the electric field strength is higher in the smaller core which accelerate to degeneracy of polarization state due to above mentioned factors and

separation is higher. When the core diameter increases the air hole radius increase as a result field strength decrease which results in lower birefringence value.

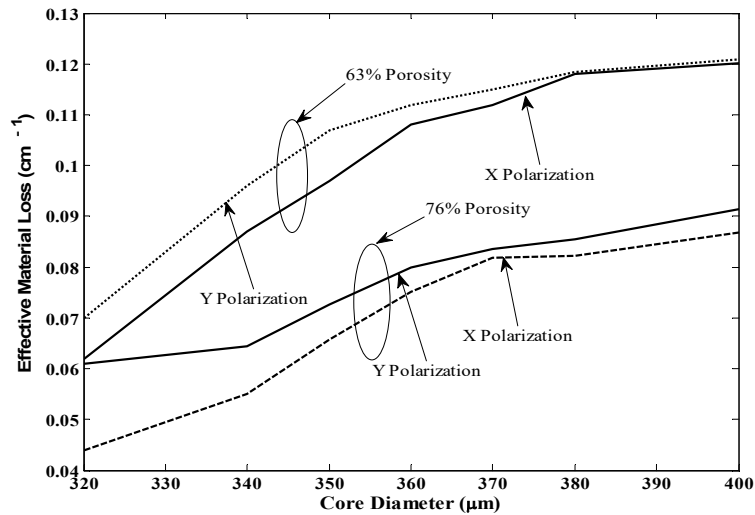


Fig. 6.6 EML versus core diameters for 63% and 76% at 0.73 THz

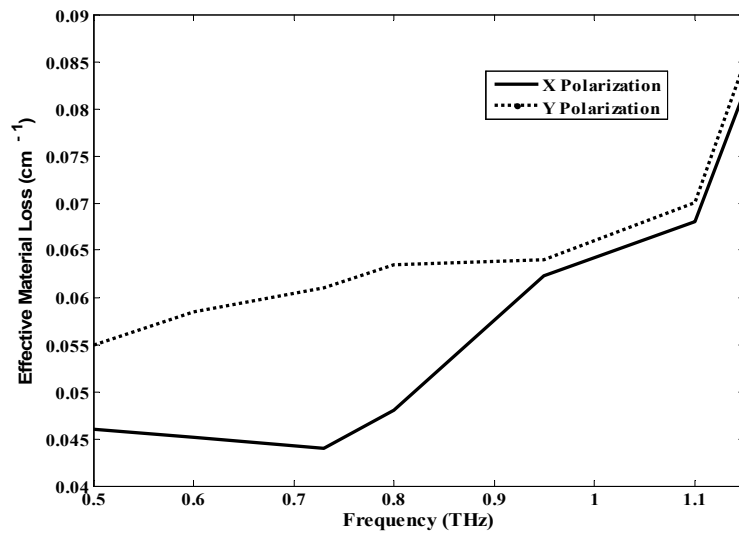


Fig. 6.7 EML versus frequency at core diameter at 320μm while porosity 42%

The foremost apprehension of designing geometry of the PC-PCF is the minimization of material absorption loss. The minimization of porosity is increases EML which is not desired. Similarly, minimization of porosity is increases value of

birefringence which as expected. The tradeoff between these two parameters should be optimized through geometrical structure of the proposed fiber.

The EML for X and Y polarization have depicted in Fig. 6.6 while porosity is set 63% and 76% for the simulation respectively. The X-polarization exhibits lower EML compared to Y-polarization. The optimized result for EML is achieved at 76% porosity which is 0.044 cm^{-1} . The scattering of light causes when the diameter of the core increase. The same phenomena can be found here from the Fig. 6.6. Thus, the effective material loss increases while the diameter of the core increases.

The behavior of EML for two degenerated optical mode with respect to variation of frequency has presented in Fig. 6.7. During the obtaining the optimize value EML, the porosity has set to 76%, frequency 0.73 THz and core diameter to $320 \mu\text{m}$. Minimum value of EML has found in case X-polarization which is 0.044 cm^{-1} .

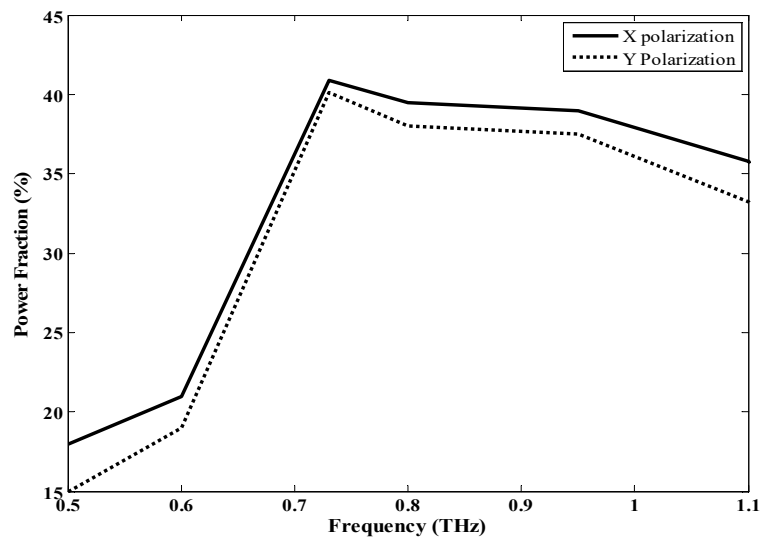


Fig. 6.8 Core power fraction versus various frequencies while porosity 42% and at core diameter $320 \mu\text{m}$.

The fixed value of porosity is 42% and diameter is $320 \mu\text{m}$, confinement loss versus frequencies ranging from 0.5 THz to 1.1 THz illustrated in the Fig. 6.8 for two degenerated modes. From the Fig., the percentages of power confined in the core region for both X polarization and Y polarization are gained at 0.73 THz are 41.52% and

39.11% respectively. So, the X-polarization exhibits better power confinement through the core.

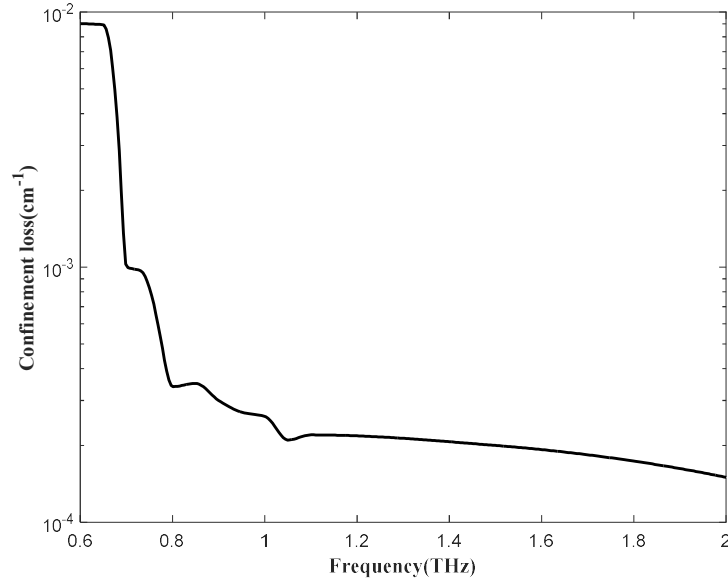


Fig. 6.9 Confinement loss is changing along with frequency at 320 μm while porosity set to 42%

The confinement loss of the crucial performance parameter in PC-PCF structure development. This parameter is function of porosity as well as total amount of air-holes designed in the cladding region. The confinement loss is achieved by considering the imaginary part of the complex refractive index profile.

The confinement loss depending on frequency has illustrated in the Fig. 6.9. The Fig. exhibits when the frequency rises, the confinement loss is reduced. In this proposed geometry structure, at $f=0.73$ THz, $D_{core}= 320\mu\text{m}$ and 42% porosity, the confinement loss of $9.7 \times 10^{-4} \text{ cm}^{-1}$ has gained which is insignificant compared to the achieved effective material loss of 0.044 cm^{-1} .

The Fig. 6.10 illustrates dispersion and frequency after altering the value of porosity of the geometry $\pm 5\%$ from the optimal value. The dispersion characteristics has been shown from 0.6 THz to 1.1 THz. The total variation of dispersion is found from 0.6 to 1 THz is $5.3 \pm 0.05 \text{ ps/THz/cm}$. The $\pm 5\%$ variation of the porosity yields same shape preserving results.

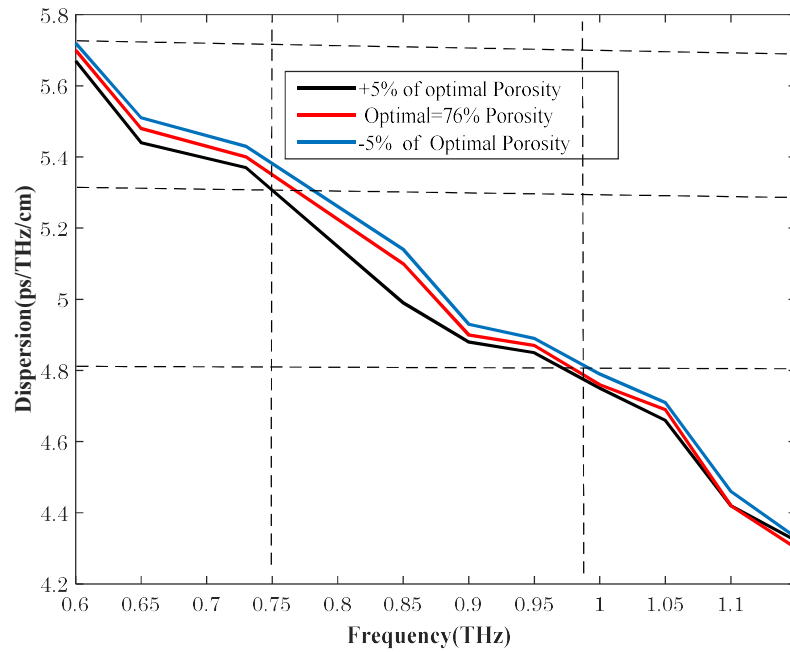


Fig. 6.10 Dispersion characteristics as a function of frequency at 1 THz at core diameter 320 μ m

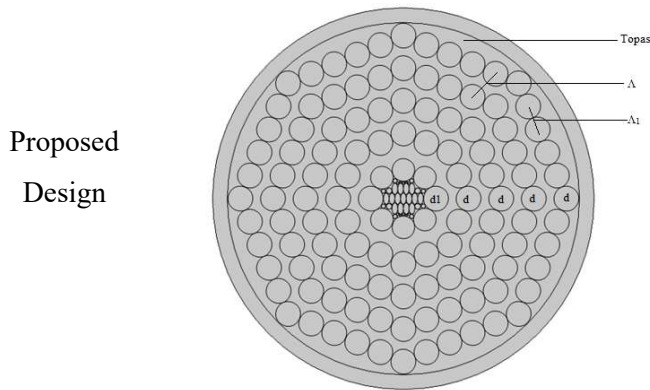
Lastly, the author has studied possible fabrication method for proposed PC-PCF. At the core of the geometry has air rings with various sizes. The implementation of the design geometry will be challenging because of its complex porous core. As expertise is evolving continuously, the implementation of the proposed geometry is therefore comprehended. The capillary stacking and sol-gel methods are the top selection toward fabrication process.

6.4 Octagonal Hybrid PCF Comparisons

In this section, the proposed PCF with other reported octagonal PCFs has been compared critically in table 5.

Table 5 Octagonal Hybrid PCF Comparisons

| Ref. | Design | Findings |
|-------|--------|--|
| [58] | | <p>Simulation Range: 0.8 to 1.4 THz</p> <p>Material: Topas</p> <p>Results Obtained: 300μm</p> <p>Dispersion= 0.85 ± 0.05 ps/nm.cm</p> <p>BR= 0.08</p> <p>EML= 0.08 cm⁻¹</p> <p>PF=41%</p> <p>CL= 10^{-13}</p> <p>Not Shown: V-parameter</p> |
| [80] | | <p>Simulation Range: 0.5 to 1.8Thz</p> <p>Material: Topas</p> <p>Results Obtained: 350μm</p> <p>Dispersion= 0.53 ± 0.07 ps/nm.cm</p> <p>BR= 0.086(50%porosity), ~0.38(80% porosity)</p> <p>EML= 0.05 cm⁻¹</p> <p>CL= 10^{-9}</p> |
| [100] | | <p>Simulation Range: 2-4 THz</p> <p>Material: Topas</p> <p>BR= 0.03</p> <p>EML= 0.06 cm⁻¹</p> <p>PF=30%</p> <p>CL= 0.01 cm⁻¹</p> |



Simulation Range: 0.6-1.1 THz

Material: Topas

AFF= $d/\Lambda = d/\Lambda = 0.75$

Porosity=42%

$D_{\text{core}} = 2(\Lambda - d/2) = 320 \mu\text{m}$

Results Obtained: 0.73 THz

EML= 0.044 cm^{-1}

CL= $9.7 \times 10^{-4} \text{ cm}^{-1}$

BR=0.043

It can be found from the comparisons (table 5), the proposed design has presented more performance parameters. Also, material and geometric parameters are different as the operating ranges of fibers are different. The design reported in the references [58,80] is in our simulation range. It can be found that proposed design has higher EML compared to them. Finally, the proposed design exhibits competitive performance with references in [58, 80]. Further, better behavior over reference [100] due to greater number of air holes inside the core.

6.5 Summary of the Chapter

A novel porous geometry design having hybrid core has been proposed in the chapter. This PC-PCF is significant for polarization state preserving applications in terahertz spectrum. It is revealed that despite of breaking symmetry of the fiber core, still the proposed PC-PCF achieved EML of 0.044 cm^{-1} while the birefringence is found ~ 0.043 . The proposed geometry design is very complex. So, the fabrication method will face lots of challenges. The fabrication method could be combination of extrusion and sol-gel technique. For polarization maintaining as well as for long distance terahertz communication the proposed design may be examined.

The circular core and circular cladding PC-PCF has been proposed in next chapter to minimize losses further as well as would be less complex for fabrication. The background material would be same that is Topas.

CHAPTER 7

CIRCULAR POROUS CORE PHOTONIC CRYSTAL FIBER

7.1 Introduction

The author has presented a comprehensive numerical investigation of a low loss PC-PCF with circular cladding and core structure for terahertz optical wave propagation. The anticipated PC-PCF exhibits low EML while having high power fraction in the frequency spectrum of 0.8- 1.15 THz accompanied by single mode operation at core diameter 350 μm . The numerical outcomes attained employing finite element method (FEM) that established EML of 0.04 cm^{-1} and high core power fraction of 55.8% at 1.05 THz working frequency with porosity of 84%. Also, the confinement loss obtained was $1.89 \times 10^{-4} \text{ cm}^{-1}$. So, the total loss can be considered as the EML. During the numerical investigation, solved mesh elements were 37562 including 4685 numbers of boundary elements. Furthermore, the proposed porous core structure displays moderately higher percentages of core power fraction, and lower confinement loss. The geometry structure proposed here in this chapter can be fabricated utilizing capillary stacking and sol-gel methods. The PC-PCF can be a strong candidate in ultra-broadband communication.

7.2 Geometry of the proposed Circular PC-PCF

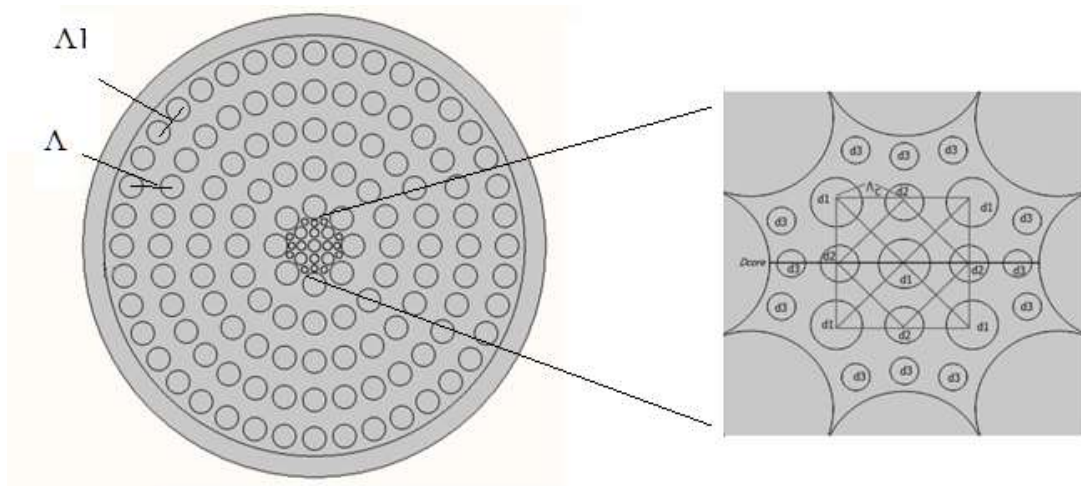


Fig. 7.1: Cross-section of the proposed PC-PCF.

The cross-section of the proposed circular core PC-PCF has presented in Fig. 7.1. The core have 21 circular air holes and radius of each air hole is correlated with the core diameter (D_{core}). The five air holes in the middle have radius of $d_1 = 0.13 D_{core}$, the next four air holes have $d_2 = 0.1 D_{core}$ and finally outmost air holes have $d_3 = 0.7 D_{core}$ of radius. The core pitch (Λ_c) is defined as the distance between two adjacent air holes in the core, which is chosen $0.12 D_{core}$. The Core pitch has carefully chosen in order to keep optical power inside fiber core. The cladding contains five layers of circular air-holes. The pitch (Λ) is separation between two adjacent air holes. The gap between two air holes of same layer is $\Lambda 1$. The core pitch is matched considering diameter of the core. The relation can be expressed as $D_{core} = 2 (\Lambda - d/2)$. The normalized diameter (d/Λ) was kept fixed at a value as high as 0.75 for a good confinement factor.

Table 6 Optimize Parameter for Circular PCF simulations at 1.05 THz

| Parameter | Values |
|-----------------------------------|---|
| No. of Air holes (Cladding+ Core) | 141(120+21) |
| Radius of core | 350 μm |
| Cladding air-hole radius | $1.014 \times 10^{-4} \text{m}$ |
| Core air-hole radius | Varies:13%, 10%, and 7 % of D_{core} |
| AFF | 0.76 |
| PML | 10% |
| Number of elements | 37562 |

Topas has been selected as host material for the geometry structure. The motive of choosing this host material over various types of polymer materials are minimum material absorption loss, high glass transition temperature and flat refractive index of 1.53 in the THz frequency spectrum. In addition, null dispersion and negligible response to humidity.

7.3 Numerical results and discussions

To calculate the optical light confinement features of the proposed geometry structure, FEM build commercially available COMSOL multiphysics has been adapted. Afterward, PML border condition is employed around the exterior part of computational domain for approximation of confinement losses. The numerical investigation has executed inside the range of 320–400 μm of core diameter with an intermission of 5 μm and within 0.7–1.3 THz of frequencies through break of 0.01 THz at 320 μm of D_{core} for various porosities.

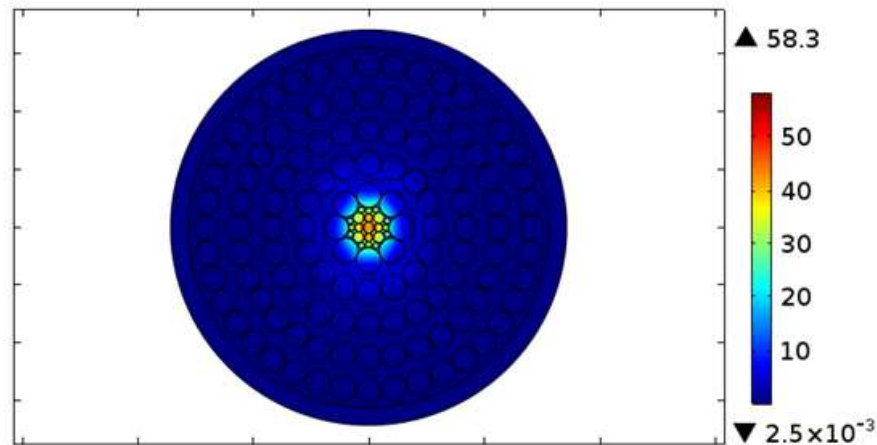


Fig. 7.2 Electric field distributions of the proposed PCF at 84% porosity at core diameter $D_{\text{core}} = 350 \mu\text{m}$

In the commencement of computational investigation, V-parameter of the proposed PC-PCF had studied to confirm single mode condition of THz wave. The normalized frequency has been calculated by using the equation 1.5. Toward confirm single mode proliferation normalized frequency values expected less than or equal to 2.405. In case of fundamental mode propagation, the delivery of light power into fiber might found tough because of shrinking size of PC-PCF core radius. Thus, investigator has proposed the single mode condition for optical mode propagation.

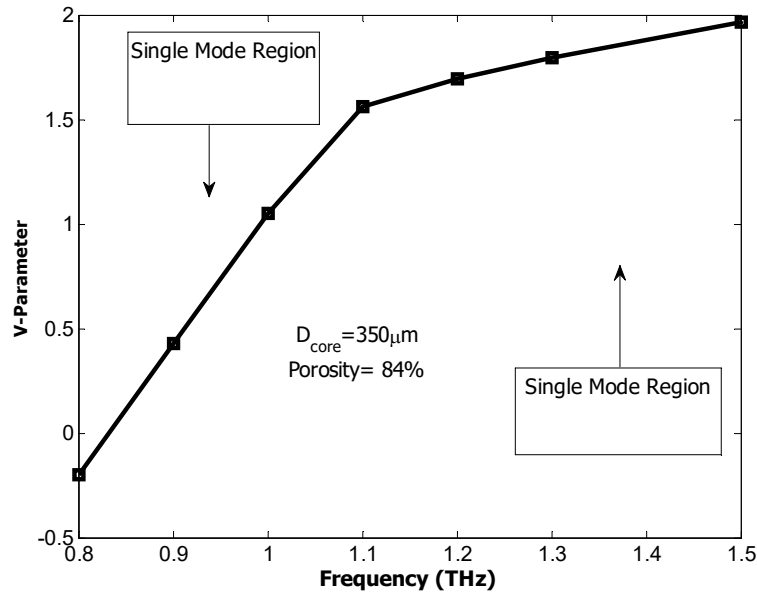


Fig. 7.3 V parameter versus frequency

The foremost concern for the fiber is minimization of EML that have to perform by the equation 1.8. The EML depends on operating frequency having various core porosities is shown in Fig. 7.4. The frequency response of EML increases with frequency from 1.05 THz. This behavior due to the optical frequency is proportional to EML. Therefore, it is found that when the frequency rises, EML rises accordingly. Also, from Fig. 7.4, the EML is lowest and core power fraction has found high at 1.05 THz frequency. It has been found that at 1.05 THz, $D_{\text{core}} = 350 \mu\text{m}$, and 84% porosity optimal results for the design structure can be achieved. The achieved value of EML is visibly better than formerly reported literatures [69, 84].

The EML versus function of diameter of the core by means of various core porosities has illustrate in Fig. 7.5. At this point, EML mostly rely on the amount of background material available inside the porous core. The amount of material inside the core rely on core porosity. Higher values of core porosity results in reducing host material from the core and thus, the EML decreases. It can be noticed form Fig. 7.5 that lowest minimum value of EML is 0.04 cm^{-1} achieved at $350 \mu\text{m}$ with 84% porosity.

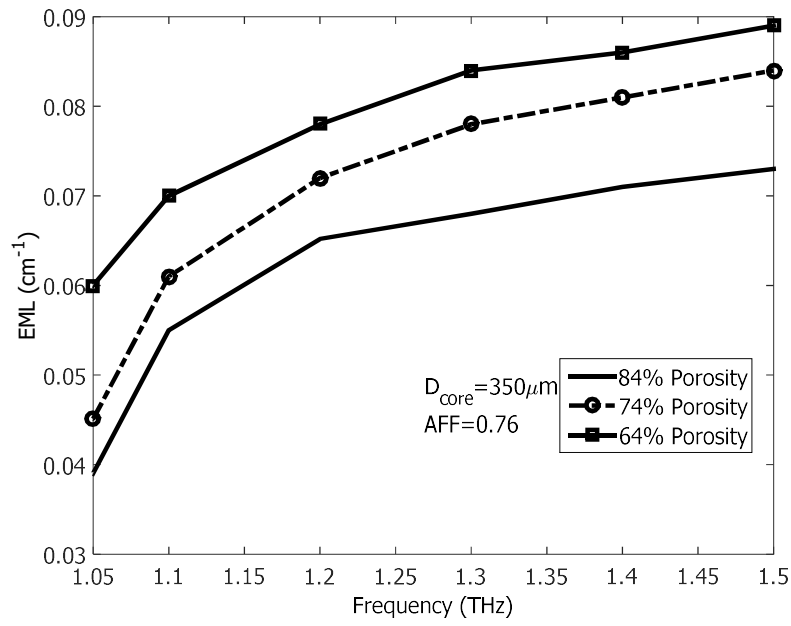


Fig. 7.4 Behavior of EML with frequency at 350 μm

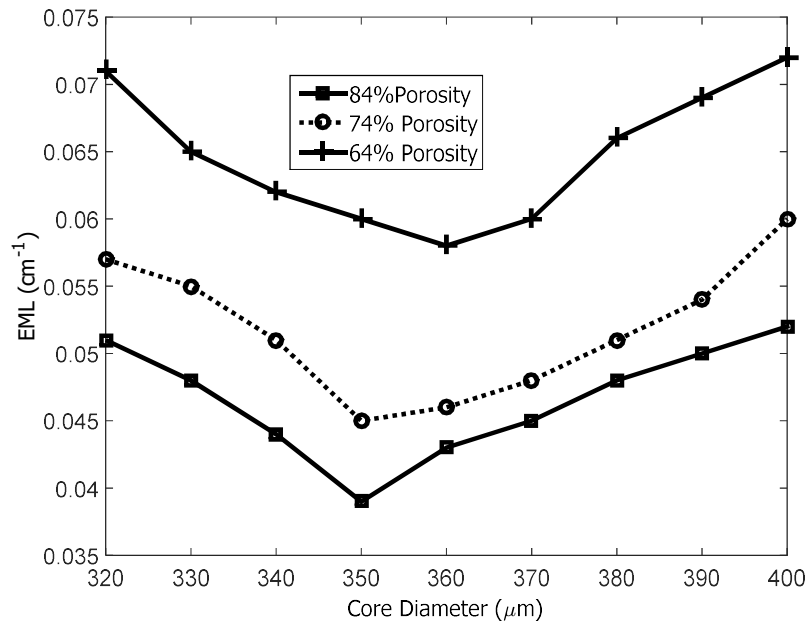


Fig. 7.5 Behavior of EML with Core diameters at 1.05 THz

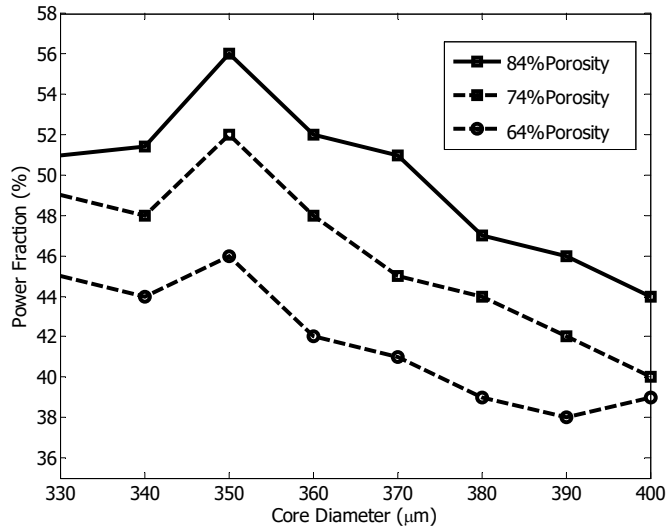


Fig. 7.6 Behavior of power fraction versus core diameters while frequency 1.05THz.

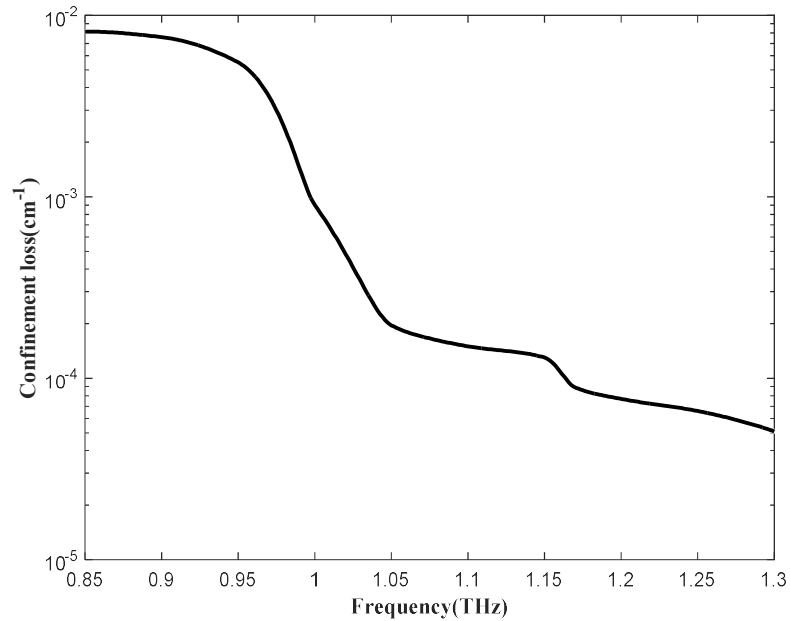


Fig. 7.7 Confinement loss vs frequency at 350μm using porosity of 84%

For various core porosities, the core power fraction is variable of fiber core diameter has represented in Fig. 7.6. If the core porosity is increased, the core power fraction similarly rises. This happens due to increase in core porosity directly decreases the amount of solid material inside core area. Therefore, maximum mode power travels

inside air holes in absence of solid material. This helps to obtain higher value core power fraction. Thus, from Fig. 7.7, for 84% core porosities, uppermost value of 55.8% is gained while core diameter is set to 350 μm and frequency is 1.05 THz.

The confinement loss of the crucial performance parameter in PC-PCF structure development. This parameter is function of porosity as well as total amount of air-holes designed inside cladding region. The confinement loss is found from the complex part of the index of refraction throughout the numerical simulation. The confinement loss should be found by using equation 1.3.

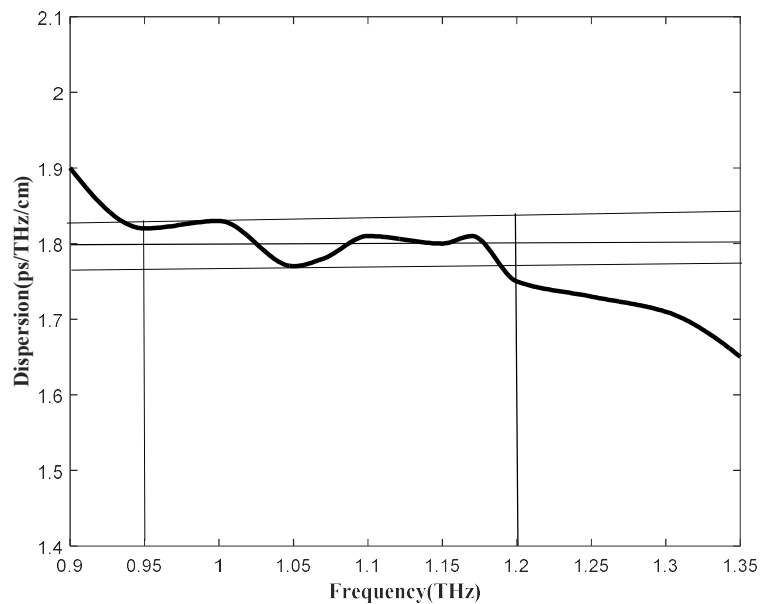


Fig. 7.8 Dispersion as a function of frequency at 350 μm using porosity of 84%

The confinement loss versus frequency while 84% porosity of the core represented in Fig. 7.7. The Fig. displays as the confinement loss is insignificant compared to the gained EML. As, the confinement loss of $1.89 \times 10^{-4} \text{cm}^{-1}$ was achieved. The confinement loss is decreasing along with increasing frequency. This happens due to increase in frequency the maximum propagating optical power starts to tighten in the desired porous core region. For further minimization of confinement loss, the amount of air holes inside cladding region should be increased. Fabrication process might be challenging for further incrementation number of air-holes in both core-cladding regions.

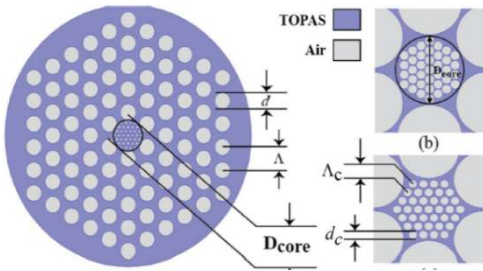
Dispersion characteristics have presented in the Fig. 7.8. It can be observed that steady dispersion has found from frequency span of 0.95 to 1.2 terahertz. Also, it is found $\beta_2 < 1.825$ ps/THz/cm and $\beta_2 > 1.78$ ps/THz/cm. Therefore, the alternation of dispersion is less than 1.8 ± 0.225 ps/THz/cm. The measure of dimension of β_2 for terahertz optical waveguide is in ps/THz/cm, which specifies how much signal broadens in time (ps) per unit bandwidth (THz) for the travelling distance of one centimeter. Having closely equal signal spreading designed fiber should allow multiple transmission of signal at same time is desirable.

Finally, the investigation of fabrication feasibility of this proposed geometry structure shall be explored. From the understanding of the proposed PC-PCF, as there is outstanding development in PC-PCF fabrication methods leads to in the possible scope of fabrication. Stack and drilling, capillary stacking, and sol-gel methods can be considered for PCF fabrication. The stack and draw process fail to create circular airhole. Drilling method does not appropriate for the proposed structure of PC-PCF as the procedure is restricted to small number of airholes. Since, the proposed structure made of a good number of micro-structured circular shape airholes, capillary stacking as well as sol-gel methods are the top adoptions to fabricate where the dimension of the proposed geometry of PC-PCF can be tuned spontaneously.

7.4 Circular comparisons

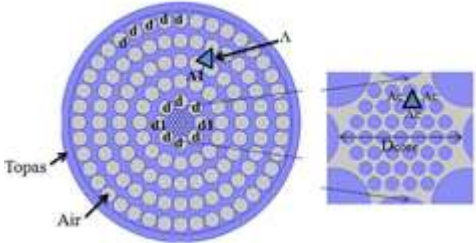
In this section, the proposed PC-PCF with other reported circular designs has been compared critically in table 7.

Table 7 Circular PCF Comparisons

| Ref. | Design | Findings |
|------|---|--|
| [62] |  | <p>Simulation parameters:</p> <p>0.5 to 1.08THz</p> <p>Material: Topas</p> <p>Porosity=60%</p> <p>Core Diameter =300μm</p> <p>Results Obtained: 1 THz</p> <p>EML:0.066 cm⁻¹</p> |

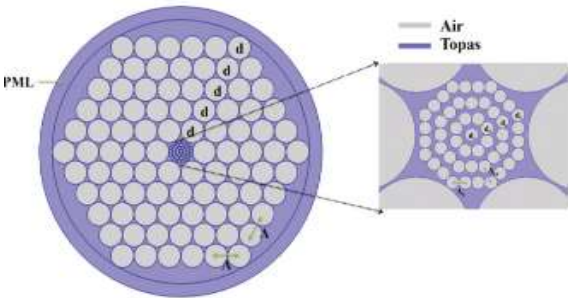
$CL= 10^{-4} cm^{-1}$

[69]



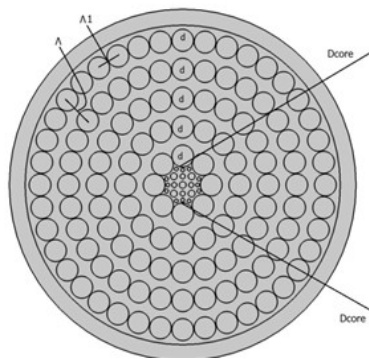
Simulation Range:
 9 to 1.3 THz
 Material: Topas
 Porosity:81%
 Core Diameter: 300μm
 Results Obtained: 1THz
 $CL= 10^{-3} cm^{-1}$
 $EML= 0.043 cm^{-1}$
 PF 47%

[84]



Simulation Range:
 0.3 to 1 THz
 Material: Topas
 Core Diameter: 400μm
 Results Obtained: 1THz
 $CL= 10^{-5} cm^{-1}$
 $EML= 0.08 cm^{-1}$

Proposed design



Range: 0.8 to 1.5 THz
 Material: Topas
 At 84% core porosity, $f = 1.05$ THz frequency
 $D_{core}=350\mu m$
 $PF=55.8\%$
 $EML=0.04cm^{-1}$
 $CL=1.89 \times 10^{-4} cm^{-1}$

It can be seen from the comparisons (table 7) that the proposed design has presented more performance parameters. The design reported in [69,84] is in our simulation range.

It can be found, the EML is low compared to them. Finally, the proposed design is better than because of its geometric structure.

7.5 Conclusion of the Chapter

A flexible topas as host material, circular core-cladding PC-PCF has been proposed at 1.05 THz having material absorption loss of 0.04 cm^{-1} . Further, having maximum core power fraction of 55.8%, and low confinement loss values are achieved. Consequently, the proposed PC-PCF structure possibly will be the prospective applicant for high data rate communication in THz spectrum.

CHAPTER 8

CONCLUSION AND FUTURE WORK

8.1 Conclusion of the Thesis

The exploration conveyed in this thesis is intended to know the optical light guiding properties of proposed PC-PCF and how these proposed structures can be applied in the field of ultra-broadband communication in THz regime. The author has focused on designing PC-PCFs with low losses and high core power fractions. The computational investigation is based on modeling of the proposed PC-PCF geometric structures using numerical technique to achieve the light guiding properties. The technique employed here is FEM. FEM is selected due to its flexibility in offering random boundaries. The proposed PC-PCF structure has a complex boundary and needs well-organized discretization of domain to analyze the fiber precisely. Additionally, the perfectly matched layer in FEM to limit error prone solutions as well as absorb unwanted radiations, correspondingly. The author has proposed four PC-PCFs and the best suitable application for each design. In each proposed design, PC-PCF core structure has been modeled carefully to increase modal power propagation through higher air filling fraction. In order to obtain an overall satisfactory result, porosity is varied intentionally to a certain extent by considering existing fabrication techniques.

Table 8 depicts the summary of results for the thesis works. It can be seen that comparatively better result has been found in case of circular cladding and core combination. In this design lower EML and CL have been found. Also, the design has exhibited high core power fraction which is considered good for THz communications compared to other proposed design. If polarization maintaining fiber is required along with low losses, then proposed design octa-hybrid can be taken into consideration.

The author has observed few expected behaviors of modal parameters throughout the thesis work. As photonics is a quantum mechanical phenomenon, the author has also observed some unexpected behavior as well. This was due to geometric structures of the porous core photonic crystal. But the impacts of unexpected behaviors are negligible. In this thesis, it is found that EML increases along with increasing frequency. It is likewise found that increasing value of core diameter results in higher EML. Finally, the author

has concluded that porosity has an inverse relation with EML. On the other hand, a confinement loss was decreasing with increasing core diameters and frequencies. In this thesis, it is also seen that birefringence is dependent on core diameter, porosity and frequency. Birefringence is increased when the values of core diameter and porosity goes down. Similarly, it also displayed inverse relation with frequency which is expected. Core power fraction which is another important modal parameter increased with porosity and core diameter.

Table 8 Light guiding properties of the proposed PC-PCFs in THz regime

| Modal Properties | Deca-Hexa | Octa-Hexa | Octa-Hybrid | Circle-Circle |
|--------------------------|-----------------------|----------------------|----------------------|-----------------------|
| Frequency (THz) | 1 | 1 | 0.73 | 1.05 |
| EML (cm^{-1}) | 0.049 | 0.045 | 0.044 | 0.040 |
| CPF (%) | 43 | 58.2 | 40 | 57 |
| CL (cm^{-1}) | 1.35×10^{-3} | 9.8×10^{-4} | 7.9×10^{-4} | 1.89×10^{-4} |
| BR | - | - | 0.043 | - |
| Dispersion $ps/THz/cm$ | 1.58 ± 0.02 | 1 ± 0.225 | 5.3 ± 0.05 | 1.8 ± 0.225 |
| Total Loss (cm^{-1}) | 0.0504 | 0.046 | 0.044 | 0.040 |

The proposed PC-PCF has shown several advantages over other PC-PCF in many applications and there are more to be explored and exposed in these unique proposed designs.

8.2 Scope for Future Works

This research is focused on the investigation of PC-PCF and to carry forward their exclusive modal properties over traditional fibers as well as other PCFs. PC-PCFs

normally have several benefits over traditional fiber optics and few of them are discussed in the work. High birefringence can be obtained by using dual unit based porous core and rotating core air holes at different angles. High birefringence with reasonable EML can also be achieved by using microstructure cladding air holes and elliptical core air holes. Effective material loss can be reduced further by increasing the porosity. Also, new type of materials like zeonex can be used as host material. Further, a PCF can be designed for optical communication and sensing. In this case, the tradeoff between EML and relative sensitivity should be taken care of.

In this thesis work, the author has tried to improve some particular properties keeping others in a tolerable range. Hence, there are scope of improving other optical properties. Besides, we cannot fabricate the proposed fiber which is also a big challenge. Moreover, there are also some nonlinear optical properties at higher frequencies which have unavoidable effect. We could not find these effects because of constraints of time and resource. Those properties should also be taken under consideration while designing a THz PC-PCFs.

The simulations of proposed PC-PCFs have established their benefits over other micro-structured fibers. The theoretical investigations are obtained in these works and articles are published. However, the obligation is to validate the obtained results using practical fabrication in the specified THz spectrum. The fabrication of these fibers will open the new horizon to researchers to examine the unique properties of proposed PC-PCF as well as implement those designs in the relevant fields.

APPENDICES

In this section the author has derived two important light guiding parameters for the proposed PC-PCF. They are core power fraction in Appendix A and effective material absorption loss in Appendix B.

APPENDIX A: CORE POWER FRACTION

If the waveguide has cylindrical symmetry, the modal field can be written in separable form in three dimensions [101].

$$\mathbf{E}_j(x, y, z) = \mathbf{e}_j(x, y) e^{i\beta_j z} \quad (a1)$$

$$\mathbf{H}_j(x, y, z) = \mathbf{h}_j(x, y) e^{i\beta_j z} \quad (a2)$$

Where β_j is denoted as propagation constant or Eigen value of j^{th} mode. Each propagation mode has single value of β_j .

If the medium has non-absorbing properties then $n(x,y)$ is real. Then field component of each bound mode,

$$\mathbf{e}_{tj}, \mathbf{h}_{tj} \text{ is pure real and} \quad (a3)$$

e_{zj}, h_{zj} is pure imaginary.

When the optical mode has excitation, the corresponding mode will convey power. If the waveguide is non-absorbing then power flows parallel along axis, for the j^{th} mode, power flow scattered through infinite cross-section area having intensity, S_j using equations (a1),(a2), (a3),

$$P_j = \frac{1}{2} |a_j|^2 \text{RE}\{\mathbf{E}_j \times \mathbf{H}_j^*\} = \frac{1}{2} |a_j|^2 \mathbf{e}_j \times \mathbf{h}_j^* \cdot \hat{\mathbf{z}} \quad (a4)$$

Here a_j is modal amplitude. Net power every guided mode obtained using integration, S_j across infinite area, A_∞ . Now, the j^{th} forward and backward propagation mode we can write,

$$P_j = \frac{1}{2} |a_j|^2 \int_\infty \mathbf{e}_j \times \mathbf{h}_j^* \cdot \hat{\mathbf{z}} dA, \quad (a5)$$

$$P_{-j} = -\frac{1}{2} |a_j|^2 \int_\infty \mathbf{e}_j \times \mathbf{h}_j^* \cdot \hat{\mathbf{z}} dA \quad (a6)$$

Where $P_j > 0$ indicates power flows in positive z -direction and $P_{-j} < 0$ indicates power flows in negative z -direction.

As the refractive index is different in two regions core and cladding leads to distinct behavior in waveguide. Using above equations (a5 and a6), the total power propagates through the core can be derived. Now we define a new parameter called core power fraction, η_j .

$$\eta_j = \frac{\text{Power flow into the core}}{\text{Power flow of the mode}}$$

$$\eta_j = \eta_{-j} = \frac{\frac{1}{2} \int_{Core} \mathbf{e}_j \times \mathbf{h}_j^* \cdot \hat{\mathbf{z}} dA}{\frac{1}{2} \int_{\infty} \mathbf{e}_j \times \mathbf{h}_j^* \cdot \hat{\mathbf{z}} dA} \quad (a7)$$

For forward or backward propagation above equation (a7) [101] tells how much energy is propagating through the core area.

APPENDIX B: DERIVATION OF EML

The material absorption loss can be derived using conjugate and non-conjugate reciprocity theorem of Maxwell's laws [105]. This needs two different electromagnetic conditions: firstly, characterize index of refraction n , current density, \mathbf{J} , electric and magnetic fields \mathbf{E} and \mathbf{H} respectively while another characterize by \bar{n} , $\bar{\mathbf{J}}$, $\bar{\mathbf{E}}$, and $\bar{\mathbf{H}}$. All vector components hold the time dependence, $e^{-j\omega}$, where ω is angular frequency. Index refraction profiles n and \bar{n} determined spatial variables.

Using conjugate form, we define a vector function \mathbf{F}_c by

$$\mathbf{F}_c = \mathbf{E} \times \bar{\mathbf{H}}^* + \bar{\mathbf{E}}^* \times \mathbf{H} \quad (b1)$$

Here $*$ is complex conjugate. The fields satisfy conjugate form of Maxwell's equations [101].

$$\begin{aligned} \nabla \times \bar{\mathbf{E}}^* &= -i \left(\frac{\mu_0}{\varepsilon_0} \right)^{\frac{1}{2}} k \bar{\mathbf{H}}^* \\ \nabla \times \bar{\mathbf{H}}^* &= \bar{\mathbf{J}} + i \left(\frac{\mu_0}{\varepsilon_0} \right)^{\frac{1}{2}} k (\bar{n}^*)^2 \bar{\mathbf{E}}^* \end{aligned} \quad (b2)$$

Where μ_0 , ε_0 and k are real. We need following vector identity to express equation (b2)

$$\nabla_t \cdot (\mathbf{A} \times \mathbf{B}) = \mathbf{B} \cdot (\nabla_t \times \mathbf{A}) - \mathbf{A} \cdot (\nabla_t \times \mathbf{B})$$

Now, equation b2 becomes:

$$\nabla \cdot \mathbf{F}_c = -i \left(\frac{\mu_0}{\varepsilon_0} \right)^{\frac{1}{2}} k \{ (\bar{n}^*)^2 - n^2 \} \mathbf{E} \cdot \bar{\mathbf{E}}^* - (\bar{\mathbf{E}}^* \cdot \mathbf{J} + \bar{\mathbf{J}} \cdot \mathbf{E}) \quad (b3)$$

Now, applying divergence theorem. The form is

$$\int_S \nabla \cdot \mathbf{A} \, ds = \frac{\partial}{\partial z} \int_S \mathbf{A} \cdot \hat{\mathbf{z}} \, ds + \int_l \mathbf{A} \cdot \hat{\mathbf{n}} \, dl$$

The \mathbf{F}_c can be written as

$$\int_A \nabla \cdot \mathbf{F}_c \, dA = \frac{\partial}{\partial z} \int_A \mathbf{F}_c \cdot \hat{\mathbf{z}} \, dA + \int_l \mathbf{F}_c \cdot \hat{\mathbf{n}} \, dl \quad (b4)$$

Here A is arbitrary cross-sectional area, $\hat{\mathbf{z}}$ is the unit vector parallel to the z -axis. For optical waveguides, the line integral over the circle $r = \infty$, where r represents cylindrical radius. So, \mathbf{F}_c vanishes as $r \rightarrow \infty$, since the bound node amplitude falls exponentially. Thus, we drop the line integral equation from (b4) and obtain the reciprocity theorem

$$\frac{\partial}{\partial z} \int_{A_\infty} \mathbf{F}_c \cdot \hat{\mathbf{z}} dA = \int_{A_\infty} \nabla \cdot \mathbf{F}_c dA \quad (b5)$$

Where \mathbf{F}_c defined by equation(b1) and $\nabla \cdot \mathbf{F}_c$ by equation(b3). This result effective for uninformed refractive index profile, including material absorption, when n has imaginary part.

The propagation constant has the attenuation portion. Now, we will derive the integral expression of the propagation constant. In equation (b1) where \mathbf{F}_c will be replaced by \mathbf{G}_c .

$$\mathbf{G}_c = \mathbf{E} \times \bar{\mathbf{H}}^* \quad (b6)$$

The Maxwell's equation for no-magnetic material that constitutes the waveguide [101]. The magnetic permeability μ is close to free space value μ_0 .

$$\begin{aligned} \nabla \times \mathbf{E} &= i \left(\frac{\mu_0}{\epsilon_0} \right)^{\frac{1}{2}} k \mathbf{H} \\ \nabla \times \mathbf{H} &= \mathbf{J} - i \left(\frac{\mu_0}{\epsilon_0} \right)^{\frac{1}{2}} kn^2 \mathbf{E} \\ \nabla \cdot (n^2 \mathbf{E}) &= \frac{\sigma}{\epsilon_0} \\ \nabla \cdot \mathbf{H} &= 0 \end{aligned} \quad (b7)$$

Assume $n = \bar{n}$, $\mathbf{J} = \bar{\mathbf{J}} = 0$. With the help of equation (b7) and the vector identity, we deduce that,

$$\nabla \cdot \mathbf{F}_c = ik \left\{ \left(\frac{\mu_0}{\epsilon_0} \right)^{\frac{1}{2}} k \mathbf{H} \cdot \bar{\mathbf{H}}^* - \left(\frac{\mu_0}{\epsilon_0} \right)^{\frac{1}{2}} (n^2)^* \mathbf{E} \cdot \bar{\mathbf{E}}^* \right\} \quad (b8)$$

Replacing \mathbf{F}_c with \mathbf{G}_c in (b5) leads to

$$\frac{\partial}{\partial z} \int_{A_\infty} \mathbf{E} \times \bar{\mathbf{H}}^* \cdot \hat{\mathbf{z}} dA$$

$$= \int_{A^\infty} \left\{ \left(\frac{\mu_0}{\varepsilon_0} \right)^{\frac{1}{2}} k \mathbf{H} \cdot \bar{\mathbf{H}}^* - \left(\frac{\mu_0}{\varepsilon_0} \right)^{\frac{1}{2}} (n^2)^* \mathbf{E} \cdot \bar{\mathbf{E}}^* \right\} dA \quad (b9)$$

The fields with forward and backward propagation mode with propagation constant β_j ,
Therefore:

$$\begin{aligned} \mathbf{E} &= \mathbf{e}_j e^{i\beta_j z}, \\ \mathbf{H} &= \mathbf{h}_j e^{i\beta_j z} \\ \bar{\mathbf{E}} &= \mathbf{e}_{-j} e^{-i\beta_j z} \\ \bar{\mathbf{H}} &= \mathbf{h}_{-j} e^{-i\beta_j z} \end{aligned} \quad (b10)$$

Now, equation (b9) can be deduced to using equation (b10)

$$\beta_j = \frac{\frac{k}{2} \int_{A^\infty} \left\{ \left(\frac{\mu_0}{\varepsilon_0} \right)^{\frac{1}{2}} \mathbf{h}_j - \left(\frac{\mu_0}{\varepsilon_0} \right)^{\frac{1}{2}} (n^2)^* |\mathbf{e}_j|^2 \right\} dA}{\int_{A^\infty} \mathbf{e}_j \times \mathbf{h}_j \cdot \hat{\mathbf{z}} dA} \quad (b11)$$

Which is valid for absorbing waveguide. For non-absorbing waveguide (b11) becomes

$$\beta_j = \frac{k \left(\frac{\mu_0}{\varepsilon_0} \right)^{\frac{1}{2}} \int_{A^\infty} \{ n^2 \mathbf{e}_j \times \mathbf{h}_j^* \} dA}{\int_{A^\infty} n^2 |\mathbf{e}_j|^2 dA} \quad (b12)$$

The above equation in terms of attenuation from [169]

$$\gamma_j = 2k \left(\frac{\mu_0}{\varepsilon_0} \right)^{\frac{1}{2}} \frac{\int_{A_x} n^r n^i |\mathbf{e}_j|^2 dA}{RE \left\{ \int_{A_{ll}} \mathbf{e}_j \times \mathbf{h}_j^* \cdot \hat{\mathbf{z}} dA \right\}} \quad (b13)$$

Where γ_j is the power attenuation constant. The above equation is simplified in [91] as effective material loss

$$\alpha_{eff} = \left(\frac{\mu_0}{\varepsilon_0} \right)^{\frac{1}{2}} \frac{\int_{A_{mat}} n \alpha_{mat} |\mathbf{E}|^2 dA}{RE \left\{ \int_{A_{ll}} \mathbf{E} \times \mathbf{H}^* \cdot \hat{\mathbf{z}} dA \right\}} \quad (b14)$$

where RE denotes the real part, n indicates refractive index, and α_{mat} represents the material loss. \mathbf{E} represents electric field and \mathbf{H}^* signifies complex conjugated magnetic field component. $\hat{\mathbf{z}}$ is unit vector in z -direction.

The numerator part carries out through solid material (A_{mat}) because the propagation loss of terahertz radiation in air is negligible.

REFERENCES

- [1] S. Atakaramians, S. Afshar V., T.M. Monro, and Derek Abbott, "Terahertz dielectric waveguides", *Advances in Optics and Photonics*, vol. 5, pp. 169-215, 2013.
- [2] A. Mendez and T. Morse, *Specialty Optical Fibers Handbook*. 1st ed., Elsevier, 2007.
- [3] R. J. Mears, L. Reekie, I. M. Jauncey, and D. N. Payne, "Low-noise erbium doped fiber amplifier operating at 1.54 μm ", *Electronics Letters*, vol. 23, no. 19, pp. 1026–1028, 1987.
- [4] M. Bass, C. DeCusatis, J. Enoch, V. Lakshminarayanan, G. Li, C. MacDonald, V. Mahajan, and E. V. Stryland, *Handbook of Optics, Volume V: Atmospheric Optics, Modulators, Fiber Optics, X-Ray and Neutron Optics*, 3rd ed., 2009.
- [5] S. Atakaramians, "Terahertz Waveguide: A study of Microwires and Porous Fiber", Ph.D. dissertation, Dept. of Electrical and Electronic Engineering., Univ. of Adelaide, Adelaide, 2011.
- [6] Terahertz Sources (May 10, 2020). RP Photonics Encyclopaedia [online]. Available: https://www.rp-photonics.com/terahertz_sources.html
- [7] Charrada K, Zissis G and Aubes M, "Two-temperature,two-dimensional fluid modelling of mercury plasma in high-pressure lamps", *J. Phys. D: Appl. Phys.*, vol. 29, pp.2432–8, 1996.
- [8] Shin Y M, Park G S, Scheitrum G P and Caryotakis G, "Circuit analysis of an extended interaction klystron." *J. Korean Phys. Soc.*, vol. 44, pp. 1239–1245, 2004.
- [9] Bhattacharjee S., "Folded waveguide traveling-wave tube sources for terahertz radiation.", *IEEE Trans. Plasma Sci.*, vol. 32, pp. 1002–1014, 2004.
- [10] B. A. Knyazev, G. N. Kulipanov and N. A. Novosibirsk, "terahertz free electron laser: instrumentation development and experimental achievements.", *Meas. Sci. Technol.*, vol. 21, pp. 054017, 2010.

- [11] L. A. Yang, Y. Hao, Q. Yao and J. Zhang, "Improved negative differential mobility model of GaN and AlGaIn for a terahertz Gunn diode.", *IEEE Trans. Electron Devices*, vol. 58, pp. 1076–83, 2011.
- [12] W. Knap, J. Lusakowski, T. Parenty, S. Bollaert, A. Cappy, and M. S. Shur, "Terahertz emission by plasma waves in 60 nm gate high electron mobility transistors." *Appl. Phys. Lett.*, vol. 84, pp. 2331–2333, 2004.
- [13] H. Ubers, S. G. Pavlov and V. N. Shastin, "Terahertz lasers based on germanium and silicon." *Semicond. Sci. Technol.*, vol. 20, pp. 211–21, 2005.
- [14] G. Dodel, "On the history of far-infrared (FIR) gas lasers: Thirty-five years of research and application Infrared.", *Phys. Technol.*, vol. 40, pp. 127–39, 1999.
- [15] S. Hoffmann and M. R. Hofmann, "Generation of Terahertz radiation with two colour semiconductor lasers", *Laser & Photon. Rev.*, vol. 44, 2007.
- [16] F. Sizov, "THz radiation sensors.", *Opto-Electron. Rev.*, vol. 18, 2010.
- [17] H. J. Bakker, G. C. Cho, H. Kurz, Q. Wu, and X.C. Zhang, "Distortion of terahertz pulses in electro-optic sampling.", *Journal of the Optical Society of America B*, vol. 15, Issue 6, pp. 1795-1801, 1998.
- [18] Tingye Li, "Advances in Optical Fiber Communications: An Historical Perspective," *IEEE Journal on Selected Areas in Communications*, vol. 1, 1983.
- [19] R. P. Khare, *Fiber Optics and Optoelectronic*. Oxford University Press, 2nd ed., 2004.
- [20] G. Agrawal, *Nonlinear Fiber Optics*. 1st ed., Elsevier, 2013.
- [21] P. Russell, "Photonic-Crystal Fibers," *Journal of Lightwave Technology*, vol. 24, Issue 12, pp. 4729-4749, 2006.
- [22] Brief history of photonic crystal fibers J. C. Knight, "Photonic crystal fibers", *Nature*, vol. 424, pp. 847–851, 2003.
- [23] T. A. Birks, J. C. Knight, and P. S. J. Russell, "Endlessly single-mode photonic crystal fiber," *Optics Letters*, vol. 22, pp. 961–963, 1997.
- [24] M. A. Duguay, Y. Kokubun, T. L. Koch, and L. Pfeiffer, "Antiresonant reflecting optical waveguides in SiO₂/Si multilayer structures," *Applied Physics Letters*, vol. 49, pp. 13–15, 1986.

- [25] S. Atakramians, Shahraam Afshar V., Bernd M. Fischer, Derek Abbott, and Tanya M. Monro, "Porous fibers: a novel approach to low loss THz waveguides", *Applied Optics*, Vol. 16, pp. 8845-8854. 2008.
- [26] Laser and Fibers (June 23, 2020). NKT Photonics [online]. Available: <https://www.nktphotonics.com/lasers-fibers/technology/photonic-crystal-fibers>
- [27] R. F. Cregan, B. J. Mangan, J. C. Knight, T. A. Birks, P. S. Russell, P. J. Roberts, and D. C. Allan, "Singlemode photonic band gap guidance of light in air", *Science*, vol. 285, p. 1537–1539, 1999.
- [28] Y. Wang, F. Couny, P. J. Roberts, and F. Benabid, "Low Loss Broadband Transmission in Optimized Core-shape Kagome Hollow-core PCF," in *Conf. Lasers and Electro-Optics*, San Jones, CA, 2010.
- [29] F. Couny, F. Benabid, and P. S. Light, "Large-pitch kagome-structured hollow core photonic crystal fiber," *Optics Letters*, vol. 31, no. 24, pp. 3574–3576, 2006.
- [30] Md. Shariful Islam, Mohammad Faisal, S. M. Abdur Razzak, "Dispersion Flattened Porous-Core Honeycomb Lattice Terahertz Fiber for Ultra Low Loss Transmission", *IEEE Journal of Quantum Electronics*, vol. 53 , Issue: 6 , Dec. 2017.
- [31] J. D. Shephard, A. Urich, R. M. Carter, P. Jaworski, R. R. J. Maier, W. Belardi, F. Yu, W. J. Wadsworth, J. C. Knight, and D. P. Hand, "Silica hollow core microstructured fibers for beam delivery in industrial and medical applications," *Frontiers in Physics*, vol. 3, p.p. 107-114, 2015.
- [32] P. Jaworski, F. Yu, R. M. Carter, J. C. Knight, J. D. Shephard, , and D. P. Hand, "High energy green nanosecond and picosecond pulse delivery through a negative curvature fiber for precision micromachining," *Optics Express*, vol. 23, p. 8498–8506, 2015.
- [33] K. Saitoh, M. Koshiba, T. Hasegawa, and E. Sasaoka, "Chromatic dispersion control in photonic crystal fibers: application to ultra-flattened dispersion," *Optics Express*, vol. 11, no. 8, p. 843–851, 2003.
- [34] A. Ortigosa-Blanch, J. C. Knight, W. J. Wadsworth, J. Arriaga, B. J. Mangan, T. A. Birks, and P. S. J. Russell, "Highly birefringent photonic crystal fibers," *Optics Letters*, vol. 25, no. 18, pp. 1325–1327, 2000.

- [35] R. W. McGowan, G. Gallot, and D. Grischkowsky, "Propagation of ultrawideband short pulses of terahertz radiation through submillimeter-diameter circular waveguides," *Opt. Lett.*, vol. 24, pp. 1431–1433, 1999.
- [36] J. Chen, H.-W. Chen, T.-F. Kao, J.-Y. Lu, and C.-K. Sun, "Low-loss subwavelength plastic fiber for terahertz waveguiding," *Opt. Lett.*, vol. 31, pp.308–310, 2006.
- [37] C. S. Ponseca, R. Pobre, E. Estacio, N. Sarukura, A. Argyros, M. C. J. Large, and M. A. van Eijkelenborg, "Transmission of terahertz radiation using a microstructured polymer optical fiber," *Opt. Lett.*, vol. 33, pp. 902–904, 2008.
- [38] C.H. Lai, Y.-C. Hsueh, H.-W. Chen, Y.-J. Huang, H.-C. Chang, and C.-K. Sun, "Low-index terahertz pipe waveguides," *Opt. Lett.* vol. 34, pp.3457–3459, 2009.
- [39] T.I. Jeon, J. Zhang, and K. W. Goossen, "THz Sommerfeld wave propagation on a single metal wire," *Appl. Phys. Lett.*, vol. 86, pp. 161904-16909, 2005.
- [40] M. Wächter, M. Nagel, and H. Kurz, "Frequency-dependent characterization of THz Sommerfeld wave propagation on single-wires," *Opt. Express*, vol. 13, pp. 10815–10822, 2005.
- [41] S. Atakramians, S. Afshar Vahid, M. Nagel, H. Ebendorff-Heidepriem, B. M. Fischer, D. Abbott, and T. M. Monro, "THz porous fibers: design, fabrication and experimental characterization," *Opt. Express*, vol. 17, pp. 14053–14062, 2009.
- [42] Y. Kawano and K. Ishibashi, "An on-chip near-field terahertz probe and detector," *Nat. Photonics*, vol. 2, pp. 618–621, 2008.
- [43] M. Wächter, M. Nagel, and H. Kurz, "Tapered photoconductive terahertz field probe tip with subwavelength spatial resolution," *Appl. Phys. Lett.*, vol. 95, pp. 041112-18, 2009.
- [44] M. Wächter, M. Nagel, and H. Kurz, "Metallic slit waveguide for dispersion-free low-loss terahertz signal transmission," *Appl. Phys. Lett.*, vol. 90, pp. 061111-17, 2007.
- [45] S. Atakramians, S. Afshar V., H. Rasmussen, O. Bang, T. M. Monro, and D. Abbott, "Direct probing of evanescent field for characterization of porous terahertz fibers," *Appl. Phys. Lett.*, vol. 98, pp. 121104-11, 2011.

- [46] G. Gallot, S. P. Jamison, R. W. McGowan, and D. Grischkowsky, "Terahertz waveguides," *J. Opt. Soc. Am. B*, vol. 17, pp. 851–863, 2000.
- [47] R. Mendis and D. Grischkowsky, "Undistorted guided-wave propagation of subpicosecond terahertz pulses," *Opt. Lett.*, vol. 26, pp. 846–848, 2001.
- [48] K. Wang and D. M. Mittleman, "Metal wires for terahertz wave guiding," *Nature*, vol. 432, pp. 376–379, 2004.
- [49] B. Bowden, J. A. Harrington, and O. Mitrofanov, "Silver/polystyrene-coated hollow glass waveguides for the transmission of terahertz radiation," *Opt. Lett.*, vol. 32, pp. 2945–2947, 2007.
- [50] A. Barh, R. K. Varshney, and B. P. Pal, "THz guidance through hollow-core plastic photonic bandgap fiber: Sensitivity to structural parameters," *Recent Adv. Photonics*, WRAP 2015, pp. 1–4, 2015.
- [51] M. Azadeh, *Fiber Optics Engineering*, 1st ed., Springer, 2009.
- [52] MS Islam, S Rana, MR Islam, M Faisal, H Rahman, J Sultana, "Porous core photonic crystal fibre for ultra-low material loss in THz regime", *IET Communications*, vol. 10, pp. 2179-2183, 2016.
- [53] MS Islam, J Sultana, J Atai, D Abbott, S Rana, MR Islam "Ultra low-loss hybrid core porous fiber for broadband applications", *Applied optics*, vol. 56, pp. 1232-1237, 2017.
- [54] R. P. Khare, *Fiber Optics and Optoelectronic*, 1st ed., Oxford University Press, 2004.
- [55] M. D. Nielsen, R. S. Jacob and K. P. Hansen, "Modal cut-off and the V – parameter in photonic crystal fibers," *Optics Letters*, vol. 28, pp. 1879-1881, 2003.
- [56] K. Thyagarajan and A. Ghatak, *Fiber Optic Essentials*, 3rd ed., New Jersey: John Wiley & Sons, 2007.
- [57] P. Kaiser and H.W. Astle, "Low loss single material fibers made from pure fused silica," *The Bell System Technical Journal*, vol. 53, no. 6, p. 1021–1039, 1974.
- [58] K. M. Kiang, K. Frampton, T. M. Monro, R. Moore, J. Tucknott, D. W. Hewak, D. J. Richardson, and H. N. Rutt, "Extruded singlemode non-silica glass holey optical fibres," *Electronics Letters*, vol. 38, pp. 546–547, 2002.

- [59] S. Bhandarkar, "Sol-gel processing for optical communication technology," *Journal of the American Ceramic Society*, vol. 87, pp. 1180–1199, 2004.
- [60] K. Cook, G. Balle, J. Canning, L. Chartier, T. Athanaze, M. A. Hossain, C. Han, J.-E. Comatti, Y. Luo, and G.-D. Peng, "Step-index optical fiber drawn from 3D printed preforms," *Optics Letters*, vol. 41, pp. 4554–4557, 2016.
- [61] M. J. Weber, *Handbook of Optical Materials*, 2nd ed., New York: CRC Press, 2003.
- [62] A. Barh, B. P. Pal, G. P. Agrawal, R. K. Varshney, and B. M. A. Rahman, "Specialty fibers for terahertz generation and transmission: A review," *IEEE Journal of Selected Topics in Quantum Electronics*, vol. 22, pp. 365–379, 2016.
- [63] M. T. Myaing, J. Y. Ye, T. B. Norris, T. Thomas, J. J. R. Baker, W. J. Wadsworth, G. Bouwmans, J. C. Knight, and P. S. J. Russell, "Enhanced two-photon biosensing with dual-core photonic crystal fibers," *Optics Letters*, vol. 28, p. 1224–1226, 2003.
- [64] J. Anthony, R. Leonhardt, A. Argyros, and M. C. J. Large, "Characterization of a microstructured Zeonex terahertz fiber," *Journal of the Optical Society of America B*, vol. 28, pp. 1013-1018, 2011.
- [65] M. R. Islam, M. Arif Hossain, S. I. Ali, J. Sultana, and M. Saiful Islam, "Design and Characterization of an Ultra Low Loss, Dispersion-Flattened Slotted Photonic Crystal Fiber for Terahertz Application," *J. Opt. Commun.*, pp. 1–8, 2018.
- [66] N. Mahnot, S. Maheshwary, R. Mehra Overview, "Photonic crystal fiber overview," *International Journal of Scientific & Engineering Research*, vol. 6, no. 2, pp. 45–53, 2015
- [67] K. Singh, "Optical Fibre Communication: A review," *Imperial Journal of Interdisciplinary Research (IJIR)*, vol. 3, no. 8, pp. 285–288, 2017.
- [68] S. F. Kaijage, Z. Ouyang and X. Jin, "Porous-Core Photonic Crystal Fiber for Low Loss Terahertz Wave Guiding," *IEEE Photonics Technol. Lett.*, vol. 25, no. 15, pp. 1454-1457, 2013.

- [69] R. Islam, G. K. M. Hasanuzzaman, M. S. Habib, S. Rana, and M. A. G. Khan, "Low-loss rotated porous core hexagonal single-mode fiber in THz regime," *Opt. Fiber Technol.*, vol. 24, pp. 38–43, 2015.
- [70] S. F. U. Ahmed, S. Nayemuzzaman, M. Faisal, "Low Loss Porous-Core Photonic Crystal Fiber for Long-Haul Broadband THz Transmission," in *9th International Conference on Electrical and Computer Engineering*, Dhaka, Bangladesh, 2016.
- [71] M. S. Islam et al., "Extremely low material loss and dispersion flattened TOPAS based circular porous fiber for long distance terahertz wave transmission," *Opt. Fiber Technol.*, vol. 34, pp. 6–11, 2017.
- [72] S. Rana, M. S. Islam, J. Sultana, K. S. Reza, M. A. Uddin, M. Faisal, M. R. Islam and R. Islam, "A Highly Birefringent Slotted-Core THz Fiber," in *9th International Conference on Electrical and Computer Engineering*, Dhaka, Bangladesh, 2016.
- [73] S. Rana, A. S. Rakin, H. Subbaraman, R. Leonhardt, and D. Abbott, "Low Loss and Low Dispersion Fiber for Transmission Applications in the Terahertz Regime," *IEEE Photonics Technol. Lett.*, vol. 29, no. 10, pp. 830–833, 2017.
- [74] M. S. Islam, M. Faisal, and S. M. A. Razzak, "Dispersion flattened porous-core honeycomb lattice terahertz fiber for ultra-low loss transmission," *IEEE J. Quantum Electron.*, vol. 53, no. 6, pp. 1–8, 2017.
- [75] R. Islam, M. Selim Habib, G. K. M. Hasanuzzaman, S. Rana, and M. Anwar Sadath, "Novel porous fiber based on dual-asymmetry for low-loss polarization maintaining THz wave guidance," *Opt. Lett.*, vol. 41, no. 3, p. 440, 2016.
- [76] M. Shamim Anower, and M. Rabiul Hasan, "Highly birefringent and low effective material loss microstructure fiber for THz wave guidance," *Opt. Commun.*, vol. 423, pp. 140–144, 2018.
- [77] S. Ali, N. Ahmed, S. Alwee, M. Islam, S. Rana, and T. Bhuiyan, "Effects of Triangular Core Rotation of a Hybrid Porous Core Terahertz Waveguide," *Int. J. Electron. Telecommun.*, vol. 63, no. 1, pp. 25–31, 2017.

- [78] S. Ali et al., "Guiding properties of a hexagonal core porous fiber (HCPF) for terahertz wave propagation," 2nd International Conference on *Electrical, Computer & Telecommunication Engineering (ICECTE)*, 2016, Rajshahi-6204, Bangladesh.
- [79] A. Tandj, J. Yammine, G. Bouwmans, M. Dossou, A. Vianou, E. R. Andresen and L. Bigot, "Design and Fabrication of a Ring-Core Photonic Crystal Fiber for Low-Crosstalk Propagation of OAM Modes," in *European Conference on Optical Communication (ECOC)*, September 2018.
- [80] J. Sultana et al., "Highly birefringent elliptical core photonic crystal fiber for terahertz application," *Opt. Commun.*, vol. 407, pp. 92–96, 2017.
- [81] M. R. Hasan and S. Akter, "Extremely low-loss hollow-core bandgap photonic crystal fibre for broadband terahertz wave guiding," *Electron. Lett.*, vol. 53, pp. 741–743, April 2017.
- [82] R. Islam, M. S. Habib, G. K. M. Hasanuzzaman, S. Rana, M. A. Sadath and C. Markos, "A Novel Low Loss Diamond-Core Porous Fiber for Polarization Maintaining Terahertz Transmission," *IEEE Photonics Technology Letters*, vol. 28, no. 14, p. 1537–1540, 2016.
- [83] R. Ding, S. Hou, D. Wang, J. Lei, X. Li, and Y. Ma, "Novel design of a diamond-core photonic crystal fiber for terahertz wave transmission," *Prog. Electromagn. Res. Symp.–Spring (PIERS)*, no. 1, pp. 1148–1151, 2017.
- [84] I. K. Yakasai, A. Rahman, P. E. Abas, and F. Begum, "Theoretical Assessment of a Porous Core Photonic Crystal Fiber for Terahertz Wave Propagation," *Opt. Commun.*, pp. 1–11, 2018.
- [85] A. Bala, K. R. Chowdhury, and M. Faisal, "A Novel Tube Lattice Slotted Core Highly Birefringent Photonic Crystal Fiber for THz Application," *Journal of Advanced Optics and Photonics*, vol.1, No.2, 2018.
- [86] S. M. A. Razzak, Y. Namihira, "Guiding Properties of a Decagonal Photonic Crystal Fiber." *Journal of Microwaves and Optoelectronics*, vol. 6, 2007.
- [87] M. A. Motin, M. I. Hasan, M. Selim Habib, S.M. Abdur Razzak, and M. A. Goffar Khan, "Dispersion and Confinement Loss Control with Decagonal Photonic Crystal Fibers for Wideband Transmission Systems", ICIEVE, 2013.

- [88] M. A. Islam, R. Ahmad, M. S. Ali, and K. M. Nasim, "Proposal for highly residual dispersion compensating defected core decagonal photonic crystal fiber over S+C+L+U wavelength bands", *Optical Engineering*, vol. 53, pp. 076106, 2014.
- [89] M. N. Hoque, A. S. and N. Akter, "Octagonal Photonic Crystal Fibers: Application to Ultra-flattened Dispersion", *Australian Journal of Basic and Applied Sciences*, vol.4, 2274-2279, 2010.
- [90] R. A. Matej, S Dmytro, Z. Stanislav, "Modified Octagonal Photonic Crystal Fiber for Residual Dispersion Compensation over Telecommunication Bands", *Rad.Eng. Jounl.*, vol. 27, 2018.
- [91] S. Chowdhury, S. Sen K. Ahmed, B. K. Paula, and S. Islama, "Porous shaped photonic crystal fiber with strong confinement field in sensing applications: Design and analysis", *Sensing and Bio-Sensing Research*, vol. 13, pp. 63-69, 2017.
- [92] S. Sen, M. S. Islam and B. K. Paul, "Ultra-low Loss with Single Mode Polymer-Based Photonic Crystal Fiber for THz Waveguide," *Journal of Optical Communications*, vol. 40, pp. 411-417 2017.
- [93] Azabi, Y. O., "Spiral photonic crystal fibers," Ph.D. dissertation, School of Mathematics, Dept. Computer Science & Engineering, Univ. of London, London, 2017.
- [94] M. N. Sadiku, Numerical Techniques in Electromagnetics. New York: CRC Press, 2 ed., 2001.
- [95] R.Garg, Analytical and Computational Methods in Electromagnetics, 3rd ed., Norwood:Artech House, 2008.
- [96] B. M. A. Rahman and A. Agrawal, Finite Element Modeling Methods for Photonics, 2nd ed., London: Artech House, 2013.
- [97] B. A. Rahman, F. A. Fernandez, and J. B. Davies, "Review of finite element methods for microwave and optical waveguides," *Proceedings of the IEEE*, vol. 79, no. 10, pp. 1442–1448, 1991.

- [98] S. Rana, G. K. M. Hasanuzzaman, M. S. Habib, S. F. Kaijage, R. Islam., "Proposal for a low loss porous core octagonal photonic crystal fiber for T-ray wave guiding", *Optical Engineering*, vol. 53, pp. 115107, 2014.
- [99] K. Ahmed et. al, "Design of a single-mode photonic crystal fibre with ultra-low material loss and large effective mode area in THz regime." *IET Optoelectronics*, vol. 11, pp. 265-271, 2017.
- [100] Z. Wu, Z. Shi, H. Xia, X. Zhou, Q. Deng, J. Huang, X. Jiang, and W. Wu, "Design of highly birefringent and low-loss oligoporous-core THz Photonic crystal fiber with single circular , air-hole unit," *IEEE Photonics Journal*, vol. 8, pp. 4502711, 2016.
- [101] A.W. Snyder, J. Love, "Optical Waveguide Theory", Springer Science and Business Media, 1983.

LIST OF PUBLICATIONS

- [1] Md. Sohidul Islam, KM Samaun Reza, Mohammad Rakibul Islam, " Low Loss Topas Based Porous-Core Single-Mode Photonic Crystal Fiber for THz communications." *Indian Journal of Pure and Applied Physics*, vol. 57, pp. 836-841, Nov. 2019
- [2] Md. Sohidul Islam, Jamilur Rahman, Mohammad Rakibul Islam, "Topas Based Low Loss and Dispersion Flatten Decagonal Porous Core Photonic Crystal Fiber for Terahertz Communication." *Int. Jour. of Micwav. and Opt. Tech.*, vol. 14, pp. 62-69. Jan. 2019.
- [3] Md. Sohidul Islam, KM Samaun Reza, Dr. Mohammad Rakibul Islam "Topas based high birefringent and low loss single mode hybrid core porous fiber for broad band applications" *Indian Journal of Pure and Applied Physics*, vol. 56, PP. 399-404, May. May, 2018.
- [4] Mohammad Rakibul Islam, Mamoudou Mamadou, Md. Sohidul Islam, "Design and analysis of a highly sensitive hollow core photonic crystal fiber for chemical sensing ", *Journal of Nanophotonics*, vol. 14, pp. 0360141-03601415, Sept. 2020.
- [5] Md. Sohidul Islam, Mohammad Rakibul Islam, "Topas based low loss single mode circular porous core photonic crystal fiber for ultra-broadband application" *Optoelectronics and Advanced Materials-Rapid Communications*, in Review 2020.
- [6] Md. Sohidul Islam, Mamoudou Mamadou, Jamilur Rahman, Md. Shadidul Islam, Mohammad Rakibul Islam" Highly sensitive and low loss photonic crystal fiber for sensing application and wave guidance", *Turkish Journal of Physics*, submitted, September. 2020.